

(2)

# NAVAL POSTGRADUATE SCHOOL

## Monterey, California

AD-A258 019



DTIC  
ELECTE  
DEC 17 1992  
S B D

## THESIS

A COMPUTATIONAL AND EXPERIMENTAL  
INVESTIGATION OF THE PROPULSIVE AND LIFTING  
CHARACTERISTICS OF OSCILLATING AIRFOILS AND  
AIRFOIL COMBINATIONS IN INCOMPRESSIBLE FLOW

by

Kerry S. Neace  
September, 1992

Thesis Advisor:  
Co-Advisor:

M.F. Platzer  
S.K. Hebbar

Approved for public release; distribution is unlimited

92-31664



92 12 16 049

REPORT DOCUMENTATION PAGE				
1a. REPORT SECURITY CLASSIFICATION UNCLASSIFIED			1b. RESTRICTIVE MARKINGS	
2a. SECURITY CLASSIFICATION AUTHORITY			3. DISTRIBUTION/AVAILABILITY OF REPORT Approved for public release; distribution is unlimited.	
2b. DECLASSIFICATION/DOWNGRADING SCHEDULE				
4. PERFORMING ORGANIZATION REPORT NUMBER(S)			5. MONITORING ORGANIZATION REPORT NUMBER(S)	
6a. NAME OF PERFORMING ORGANIZATION Naval Postgraduate School		6b. OFFICE SYMBOL (If applicable) AA/PL	7a. NAME OF MONITORING ORGANIZATION Naval Postgraduate School	
6c. ADDRESS (City, State, and ZIP Code) Monterey, CA 93943-5000			7b. ADDRESS (City, State, and ZIP Code) Monterey, CA 93943-5000	
8a. NAME OF FUNDING/SPONSORING ORGANIZATION		8b. OFFICE SYMBOL (If applicable)	9. PROCUREMENT INSTRUMENT IDENTIFICATION NUMBER	
8c. ADDRESS (City, State, and ZIP Code)			10. SOURCE OF FUNDING NUMBERS	
			Program Element No.	Project No.
			Task No.	Work Unit Accession Number
11. TITLE (Include Security Classification) A COMPUTATIONAL AND EXPERIMENTAL INVESTIGATION OF THE PROPULSIVE AND LIFTING CHARACTERISTICS OF OSCILLATING AIRFOILS AND AIRFOIL COMBINATIONS IN INCOMPRESSIBLE FLOW				
12. PERSONAL AUTHOR(S) Kerry S. Neace				
13a. TYPE OF REPORT Master's Thesis		13b. TIME COVERED From To	14. DATE OF REPORT (year, month, day) 1992, September	15. PAGE COUNT 123
16. SUPPLEMENTARY NOTATION The views expressed in this thesis are those of the author and do not reflect the official policy or position of the Department of Defense or the U.S. Government.				
17. COSATI CODES			18. SUBJECT TERMS (continue on reverse if necessary and identify by block number)	
FIELD	GROUP	SUBGROUP	Phase relationships for oscillating airfoils, Propulsive forces (Katzmayr effect), Enhanced lift, Quasi-steady theory, Flow visualization	
19. ABSTRACT (continue on reverse if necessary and identify by block number)  Computational and experimental methods have been used to systematically study one and two airfoils undergoing unsteady motion. First, a single airfoil analysis was done with the modified computer code, U2DIIF. Thrust, efficiency, and phase relationships were computed and compared to existing theoretical results. Furthermore, to help understand the dynamic stall process, relationships were developed between steady and quasi-steady pressure distributions for an airfoil undergoing a ramp motion. Next, an unsteady analysis for two airfoils was done with the modified computer code, USPOTF2. Again, thrust and efficiencies for interfering, harmonically oscillating airfoils were computed and compared to existing theoretical results. Furthermore, an analysis was completed on the effects of a harmonically oscillating airfoil on the pressure gradient of a stationary airfoil. Finally, flow visualization experiments were conducted using a low speed smoke tunnel at the Naval Postgraduate School (NPS). This experiment demonstrated the effects of a thrust producing, oscillating airfoil on the formation of the wake vortices. Furthermore, a flow visualization experiment was conducted in the NPS low speed wind tunnel, which demonstrated the beneficial influence of a secondary airfoil oscillating in the vicinity of a stationary airfoil at high angle-of-attack.				
20. DISTRIBUTION/AVAILABILITY OF ABSTRACT <input checked="" type="checkbox"/> UNCLASSIFIED/UNLIMITED <input type="checkbox"/> SAME AS REPORT <input type="checkbox"/> DTIC USERS			21. ABSTRACT SECURITY CLASSIFICATION UNCLASSIFIED	
22a. NAME OF RESPONSIBLE INDIVIDUAL Max F. Platzer			22b. TELEPHONE (Include Area code) (408) 646-2058	22c. OFFICE SYMBOL AA/PL

Approved for public release; distribution is unlimited.

**A Computaional and Experimental Investigation  
of the Propulsive and Lifting Characteristics of Oscillating Airfoils and Airfoil Combinations  
in Incompressible Flow**

by

**Kerry S. Neace  
Lieutenant, United States Navy  
B.S., Georgia Institute of Technology, 1985**

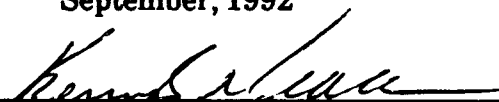
**Submitted in partial fulfillment  
of the requirements for the degree of**

**AERONAUTICAL AND ASTRONAUTICAL ENGINEER**


from the

**NAVAL POSTGRADUATE SCHOOL  
September, 1992**

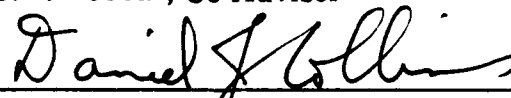
**Author:**

  
Kerry S. Neace


**Approved by:**

  
Max F. Platzner, Thesis Advisor

  
S.K. Hebbar, Co-Advisor

  
Daniel J. Collins, Chairman

**Department of Aeronautics and Astronautics**

  
Richard S. Elster  
Dean of Instruction

## ABSTRACT

Computational and experimental methods have been used to systematically study one and two airfoils undergoing unsteady motion. First, a single airfoil analysis was done with the modified computer code, U2DIIF. Thrust, efficiency, and phase relationships were computed and compared to existing theoretical results. Furthermore, to help understand the dynamic stall process, relationships were developed between steady and quasi-steady pressure distributions for an airfoil undergoing a ramp motion. Next, an unsteady analysis for two airfoils was done with the modified computer code USPOTF2. Again, thrust and efficiencies for interfering, harmonically oscillating airfoils were computed and compared to existing theoretical results. Furthermore, an analysis was completed on the effects of a harmonically oscillating airfoil on the pressure gradient of a stationary airfoil. Finally, flow visualization experiments were conducted using a low speed smoke tunnel at the Navel Postgraduate School (NPS). This experiment demonstrated the effects of a thrust producing, oscillating airfoii on the formation of the wake vortices. Furthermore, a flow visualization experiment was conducted in the NPS low speed wind tunnel, which demonstrated the beneficial influence of a or secondary airfoil oscillating in the vicinity of a stationary airfoil at high angle-of-attack.

iii

DTIC QUALITY INSPECTED

Justification	
<input checked="checked" type="checkbox"/> <input type="checkbox"/> <input type="checkbox"/>	
By _____	
Distribution/	
Availability Codes	
Dist	Avail and/or Special
A-1	

## TABLE OF CONTENTS

I. INTRODUCTION .....	1
A. GENERAL .....	1
B. SCOPE .....	2
II. SINGLE AIRFOIL ANALYSIS .....	4
A. HARMONIC MOTION .....	4
1. Introduction .....	4
2. Panel Code U2DIIF .....	7
B. PROPULSIVE EFFICIENCY .....	16
1. Introduction .....	16
2. Theory .....	17
3. Comparison to Flat Plate Theory. ....	21
4. Power Extraction for Two Degrees of Freedom .....	25
C. UNSTEADY PRESSURE DISTRIBUTIONS .....	30
1. Introduction .....	30
2. Theory .....	30
3. Description .....	32
4. Results .....	33

III.	TWO AIRFOIL ANALYSIS . . . . .	42
A.	COMPUTER CODE USPOTF2 . . . . .	42
1.	Modifications (USPOTF2A) . . . . .	43
a.	Program Output . . . . .	43
b.	Program Corrections . . . . .	45
c.	Airfoil Motion . . . . .	46
d.	Limitations . . . . .	52
B.	COMPARISON TO EXISTING COMPUTATIONAL RESULTS . .	54
C.	PROPULSIVE EFFICIENCY . . . . .	60
1.	Introduction . . . . .	60
2.	Theory . . . . .	61
3.	Comparison to Flat Plate Theory . . . . .	62
D.	UPWIND INFLUENCE STUDY . . . . .	67
1.	Introduction . . . . .	67
2.	Description . . . . .	67
3.	Results . . . . .	68
4.	Conclusion . . . . .	69
IV.	PROPULSIVE FLOW VISUALIZATION EXPERIMENT . . . . .	73
A.	INTRODUCTION . . . . .	73
B.	THEORY . . . . .	74
C.	EXPERIMENTAL SETUP . . . . .	76

1. Wave Propeller .....	76
2. Wind Tunnel .....	77
D. TEST PROCEDURE .....	79
E. RESULTS AND DISCUSSION .....	80
 V. ENHANCED LIFT FLOW VISUALIZATION EXPERIMENT .....	89
A. INTRODUCTION .....	89
B. EXPERIMENTAL SETUP .....	90
1. Wave Propeller and Stationary Wing .....	90
2. Wind Tunnel .....	91
3. Smoke Generator .....	91
C. TEST PROCEDURE .....	92
D. RESULTS AND DISCUSSION .....	92
 VI. CONCLUSION AND RECOMMENDATIONS .....	96
A. SINGLE AIRFOIL ANALYSIS .....	96
B. TWO AIRFOIL ANALYSIS .....	96
C. FLOW VISUALIZATION EXPERIMENTS .....	97
 APPENDIX A .....	99
 APPENDIX B .....	104

LIST OF REFERENCES ..... 110

INITIAL DISTRIBUTION LIST ..... 112



## TABLE OF SYMBOLS

$b, c, l$	chord or 1/2 chord, as defined
$C_L$	lift coefficient
$C_{L\alpha}$	lift curve slope
$C_D$	drag coefficient
$\bar{D}$	time averaged drag over one cycle of motion
$D$	drag force
$h_0$	plunge amplitude
$i$	denotes complex number: $\sqrt{-1}$
$l_L$	imaginary part of lift coefficient
$l_M$	imaginary part of moment coefficient
$\text{Im}(x)$	imaginary part of $x$
$k$	reduced frequency
$L$	lift force
$L_i$	imaginary part of lift
$L_R$	real part of lift
$M$	moment
$N$	normal force
$P$	power
$q$	dynamic pressure

$\text{Re}(x)$	real part of $x$
$R_L$	real part of lift coefficient
$R_M$	real part of moment coefficient
$T_s$	suction force
$t^*$	nondimensional time
$U, v$	freestream velocity
$\bar{W}$	time averaged work over one cycle of motion
$\alpha, \text{AOA}$	angle-of-attack
$\alpha_0$	pitch amplitude
$\Delta\alpha$	change in angle-of-attack
$\eta$	efficiency
$\rho$	density
$\phi$	phase angle between force and motion
$\omega$	frequency of harmonic oscillation

## **ACKNOWLEDGEMENTS**

The research for this thesis was conducted using the facilities of the Department of Aeronautics and Astronautics at the Naval Postgraduate School. I would like to give my sincere appreciation to professors M. F. Platzer and S. K. Hebbar, my thesis advisor and co-advisor, for their guidance, encouragement and many hours of council that led to the completion of this work.

I would also like to thank the professional staff of the Department of Aeronautics and Astronautics, in particular Mr. Tony Cricelli for helping me through his gifted knowledge of the different computers in the department. Furthermore, the timely and precise technical assistance provided by Mr. John Molton, Mr. Ronald Ramaker, and Mr. Don Meeks made the experimental research a success.

Finally, I would like to thank my lovely wife, Patricia, for her encouragement and support during my entire time here at the Naval Postgraduate School.

## **I. INTRODUCTION**

### **A. GENERAL**

In this thesis, several numerical methods were used to analyze the flow about one and two airfoils performing unsteady motion in an inviscid, incompressible fluid. First, the unsteady motion for a single airfoil was studied using the unsteady panel code, U2DIIF, by Teng [Ref. 1]. The primary purpose was to verify the phase lag relationships between the airfoil's motion and the build up of aerodynamic forces. To accomplish this, the time dependent output of the panel code was converted to harmonic output using a curve-fit algorithm. Furthermore, an extensive study on the production of thrust and associated efficiency for oscillating airfoils was completed using the U2DIIF code. Finally, a theory was presented that related quasi-steady ramp motion to a purely steady state phenomenon.

Next, the vortex interaction between two airfoils was studied using a computer code, USPOTF2, developed by Pang [Ref. 12] for unsteady incompressible flow. Extensive modifications were made to increase the program capabilities. Comparisons were made to flat plate, linear theory using the modified code. Again, an analysis of the propulsive forces and efficiencies associated with two airfoils was completed using the modified code and a similar curve-fit algorithm developed to convert the time dependent output to

harmonic output. This led up to a systematic study involving the influence of an oscillating airfoil in the vicinity of a stationary airfoil.

Finally, smoke flow visualization experiments were conducted using the available facilities located at the Naval Postgraduate School. These experiments were undertaken in an attempt to verify the two-dimensional theory presented here on the production of thrust associated with an oscillating airfoil. Furthermore, a visualization experiment was conducted to better understand the influence of an oscillating airfoil in the vicinity of a stationary airfoil at high angle-of-attack.

## **B. SCOPE**

Chapter II contains the complete single airfoil, theoretical analysis using the panel code, U2DIIIF. This chapter begins with the development of harmonic motion, includes an extensive verification with existing two-dimensional, linear theory, and concludes with a presented quasi-steady theory. Chapter III describes the complete two-airfoil, theoretical analysis. The development of the modified version of USPOTF2A is shown along with a complete description of the changes. Again, this code is verified with existing two-dimensional, linear theory, and used in a systematic study of interacting airfoils. Chapter IV and V incorporate some details of the flow visualization experiments and selected flow visualization photos of the results for the thrust and enhanced

lift investigation, respectively. Chapter VI contains the conclusion and recommendations.

## **II. SINGLE AIRFOIL ANALYSIS**

### **A. HARMONIC MOTION**

#### **1. Introduction**

The study of two dimensional, unsteady, harmonic motion involves an airfoil undergoing sinusoidal pitch or plunge oscillations. As the airfoil performs this oscillation, a complex flow field develops as shown in Figure 2.1. As the airfoil increases its angle-of-attack, the pressure field around the airfoil changes. These changes create a disturbance in the boundary layer due to the presence of viscosity. This disturbance builds up on the airfoil surface as it travels to the trailing edge in the form of a vortex. The vortex then sheds into the medium with a circulation strength equal in magnitude to the increase in circulation about the airfoil, but opposite in direction. These disturbances are stored in the fluid because the shed vortices convect downstream at the local flow field velocity. The counter-rotating vortices induce a sinusoidal flow field which further changes the net lift. The result of this complex flow field is a time difference or delay in the airfoil's motion and the induced aerodynamic forces. This time difference is known as the phase lag,  $\psi$  [Ref. 1].

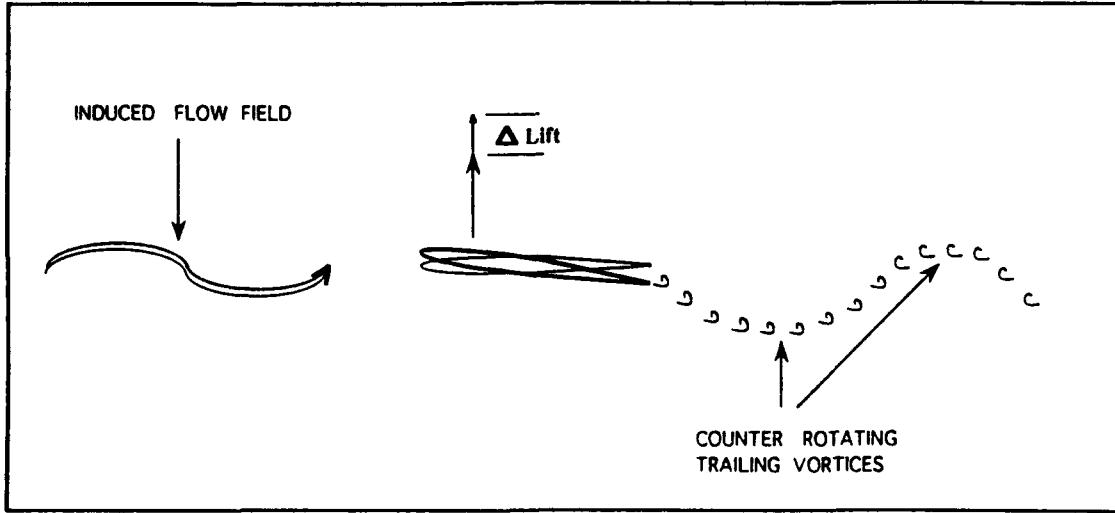


**Figure 2.1 Oscillating Flow Field**

To simplify the calculations for this type of motion it is common to describe the airfoil position and the associated aerodynamic forces with complex variables. For pure plunge oscillations the vertical motion of the airfoil is described by the real part of the following equation:

$$h(t) = h_0 e^{i\omega t} \quad (2.1)$$

where,  $h_0$  is a complex number, and  $\omega$  is the frequency of oscillation. Similarly, the lift or moment is described by:

$$L = L_0 r e^{i\omega t} \quad (2.2)$$

where,  $L_0$  is the theoretical quasi-steady lift given by the expression:

$$L_0 = \frac{1}{2} \rho U^2 S \frac{dC_L}{d\alpha} \frac{\dot{h}}{U} \quad (2.3)$$



This is termed quasi-steady because the angle of attack is represented by  $\dot{h}/U$ . The values of  $r$  and  $\psi$  represent the magnitude and phase, respectively, of the true instantaneous lift relative to the quasi-steady lift. The variables  $r$  and  $\psi$  in general depend on the reduced frequency  $k$ , the Mach number  $M$ , and the Reynolds number. For a nonviscous, incompressible fluid the values of  $r$  and  $\psi$  will be functions only of  $k$ . A complete solution for the oscillating flat-plate airfoil in incompressible flow has been obtained by Kussner and Theodorsen and is reproduced from reference 3 in Figure 2.2.

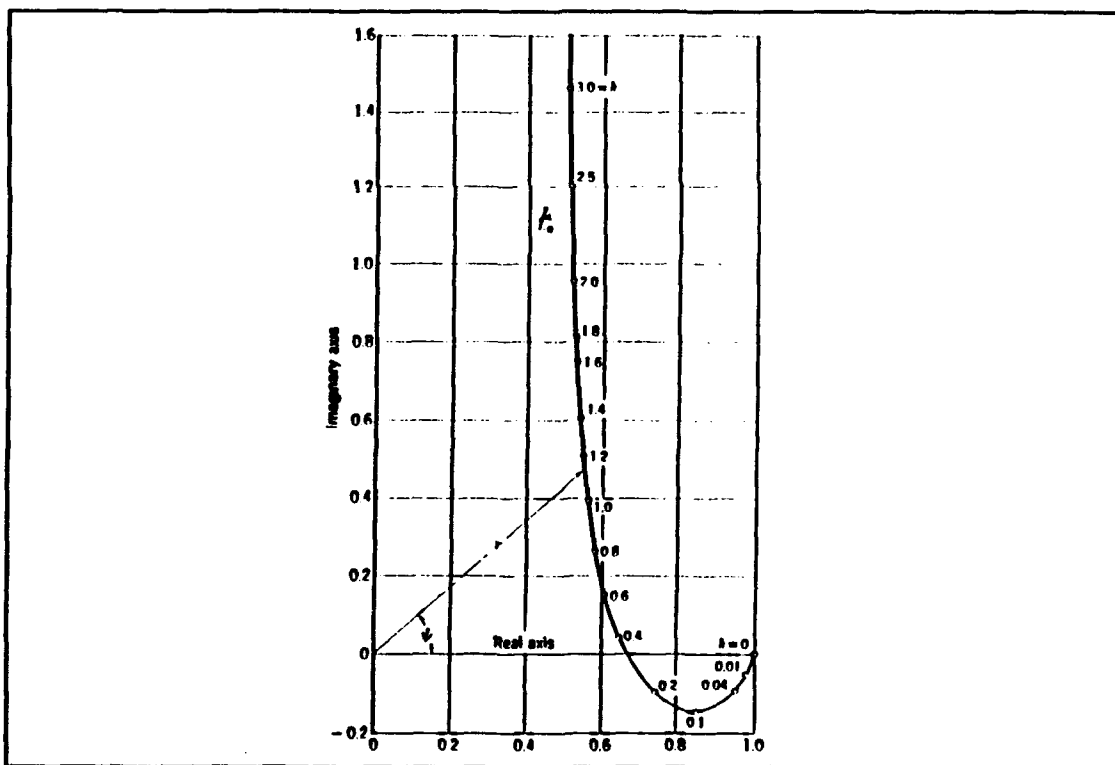


Figure 2.2. L/Lo diagram

Harmonic motion is usually characterized by non-dimensional variables. The amplitude for plunge motion is made non-dimensional by dividing by a reference length, usually the chord or half chord. Pitch amplitude is expressed in radians. The nondimensional frequency is termed the "reduced frequency" and is given by the following expression:

$$k = \frac{\omega b}{U} \quad (2.4)$$

where,  $\omega$  = frequency of oscillation,  $b$  = chord (or half-chord),  $U$  = free-stream velocity.

## 2. Panel Code U2DIIF

The computer code U2DIIF was developed by Teng [Ref. 2] for the study of unsteady, inviscid and incompressible flow over a single airfoil. The code was based on a technique called *Panel Methods* developed by Hess and Smith [Ref. 4] for steady potential flow problems. This method involves dividing the airfoil into many segments or panels. A uniform source and vorticity distribution is placed on each panel. In this code, the source strength is allowed to vary from panel to panel while the vorticity strength is held constant. This method is based on the fact that the singularity distributions automatically satisfy Laplace's equation, which is the governing equation for inviscid, incompressible flow. Furthermore, since the superposition principle applies to the Laplace equation, one can build complicated flow fields by a combination of simple flows. The unsteady potential flow model is based on

a method by Basu and Hancock [Ref. 5]. This unsteady model is governed by the Helmholtz vortex theorem which requires that any change in circulation around the airfoil must be matched by an equal and opposite change in vorticity in the wake. This is known as the vortex shedding process, which is modeled in this code by a vortex panel that is shed into the wake at each time step. The introduction of a wake model creates a non-linear, unsteady flow problem which is solved through an iterative process. No attempt is made here to reproduce the work by Teng or to explain the operation of the U2DIIF code, but instead the reader is encouraged to review reference 2. One limitation in the U2DIIF code which should be noted is the sensitivity to panel density and airfoil thickness. It can be shown that for thin airfoils of less than 8% thickness an increasing number of panels ( $< 50$ ) is required to accurately capture the leading edge suction peak. Furthermore, as the airfoil approaches a flat plate there is no amount of panels that will capture this peak. Although flat plates or NACA0001 airfoils are used in the following studies, it should be noted that the results of this code for airfoils of less than 5% thickness should be considered suspect unless it can be validated by other means.

The code was verified by comparing the time dependent output for harmonic motion to experimental results obtained by Giesing [Ref 6.]. In order to further verify the U2DIIF code and to present the results for harmonic motion in a more useful manner, a program was written to convert the time dependent output of lift and moment histories to harmonic output using an iterative, curve-

fit algorithm (appendix A). Figure 2.3 shows an example of the time dependent output, the curve fit solution, and the associated phase angles between the motion and the aerodynamic forces. In order to convert the time dependent data to harmonic output each run must proceed for at least two cycles. The first cycle is discarded because of the transient effects associated with going from steady state to unsteady motion as seen in Figure 2.3. The second cycle of data (lift and moment histories) is then curve-fitted to the following expression:

$$F(t) = Amp * Sin(\omega t + \phi) \quad (2.5)$$

where, **Amp** = amplitude of motion,  $\omega$  = frequency of motion, and  $\phi$  = phase angle between the motion and the aerodynamic forces.

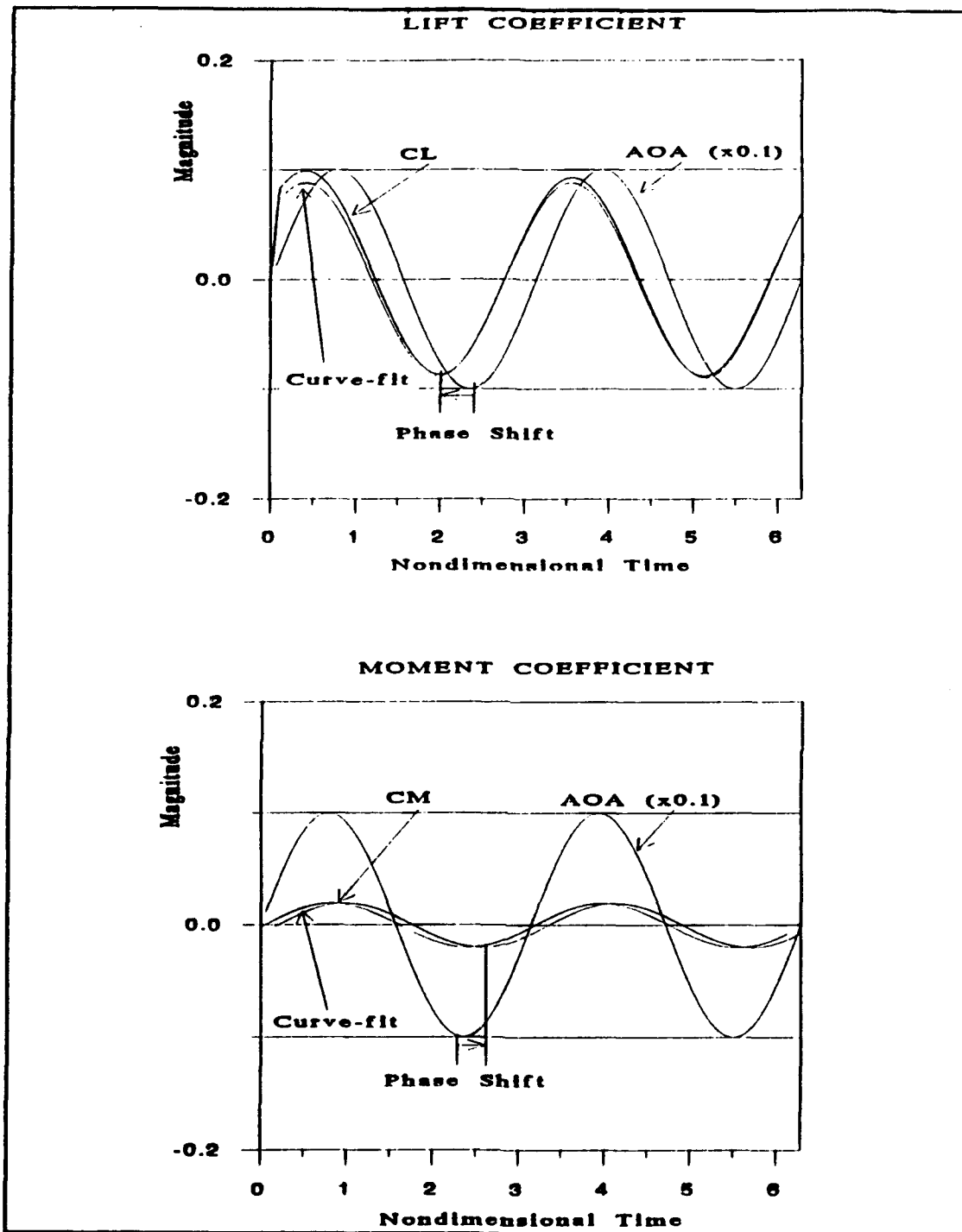


Figure 2.3 Sample Output. NACA0012 in pure pitch oscillations at a reduced frequency of 2, amplitude of  $1^\circ$ , for 2 cycles.

### 3. Comparison to Flat Plate Theory

Theoretical results for harmonic motion of a flat plate along with some experimental data were published by Halfman and reproduced in reference 7. The theoretical results for a flat plate oscillating in two degrees of freedom,  $h$  and  $\alpha$ , were used to compare the U2DIIF code with harmonic output. The expressions of aerodynamic force and moment corresponding to the harmonic motion given in reference 7 are, respectively:

$$\frac{L}{4qb} = \sqrt{R_L^2 + I_L^2} e^{i(\omega t + \phi_L)}, \quad \phi_L = \tan^{-1} \frac{I_L}{R_L} \quad (2.6)$$

$$\frac{M}{4qb^2} = \sqrt{R_M^2 + I_M^2} e^{i(\omega t + \phi_M)}, \quad \phi_M = \tan^{-1} \frac{I_M}{R_M} \quad (2.7)$$

Furthermore, the coordinate system used in the Halfman experiments was defined as positive lift acting down. A direct comparison of the U2DIIF harmonic output to these results was made by multiplying the U2DIIF output by 2 and adding  $180^\circ$  to the phase angle. This study was conducted with a panel density of 100 to accurately capture the suction peak for this very thin airfoil. The results are shown in Figures 2.4 through 2.7. It can be seen that there is very good agreement between the theoretical results and the U2DIIF code.

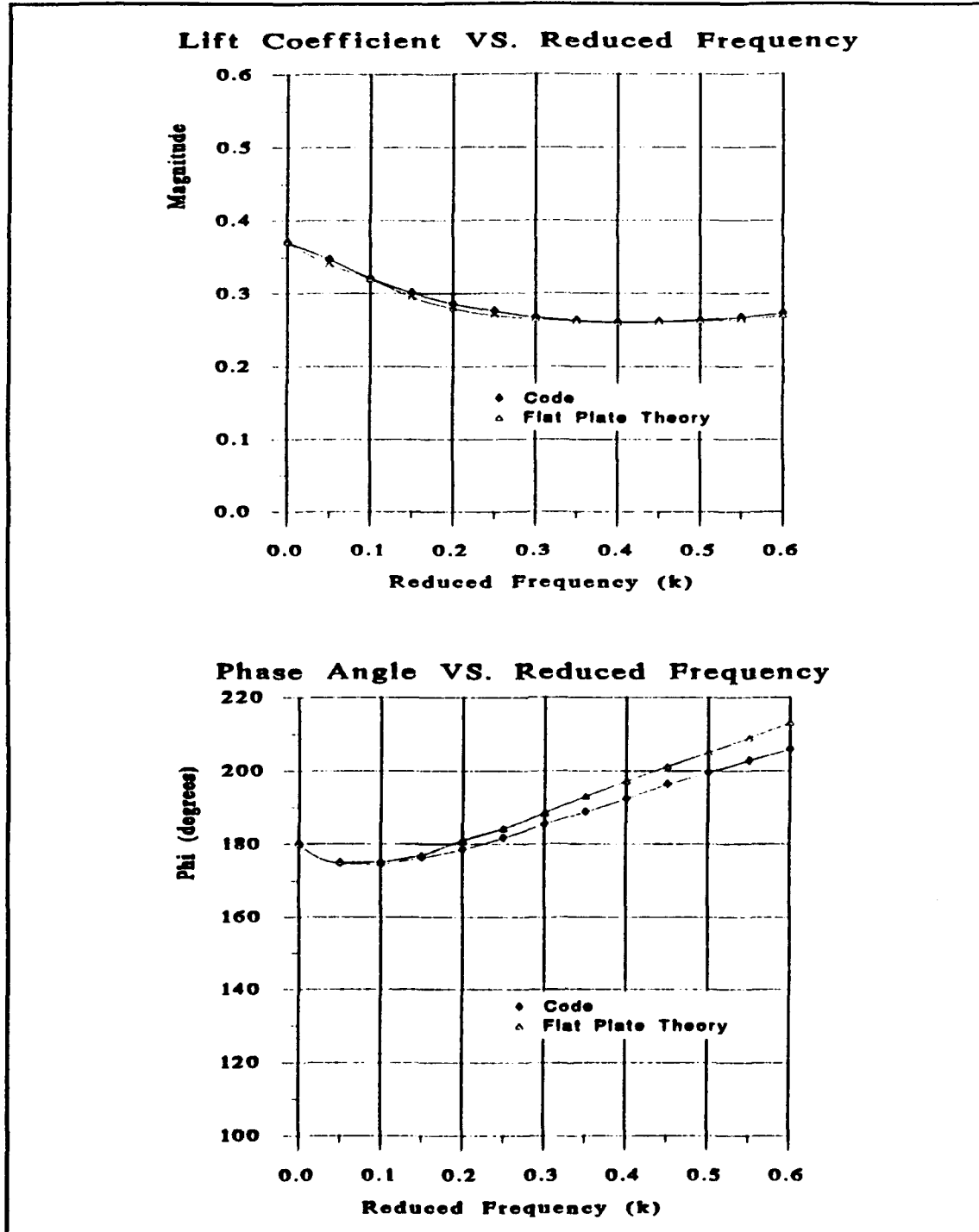


**Figure 2.4.** Lift magnitude and phase comparison for a flat plate pitching about .37c at an amplitude of 6.7°.

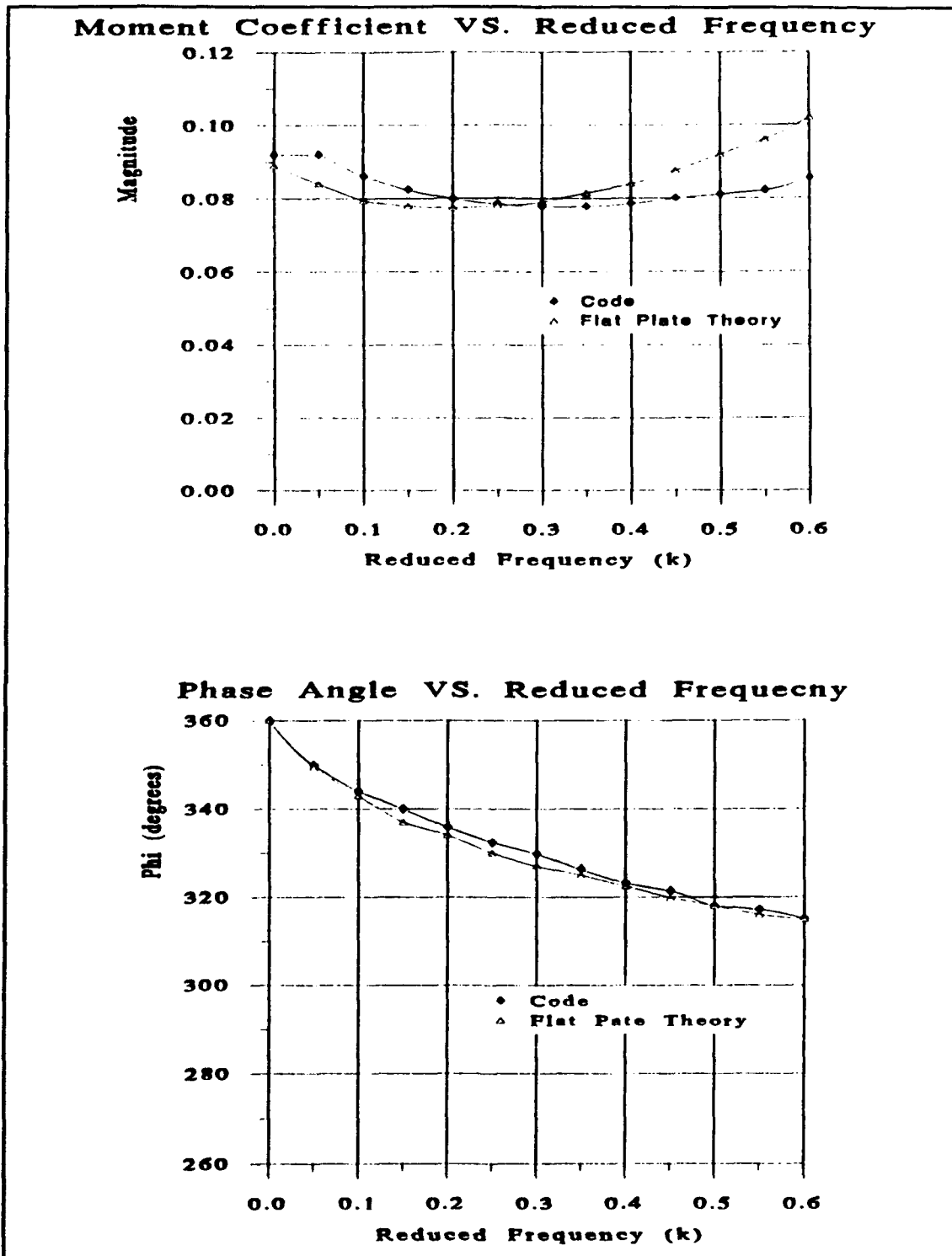


**Figure 2.5. Moment magnitude and phase comparison for a flat plate pitching about the .37c at an amplitude of 6.7°.**



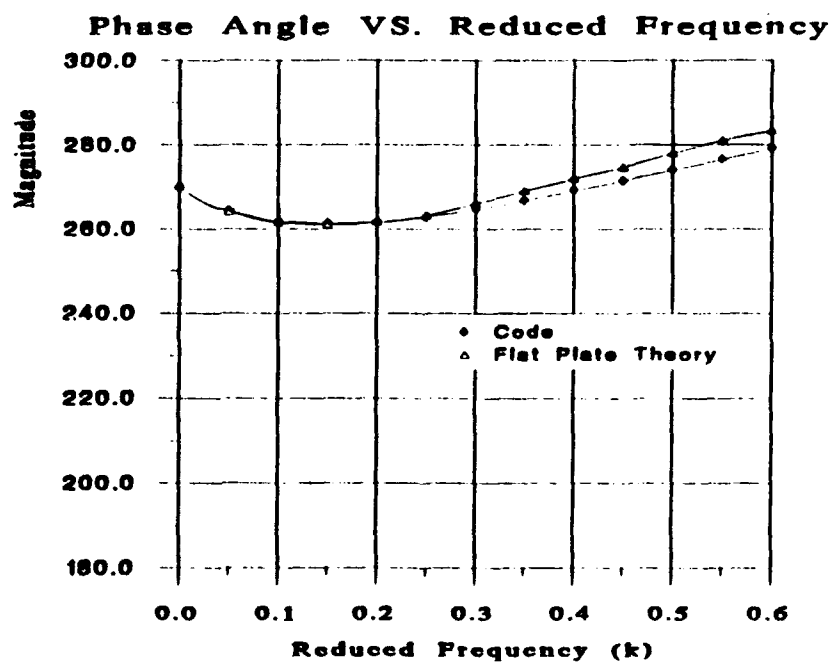
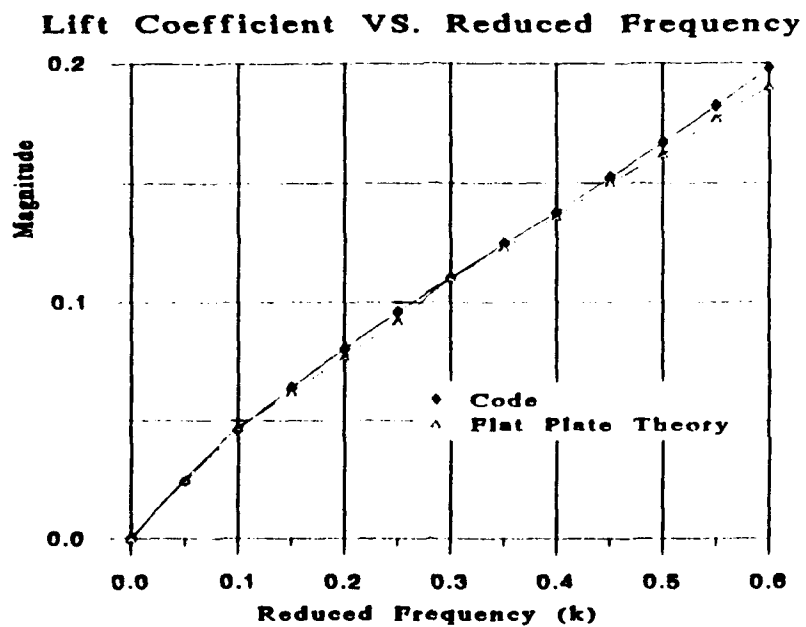
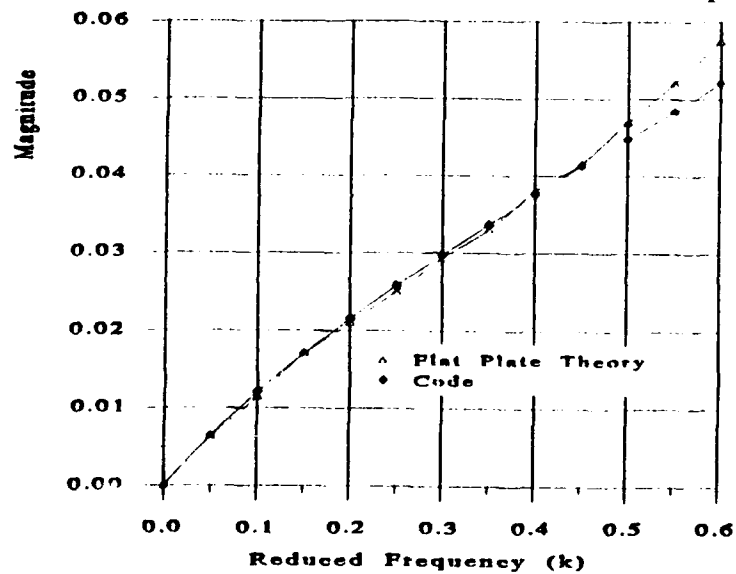


**Figure 2.6.** Lift magnitude and phase comparison for a flat plate in pure translation at a magnitude of .0833c.

Moment Coefficient VS. Reduced Frequency



Phase Angle VS. Reduced Frequency

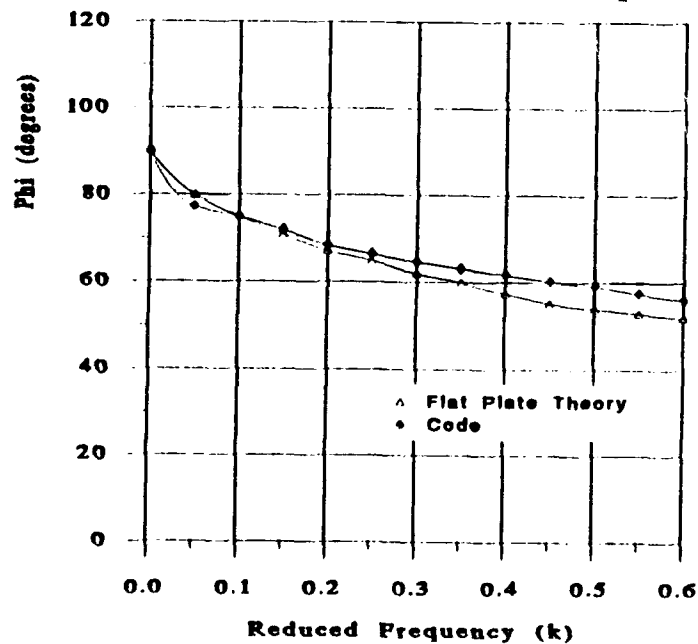


Figure 2.7. Moment magnitude and phase comparison for a flat plate in pure translation at an amplitude of .0833c.

## **B. PROPULSIVE EFFICIENCY**

### **1. Introduction**

Propulsion or thrust force from harmonically oscillating airfoils is a well known phenomenon. It has long been observed in nature from the low speed flapping of a bird's wing to the high speed flapping created by flying insects. The purpose of this study was to obtain the propulsive efficiencies associated with pure pitch and plunge harmonic motion using the nonlinear, unsteady panel code, U2DIIF. A comparison was made to the results obtained by Bosch [Ref. 8] for a flat plate undergoing harmonic motion. Bosch used a linear, analytical method to obtain the aerodynamic forces and propulsive efficiencies for a flat plate undergoing pure pitch and pure plunge harmonic motion.

The propulsive forces associated with an oscillating foil have been experimentally measured in reference 18. In this reference, Scherer measured the propulsive forces and moments associated with a rigid foil of finite span undergoing large amplitude pitching, and plunging oscillations in water. This work was undertaken for the preliminary design of an oscillating foil propulsor suitable for use on a shallow-draft boat, such as a 'ski-barge.' The results are expressed in coefficient form, and may be used in a comparative analysis with the theory presented here using the appropriate three-dimensional corrections. Sufficient time did not permit a detailed comparison in this paper.

## 2. Theory

In an inviscid, incompressible flow field propulsive forces develop over a harmonically oscillating airfoil. To better understand this process, Figure 2.8 shows the forces that develop on a harmonically plunging airfoil. It can be seen that when the airfoil is moving vertically up or down the motion creates an induced velocity component. The force that develops remains perpendicular to the relative velocity. This allows for a forward or thrust component of force while the vertical component changes sign. This is an over-simplified explanation of a complex flow field. The actual flow field that develops will depend on the type of motion, the frequency of oscillation, and the intricate system of shedding vortices that store the kinetic energy of the motion in the fluid.

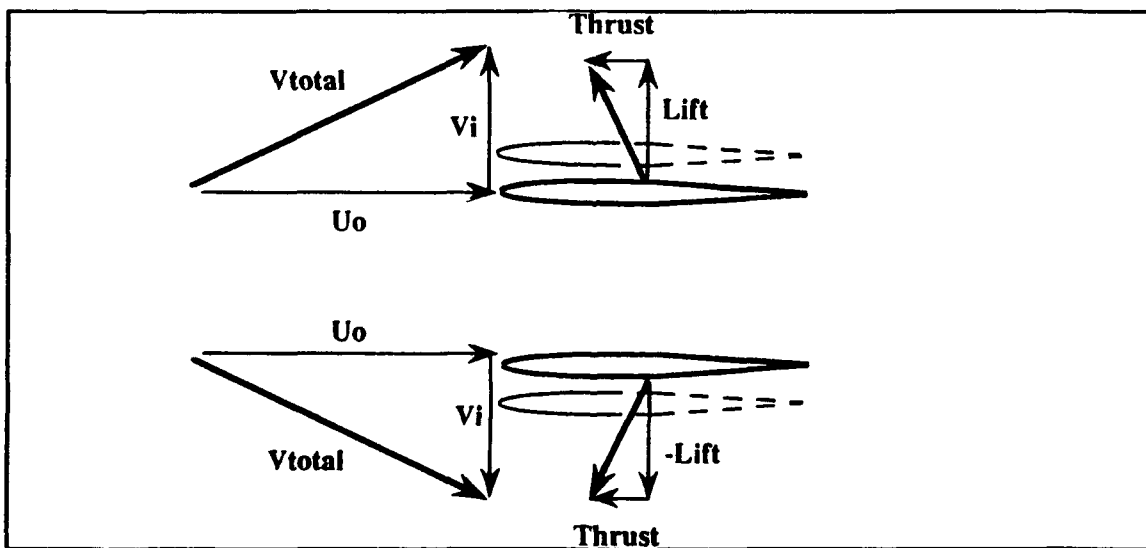


Figure 2.8. Propulsive force on plunging airfoil.

To understand how the mechanical energy of the motion is transferred to a propulsive force, it is necessary to develop the relationship for the required input work to the airfoil for both pitching and plunging motion. First, for a plunging airfoil the average work is defined as:

$$\overline{W} = \frac{1}{T} \int_0^T \text{Re}[L] * \text{Re}[\dot{h}] dt \quad (2.8)$$

$$h = h_0 e^{i\omega t}, \quad \dot{h} = i\omega h_0 e^{i\omega t}, \quad T = \frac{2\pi}{\omega} \quad (2.9)$$

The equation becomes,

$$\overline{W} = \frac{1}{T} \int_0^{\frac{2\pi}{\omega}} \text{Re}[(L_R + iL_I)] [\cos\omega t + i\sin\omega t] \text{Re}[i\omega h_0 (\cos\omega t + i\sin\omega t)] dt \quad (2.10)$$

After evaluation the equation reduces to,

$$\overline{W} = \frac{1}{T} \frac{\pi}{\omega} \omega h_0 L_I = \frac{\omega}{2} h_0 L_I \quad (2.11)$$

where, the imaginary lift and reduced frequency are given by,

$$L_I = \rho U^2 b \text{Im}(C_D) , \quad k = \frac{\omega b}{U} \quad (2.12)$$

Finally, the expression for average work reduces to,

$$\overline{W} = \frac{h_0}{b} \frac{\rho}{2} U^3 b k \text{Im}(C_D) \quad (2.13)$$

This equation for average work agrees with reference 8 if we set the value  $h_0/b = 1.0$ . This equation shows the important functional relationships between the input variables of plunge amplitude, reduced frequency, and generated lift to the output variable of average work. Furthermore, it shows that the average work is proportional to the reduced frequency and the imaginary or 'out-of-phase' component of lift.

The development for the relationship of average work for a pitching airfoil proceeds in a similar manner starting with the relation,

$$\overline{W} = \frac{1}{T} \int_0^T \text{Re}[M] * \text{Re}[\dot{\alpha}] dt \quad (2.14)$$

and the final result is,

$$\overline{W} = \alpha_0 \rho V^3 b k \text{Im}(C_M) \quad (2.15)$$

This result again matches the equation in reference 8 if we set the value of  $\alpha_0 = 1.0$  radian. This equation shows the functional relationship between the input variables of pitch amplitude, reduced frequency, and the imaginary component of moment with the output variable of average work.

A measure of the efficiency with which work input is transferred into propulsive power is given by the following expression,

$$\eta = \frac{\overline{D} \cdot v}{\overline{W}} \quad (2.16)$$

where,  $\eta$  = efficiency,  $\overline{D}$  = average drag or propulsive force,  $v$  = velocity.

This equation for efficiency is simply the drag (propulsive force) times the velocity divided by the expression for average work per unit time which is the average power output over average power required for the airfoil motion. It is clear the efficiency is primarily a function of the thrust that develops for a particular type of motion. Since the magnitude of thrust is proportional to the induced velocity ahead of the airfoil, the motion which provides the greatest induced velocity for the same work input will also provide the greatest thrust at the highest efficiency. The two types of motion studied in this paper are pitch, and plunge. Pitch motion induces a flow field in front of the airfoil that is proportional to the distance the pitch axis is from the airfoil. Furthermore, plunge motion can be thought of as pitch motion with the pitch axis at  $\infty$ .

This can be visualized as the motion of a fan blade with pitch motion similar to the blade hub, and plunge motion similar to the blade tip. Therefore, it should be no surprise that pure plunge motion provides more efficient propulsion than pure pitch.

### 3. Comparison to Flat Plate Theory.

Analytical results for a flat plate airfoil undergoing pure pitch and pure plunge motion for both propulsive force and efficiency were computed by Bosch in reference 8. To compare these results with the nonlinear code, U2DIIF, it was necessary to convert the efficiencies to aerodynamic forces. Furthermore, Bosch uses a reference length of  $b/2$  (1/2 chord length) where the U2DIIF code uses  $b$  (chord length) as the reference length. Also, Bosch defines the average drag as follows,

$$\bar{D} = \rho l v^2 \bar{C}_D \quad (2.17)$$

where  $l = 1/2$  chord. Combining equations 13, 15, and 17 into 16 gives the following relations:

$$\eta_{pitch} = \frac{\bar{C}_D}{k l m(C_M)} , \quad \eta_{plunge} = \frac{2 \bar{C}_D}{k l m(C_U)} \quad (2.18)$$

These equations for efficiency were used to compare the results obtained by Bosch. The U2DIIF code was executed at twice the reduced frequency as the one desired for comparison due to the different reference lengths.



In this study there were several problems associated with comparing analytical, linear results using a nonlinear code. First, the amplitudes used by Bosch:  $h/b = 1.0$ , and  $\alpha_0 = 1.0$  radian, (used for convenience) were well out of the linear range. For this reason much smaller amplitudes were used for the U2DIIF code:  $h/b = .05$ , and  $\alpha_0 = .0873$  radian, and the results were scaled appropriately. Scaling lift and moment results followed a linear relationship which implies that scaling the amplitude of motion by a factor results in scaling the forces up by the same factor. Drag follows a nonlinear relationship since drag is proportional to  $\alpha^2$ . Therefore, scaling the drag required multiplying the results from U2DIIF by the square of the scaling factor. After making all these conversions the U2DIIF harmonic output was compared to Bosch results in Figures 2.9 and 2.10 .

Excellent agreement is shown in plunge for both the drag coefficient, and the propulsive efficiency. This is not the case for pitch. Good agreement is shown for propulsive efficiency in pitch, but the drag coefficient does not agree well at the higher reduced frequencies. The reason for this is most likely the result of scaling errors. When small amplitudes are used for pitch motion the resulting drag coefficient magnitudes are very small  $\sim .005$ . This is near the same magnitude as the accuracy of the code. Therefore, the inherent error in the code is scaled with the coefficient of drag magnitude. Plunge drag coefficient data are an order of magnitude larger than pitch and do not have the same scaling problem.

## PLUNGE MOTION

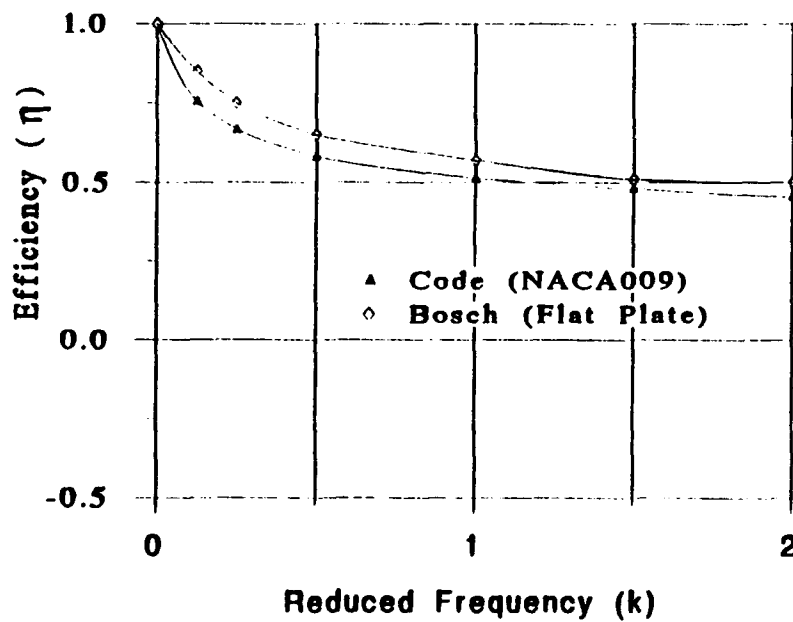
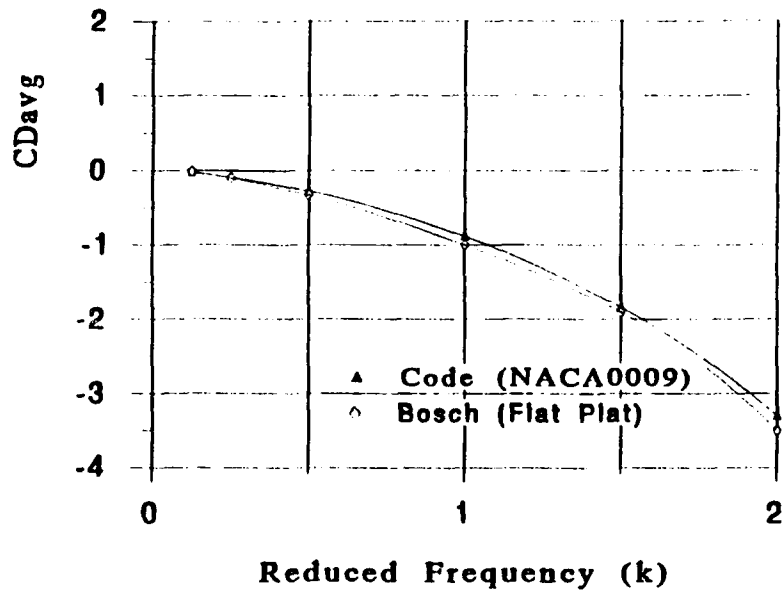


**Figure 2.9** Average drag and efficiency for a NACA0009 airfoil undergoing pure plunge oscillations at an amplitude of .05c. The results were scaled up to 1.0c (x100) for comparison to Bosch.

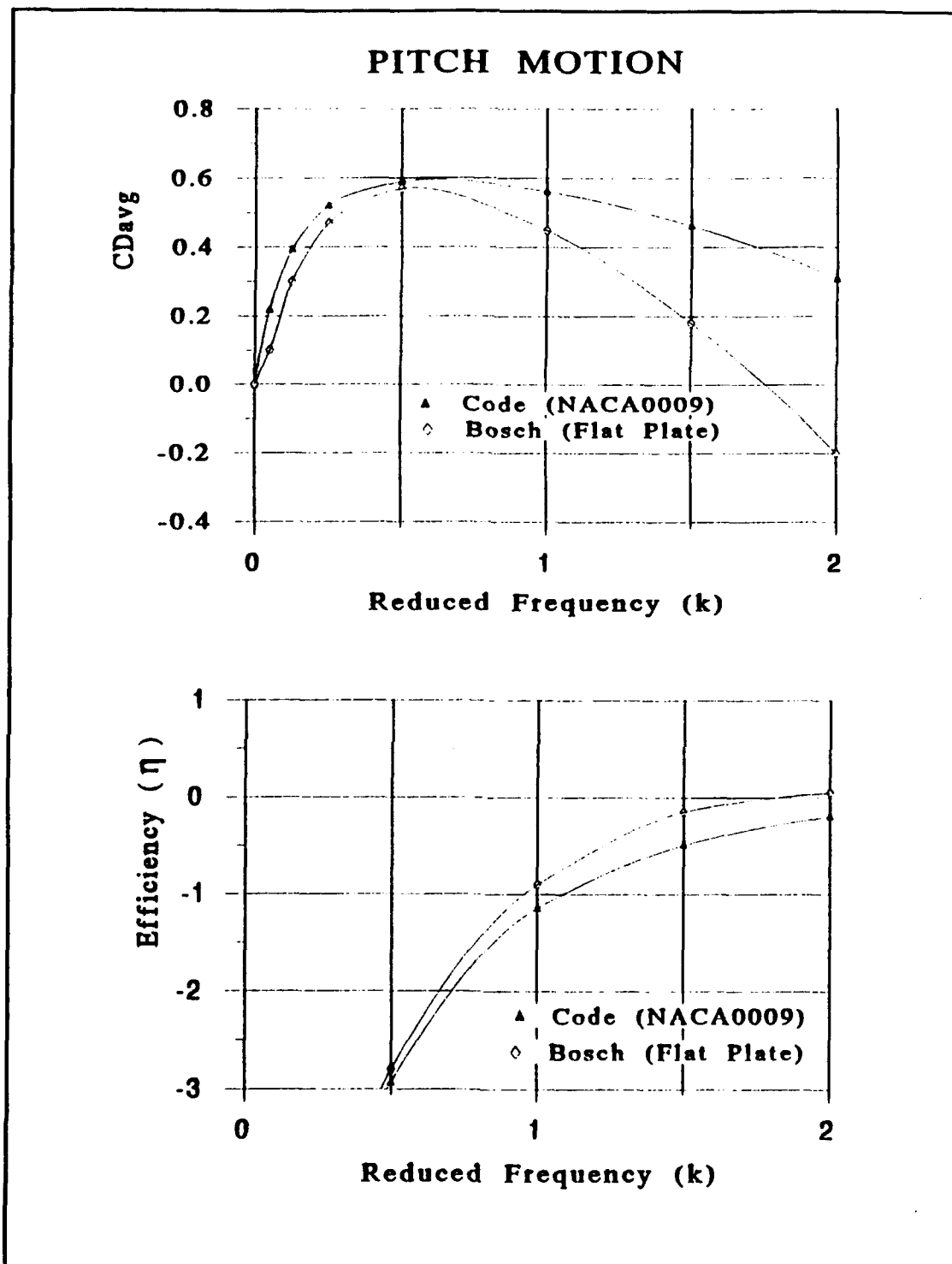


Figure 2.10 Drag and efficiency for a NACA0009 airfoil undergoing pure pitch oscillations at an amplitude of  $5.7^\circ$ . The results were scaled up to an amplitude of  $57^\circ$  ( $\times 100$ ) for comparison to Bosch.

#### 4. Power Extraction for Two Degrees of Freedom

When an airfoil undergoes both pitch and plunge motion it is oscillating with two degrees of freedom. For this condition it is possible for a phase relationship to exist between the two types of motion which results in a positive energy input into the airfoil. When this phase relationship exists energy is extracted from the airstream and transferred to the airfoil. This is the basic mechanism behind aerodynamic flutter. This may also be used as an efficient source of mechanical energy as described by McKinney and Delaurier; *The Wingmill: An Oscillating-Wing Windmill* [Ref. 9]. The objective of this study was to compare the results obtained from the U2DIIF code for power extracted from airfoil motion in two degrees of freedom to the experimental results obtained in reference 9. First, the U2DIIF code was modified to perform the following harmonic motion,

$$h = h_0 \sin(\omega t) , \quad \alpha = \alpha_0 \sin(\omega t + \phi) \quad (2.19)$$

where,  $\phi$  is the phase angle between plunging and pitching motions. Next, the equation for power extracted from the airstream is given by,

$$P = \dot{h}(N \cos \alpha + (T_s - D) \sin \alpha) + \dot{\alpha} M \quad (2.20)$$

where,  $N$  = normal force,  $D$  = drag,  $T_s$  = suction force, and  $M$  = moment about the pitch axis. Assuming small perturbations and noting the opposite signs of  $T_s$  and  $D$ , we can write,

$$(T_s - D)\sin\alpha < N\cos\alpha, \quad \text{Lift} \approx N \quad (2.21)$$

Therefore, the equation for power is reduced to,

$$P = L\dot{h} + M\dot{\alpha} \quad (2.22)$$

Equation 2.22 was used to obtain the power extracted during one cycle of motion. Experimental results are given in reference 9 for a wing undergoing the harmonic motion described in equation 2.19. The wing has a NACA0012 airfoil section and a rectangular planform of 20cm by 105cm. In the experiment  $h_0$  was kept constant at 6 cm, and  $\alpha_0$  was set to  $25^\circ$ . The reduced frequency was given to be .361 based on the half chord and the phase angle was set to  $90^\circ$ .

Figure 2.11 shows the airfoil motion for both angle-of-attack and translation as a function of time for one cycle. This plot shows the  $90^\circ$  phase difference between  $\alpha$  and  $h$ . Figure 2.12 shows the aerodynamic forces in newtons and the power extracted in watts obtained from reference 9 and the U2DIIF code. Numerically, the experimental results differ from what we obtained by a factor of 2 both in the aerodynamic forces and the power extraction. They obtained a peak normal force coefficient equal to .897, while we obtained a peak lift coefficient of 2. This difference is due to the three-dimensional effects associated with the experiment combined with our approximation of the normal force coefficient. In reference 9 a lift-curve slope of  $C_{L_\alpha} = 4.30/\text{rad}$  was used to correct the two-dimensional Theodorsen theory.

If we apply the same correction to the theoretical lift-curve slope of  $c_{l\alpha} = 2\pi$  used in U2DIIF along with the normal force correction, we obtain a normal force coefficient equal to 1.23. This is slightly greater than the results of reference 9. This is what we expected considering the low Reynolds number and added mass term used in the wind tunnel experiments which would tend to lower the results from theoretical predictions.

The power extraction curve followed the same trend as the aerodynamic forces, and again was off by a factor of 2. After applying the same corrections as above we obtain a peak power equal to 16.6 watts compared to the experimental value of 13.5 watts. It was encouraging to see the predictions from U2DIIF produce the same shape and phasing as the experimental results. Furthermore, we accurately predict positive work (power) over most of the cycle, as is expected for a phase angle of  $90^\circ$ .

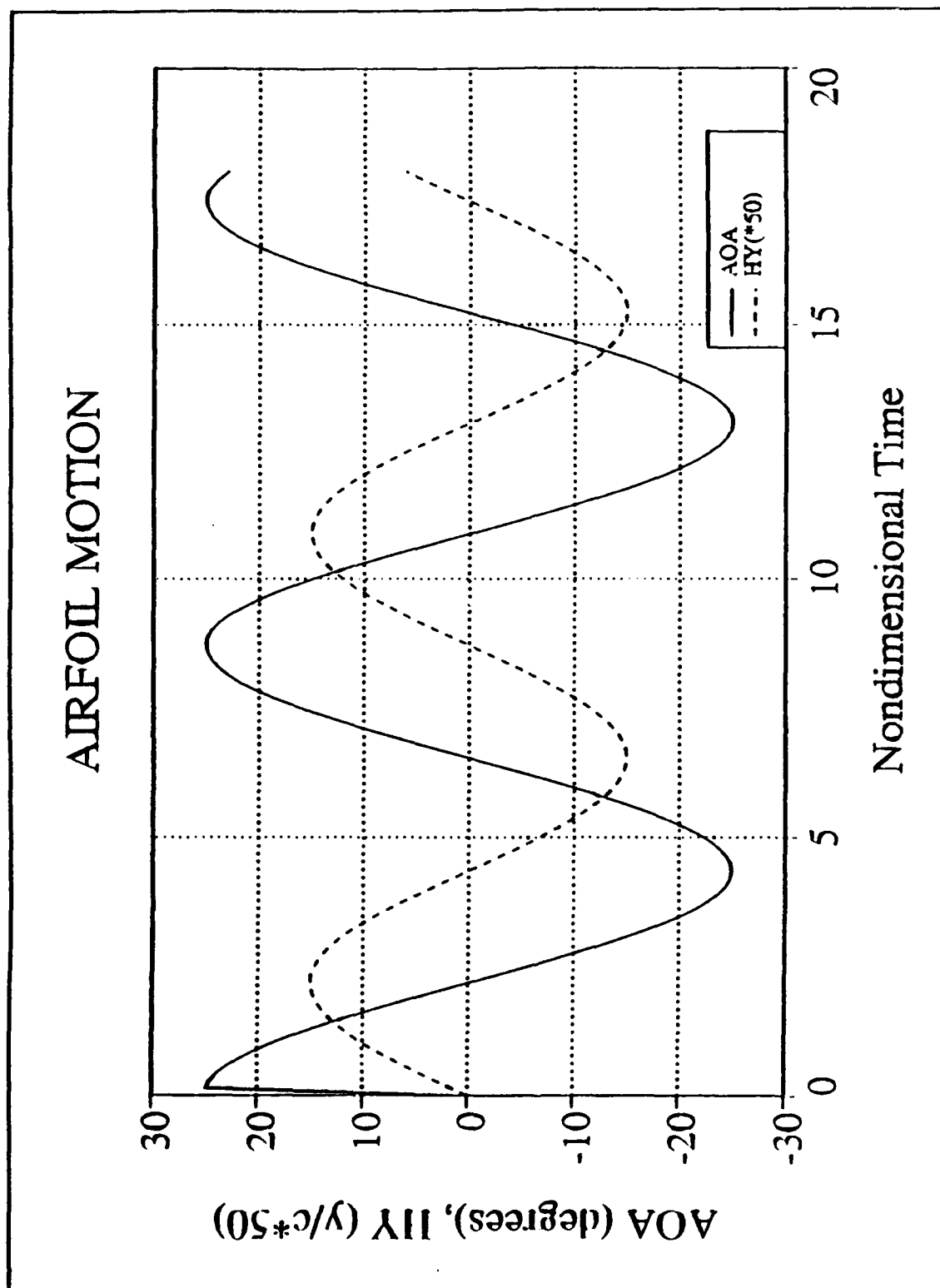
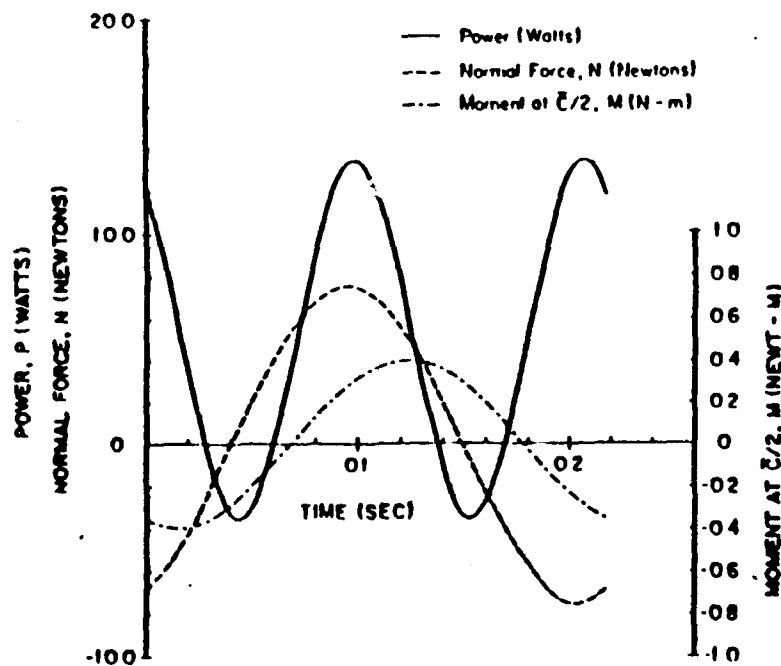


**Figure 2.11** Airfoil motion over two cycles for combined pitch and translation showing the 90 degree phasing between the two.



### POWER & AERODYNAMIC FORCES

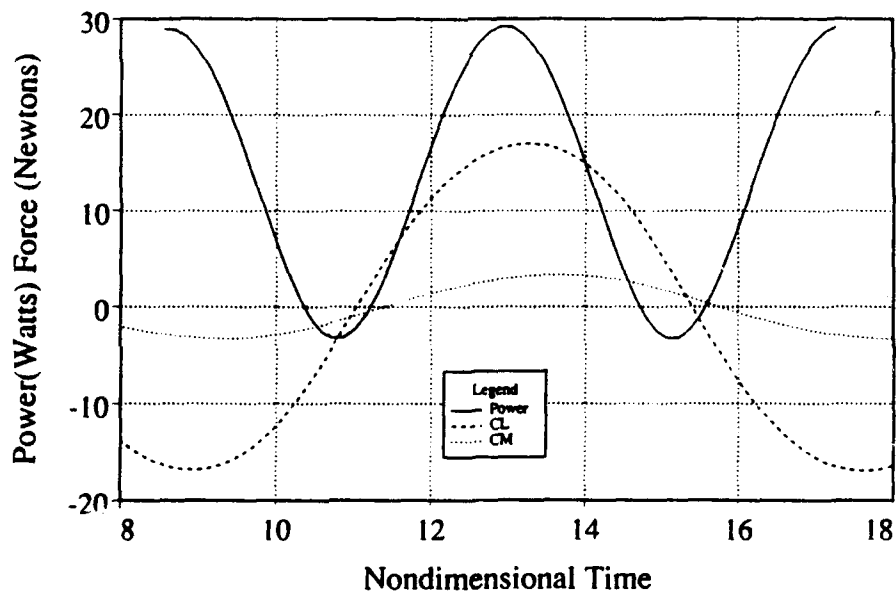


**Figure 2.12** The aerodynamic forces (newtons) and power extracted (watts) for both the results obtained by McKinney [Ref. 9] and the results from the U2DIIF code respectively.



## **C. UNSTEADY PRESSURE DISTRIBUTIONS**

### **1. Introduction**

The purpose of this study was to establish relationships between steady state pressure distributions and unsteady pressure distributions for a NACA0012 airfoil using the panel code U2DIIF. The study centered on finding an unsteady pressure distribution on the upper surface of an airfoil undergoing a ramp motion which would match a pressure distribution from the same airfoil at some steady state value. Once the relationship was developed between steady and unsteady pressure distributions, the results could be used as an input in a direct boundary layer code. This would give a quick and efficient method of determining unsteady boundary layer profiles and the onset of dynamic stall using a simple panel code coupled with a direct boundary layer code.

### **2. Theory**

The principal theory or hypothesis is that an airfoil undergoing a quasi-steady ramp motion can be analyzed as a steady-state process. The current thought process is that a ramp motion is a purely unsteady phenomenon which requires an unsteady analysis (ie. Navier Stokes) to determine the boundary layer and the onset of dynamic stall. In fact, as pointed out in reference 11, dynamic stall is strongly dependent upon airfoil geometry, Mach number, pitch rate, Reynolds number, state of the airfoil boundary layer, type of motion, etc.

Furthermore, the computation of unsteady, compressible flows can be a long and complicated process, even assuming the flow can be modeled appropriately. The next thought process is to assume that the boundary layer behaves in a quasi-steady fashion. This implies that the boundary layer reacts nearly instantaneously to the pressure distribution. More precisely, the boundary layer will react to the pressure gradients. The stronger the adverse pressure gradient the more likely the boundary layer tendency is to separate. To check this theory, a study was done in reference 10 where the unsteady pressure distribution for a particular motion was input into a steady direct boundary layer code. The direct boundary layer code can then accurately predict the onset of separation or flow reversal, although the code breaks down after separation due to the formulation of the direct boundary layer problem [Ref. 10]. The onset of separation for different pitch rates was compared to experimental results obtained by Chandrasekhara, Carr, and Ahmed at NASA Ames Research Center [Ref. 11]. This process covers all the variables stated above that influence dynamic stall with some limitations. First, the airfoil geometry, type of motion, and pitch rate are covered in the unsteady panel code. The effects of Reynolds number, and Mach number are covered in the direct boundary layer code because this code was modified to include the Prandtl-Glauert compressibility correction factor. The primary limitations in this analysis are that the three-dimensional effects are not considered, and at higher

pitch rates the flow becomes transonic making the compressibility correction less accurate.

Once it has been established that the boundary layer behaves in a quasi-steady fashion for certain flows, a relationship can be obtained that links the quasi-steady pressure distribution on the upper surface to a purely steady state pressure distribution. For this to be true we must assume that the entire flow field is quasi-steady. This requires keeping the ramp motion sufficiently slow to satisfy this assumption. When an airfoil moves in a quasi-steady ramp motion the pressure field will require a finite amount of time to react as explained in the first section. For this reason the pressure distribution on the upper surface of the ramping airfoil will match a steady state pressure distribution at some earlier AOA. The purpose of this study was to verify this hypothesis and to determine the relationship between steady and quasi-steady flow fields.

### **3. Description**

This study involved using the U2DIIIF code for NACA0012 airfoils undergoing a ramp motion at various rise times to determine the relationship between steady and quasi-steady flows. It was first necessary to determine the range of rise times for which the assumption of quasi-steady flow would hold true. The rise time is defined as the time required for the airfoil to ramp from the initial AOA to the final AOA. The rise time is expressed in

nondimensional units by Teng [Ref 2.] and is defined as the time required for a fluid particle to travel from the leading edge to the trailing edge,

$$t^* = \frac{tV_\infty}{c} \quad (2.23)$$

Since experimental results can normally be assumed quasi-steady due to mechanical limitations, the experimental results in reference 11 were used as a guide. In these experiments the ramp motion goes from 0 to 5° in 0.00167sec. The fluid particle takes 0.0005 sec to go from the leading edge to the trailing edge. Therefore, the nondimensional rise time is equal to 3.34. This is equivalent to a nondimensional pitch rate as defined in reference 11 of .027 units. Since this study involved ramp motions from 0 to 15°, rise times on the order of 10 units were considered quasi-steady.

The study involved running the U2DIIF code for a particular rise time. The pressure distribution output was then compared to the steady state pressure distribution for AOA's of 6, 8, and 10 degrees. The comparison continued until the best match was found between the unsteady pressure distribution and the steady state distribution. In order to compare the pressure gradients on the upper surface, the pressure distribution from the U2DIIF output was differentiated using a four point central difference scheme.

#### **4. Results**

Figures 2.13 and 2.14 show a typical comparison study of the pressure distributions and pressure gradients. The steady state distribution is

plotted for a particular AOA along with several unsteady distributions for different AOA's until a 'best' match is found. In this particular study the match for a  $10^\circ$  AOA steady distribution was found at the unsteady AOA of  $13.34^\circ$  for a relatively fast rise time of 3 units. Figure 2.15 shows the AOA and the aerodynamic forces as a function of time for this ramp motion. This important result verifies that there does exist an unsteady pressure distribution that will match a steady state pressure distribution on the upper surface.

One of the first results discovered in this study was that when the rise times were decreased from 10 to 3 units the best match became increasingly off. This was to be expected as the ramp motion increased to where the quasi-steady assumption would be invalid. It was found that rise times faster than 3 units would not match steady state pressure distributions. To show the trend, Figures 2.16 and 2.17 show the best match of a  $10^\circ$  AOA steady pressure distribution and the corresponding unsteady pressure distribution for a rise time of 10 and 3 units respectively. As can be seen, the match becomes progressively worse with the faster rise times.

The numerical results for this study are tabulated in Table 2.1. Certain trends can be observed from these results. First, the steady state lift coefficient at a particular AOA is always greater than the corresponding unsteady lift coefficient at the same AOA. This is consistent with Theodorsen theory. Next, the peak unsteady lift coefficient is always greater than its corresponding steady state value and increases with increasing pitch rate. This

is consistent with the increased maximum AOA and corresponding lift obtained from dynamic motion over steady state results as shown in reference 11.

The AOA for which a particular match was found also followed certain trends. First, the delta AOA at the smaller steady state angle-of-attack ( $6^\circ$ ) was almost independent of the rise time. This is equivalent to stating that it is independent of the pitch rate. A nominal value of two degrees was found between the unsteady and steady distributions for the smaller steady state AOA's. Next, the higher the steady state AOA, the more dependency on pitch rate was found. At  $10^\circ$  AOA steady the delta AOA went from 2.13 degrees for a rise time of 10 units to a delta AOA of 3.2 degrees at a rise time of 3 units.

When comparing this data to the experimental results of reference 11, it was not straight forward. The best we could do was compare the effects of pitch rate on the onset of separation. Reference 11 notes that when the pitch rate is doubled from .03 to .05 units the onset in separation is delayed by  $2^\circ$  (from  $14^\circ$  to  $16^\circ$ ). Although we do not compute separation, we can compare the delay in matching the steady state values at an AOA of  $14^\circ$  for the pitch rates used in reference 11. The results of this study are tabulated at the end of Table 2.1. As can be seen, we achieve the same delay of  $2^\circ$  when we double the pitch rate for a rise time of 14 to 7 units with a ramp change of  $20^\circ$ .

**TABLE 2.1** Results of unsteady to steady pressure distribution matching.

Steady AOA	Steady $C_L$	Unsteady AOA	Delta AOA	Unsteady $C_L$
<b>Rise Time = 10 units (0° - 15°)</b>				
6	.723	7.72	1.72	.835
8	.960	10.14	2.14	1.067
10	1.198	12.13	2.13	1.254
<b>Rise Time = 8 units (0° - 15°)</b>				
6	.723	7.78	1.78	.856
8	.960	10.12	2.12	1.07
10	1.198	12.33	2.33	1.26
<b>Rise Time = 6 units (0° - 15°)</b>				
6	.723	7.87	1.87	.902
8	.960	10.25	2.25	1.104
10	1.198	12.51	2.51	1.281
<b>Rise Time = 4 units (0° - 15°)</b>				
6	.723	7.9*	1.9	.999
8	.960	10.36*	2.36	1.18
10	1.198	12.82	2.82	1.32
<b>Rise Time = 3 units (0° - 15°)</b>				
6	.723	8.1**	2.1	1.11
8	.960	10.43*	2.43	1.26
10	1.198	13.2	3.2	1.35
<b>Rise Time = 14 units (0° - 20°)</b>				
14	1.67	16.1	2.1	
<b>Rise Time = 7 units (0° - 20°)</b>				
14	1.67	18.1	4.1	1.8

# Cp PLOT

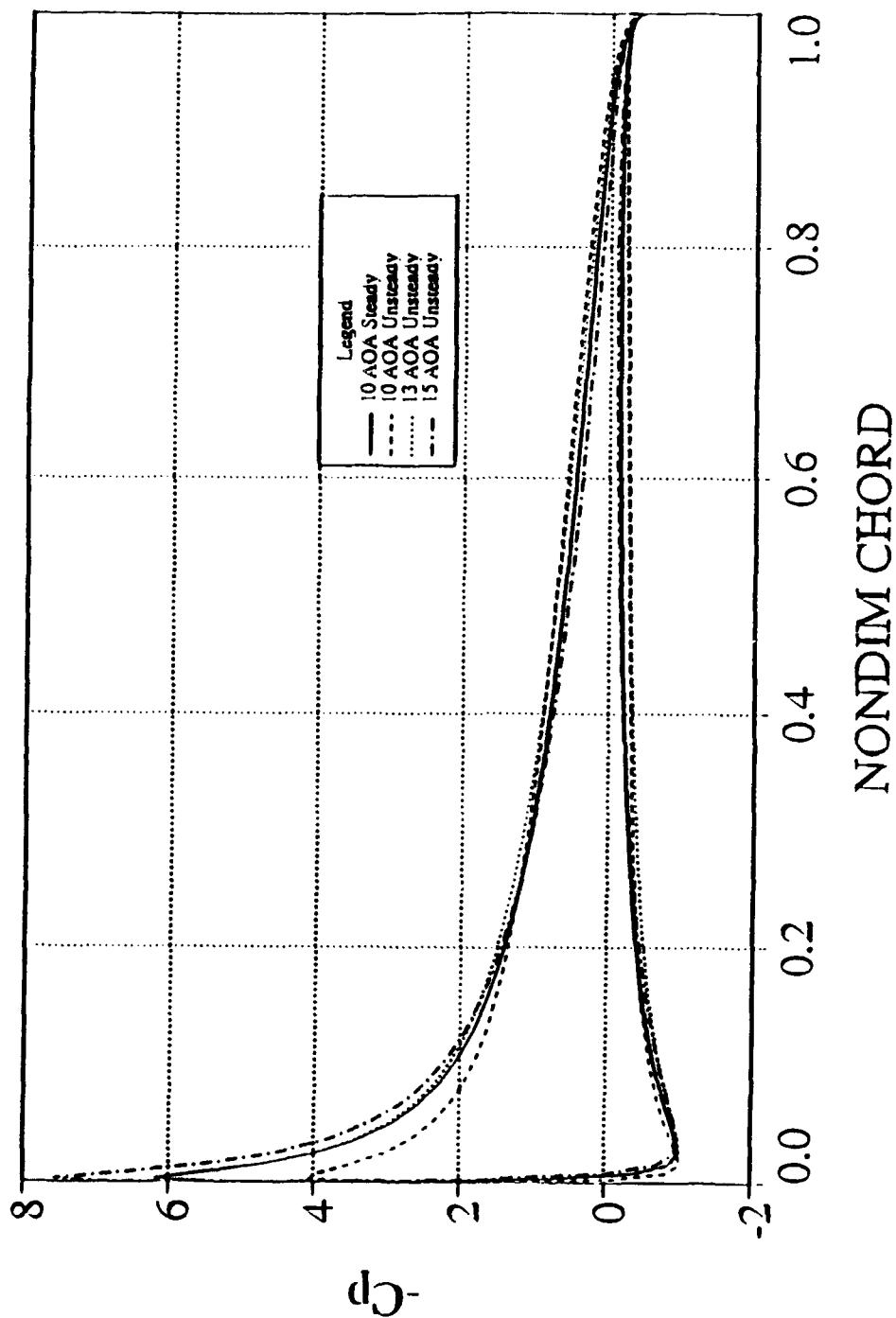
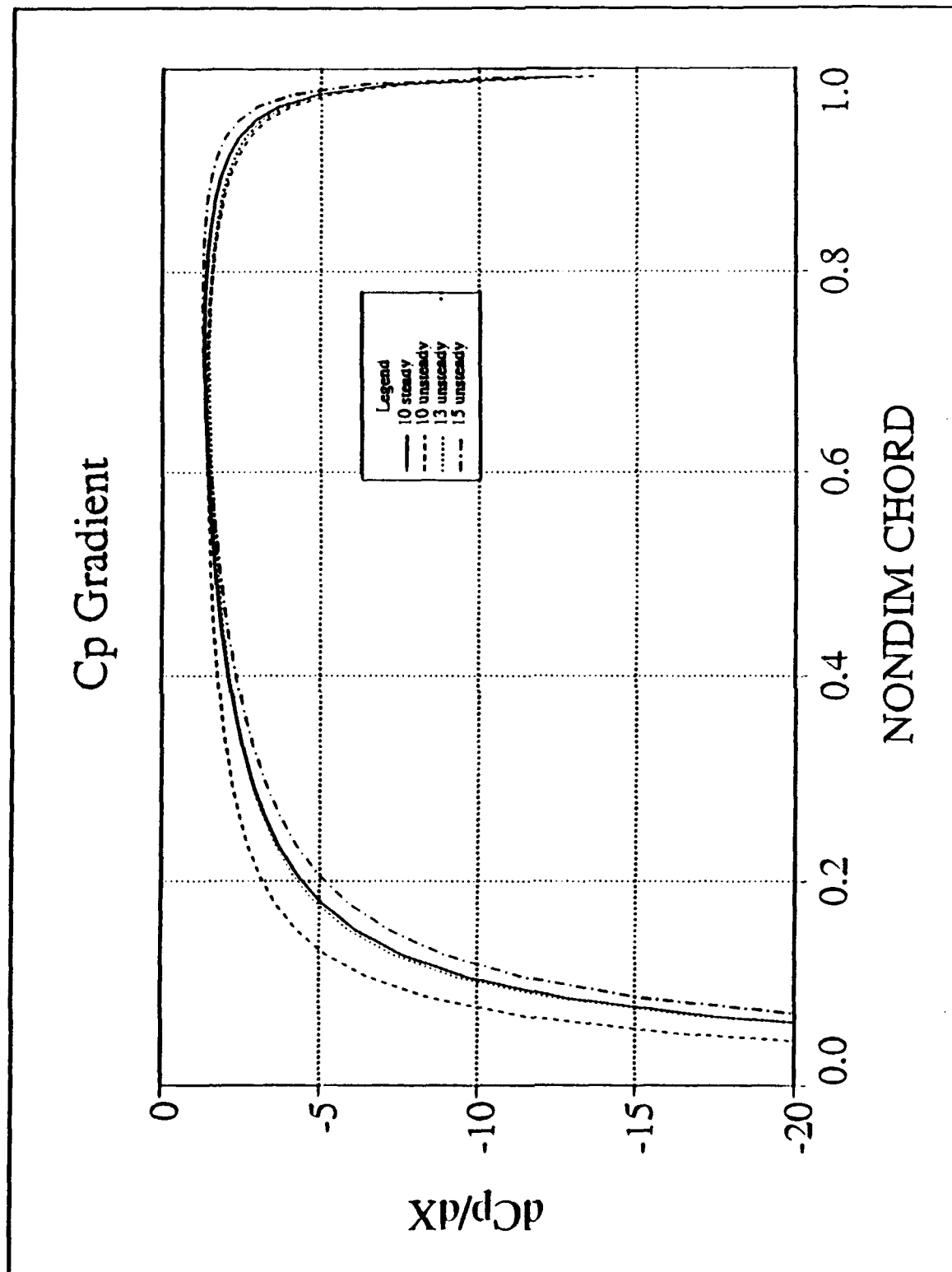
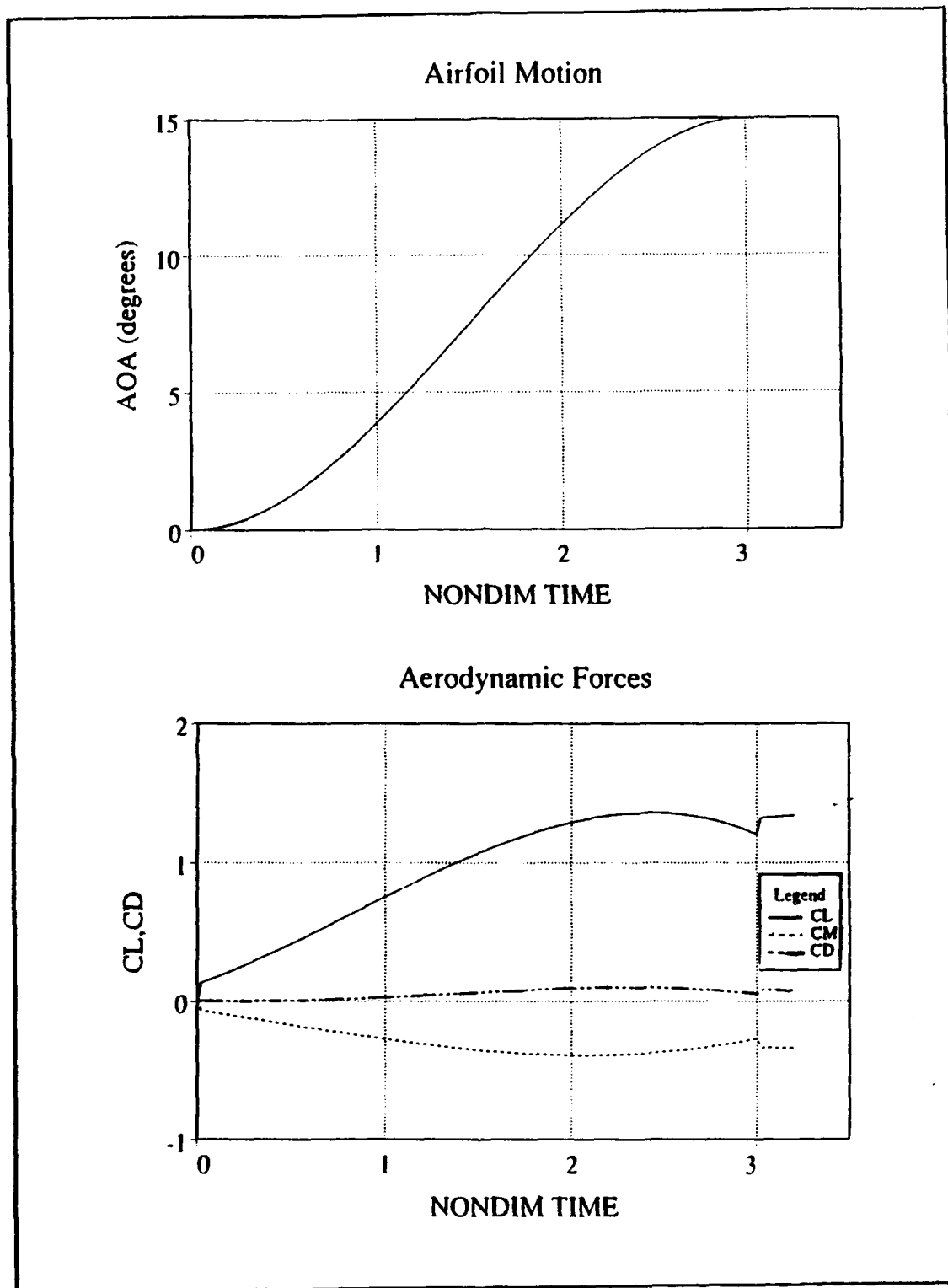


Figure 2.13 Pressure distribution match for a steady AOA of 10 degrees and a rise time of 3 units.





**Figure 2.14** Pressure gradient match for a steady AOA of 10 degrees and a rise time of 3 units.



**Figure 2.15** Airfoil motion and aerodynamic forces for a NACA0012 airfoil undergoing a ramp motion from 0 to 15° in a rise time of 3 units.

# Cp and Gradient Plot (rise time = 10 units)

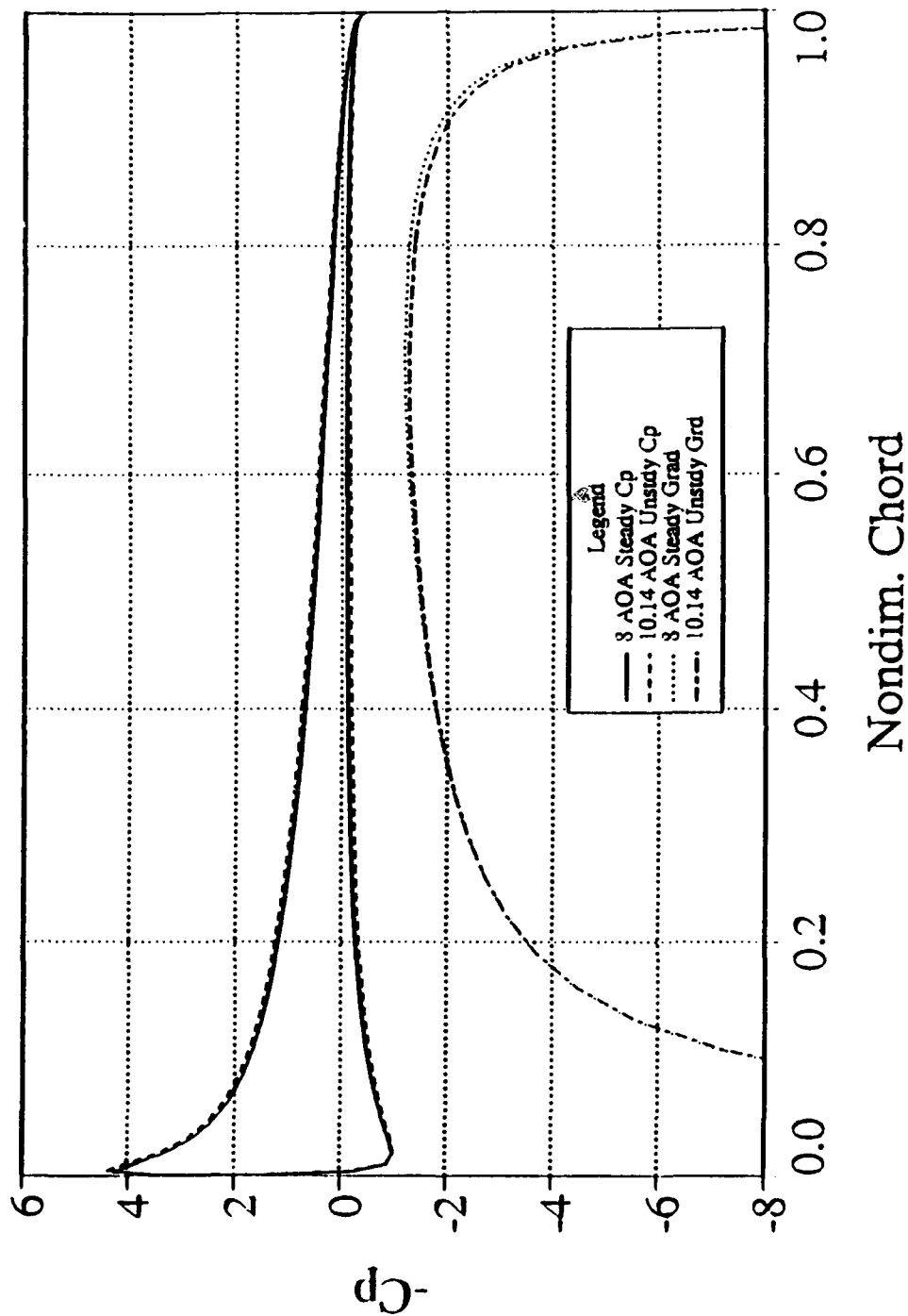


Figure 2.16 Pressure distribution match for a steady AOA of 8 degrees and a rise time of 10 units.

# Cp and Gradient Plot (rise time = 3 units)

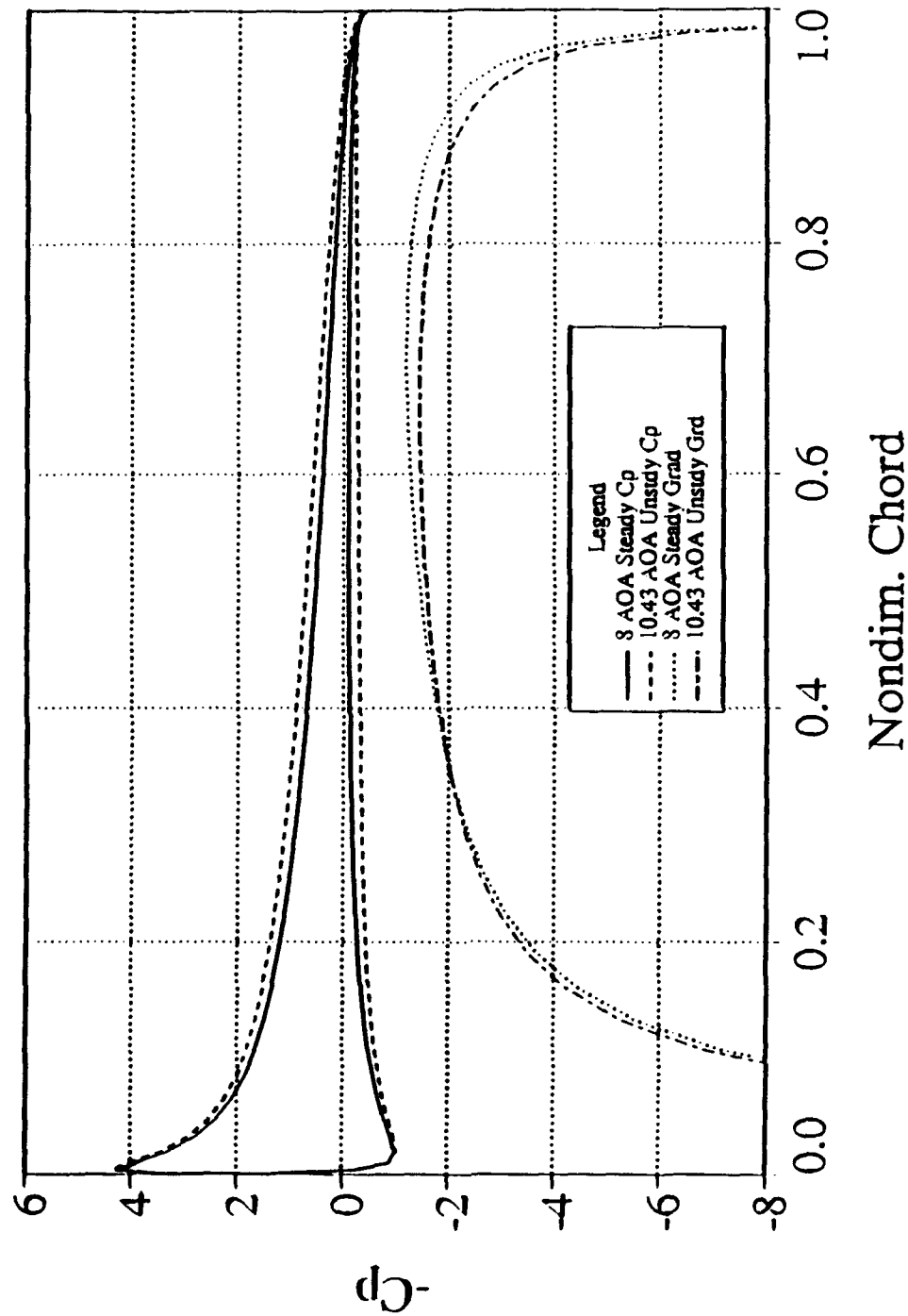


Figure 2.17 Pressure distribution match for a steady AOA of 8 degrees and a rise time of 3 units.

### **III. TWO AIRFOIL ANALYSIS**

#### **A. COMPUTER CODE USPOTF2**

The computer code written by Pang [Ref. 12] was the primary method used in the following studies of two airfoils undergoing harmonic motion. The computer code, USPOTF2, was written to solve the potential flow for two airfoils executing unsteady motions in an inviscid, incompressible flow medium. This code is an extension of the single airfoil code, U2DIIIF [Ref. 2], which uses the technique known as *Panel Methods* for steady flow and extends it to unsteady flow by introducing a wake model. This creates a non-linear problem due to the continuous shedding of vortices into the trailing wake. Furthermore, the presence of the second airfoil introduces a set of non-linear coupled equations for the Kutta condition. The solution requires an iterative procedure to compute the two vorticity strengths. Although no attempt is made here to reproduce the work by Pang, a general list of the modifications required to enhance the original code to a two-airfoil code is shown here. This will provide the reader with the necessary information to understand the modifications made by this author:

1. The establishment of five frames of reference: one fixed inertia frame of reference (global), two moving local frames of reference and two frozen local frames of reference.

2. Reformulation of the two Kutta conditions which are coupled non-linear.
  3. The creation of a new subroutine (NEWPOS) which transforms all coordinates in either of the two respective local frames of reference to the global frame of reference.
  4. The introduction of a more accurate method to obtain the velocity potential by integrating the velocity over smaller panels on the airfoil.
  5. Extension of the influence coefficient to include the effects of the second airfoil with its own peculiar wake. This also requires an introduction of an additional influence coefficient, that on the wake element due to the wake element from the other airfoil.
  6. The program is restricted to the following types of motion:
    - In-phase and out-of-phase Step Input
    - In-phase and out-of-phase Modified Ramp Input
    - In-phase and out-of-phase Translational Harmonic Oscillation
    - In-phase and out-of-phase Rotational Harmonic Oscillation
    - Sharp Edge Gust Field Penetration
1. **Modifications (USPOTF2A)**

***a. Program Output***

The code was originally written on the IBM mainframe at the Naval Postgraduate School. It has been transferred to the Stardent machine of the Department of Aeronautics and Astronautics. This allowed for increased storage capacity and a decrease in run times. For this reason, the total number of panels used to describe both airfoils has been increased from 200 to 400. The program was also transferred to the Iris workstation in the department. Although the program would compile on the workstation, this author could not

get the program to run on the Iris. It was believed to be a memory storage problem, but a thorough investigation was not completed. This program produces an extremely large amount of output to the screen. It is usually convenient on a Unix based machine to redirect screen output to a file during program runs. This file can get very large for long program runs, and may cause a problem in the temporary storage capacity. For this reason, the logical variable 'output' was added to the input file, FOR001.DAT. When this variable is set to *false*, most of the screen output will not be printed, thus reducing the size of the output file. Furthermore, the important output has been separated into different files for easier analysis, and is not affected by the variable output. The following list describes the input/output files and the data they contain:

1. FOR001.DAT: This is the input file (see Figure 3.1).
2. FOR002.DAT: This is for user supplied airfoil coordinates, if desired.
3. FOR003.DAT: This file contains the global coordinates of the first airfoil at each time step.
4. FOR004.DAT: This file contains the global coordinates of the second airfoil at each time step.
5. FOR007.DAT: This file contains the lift, drag, and moment coefficients for both airfoils at each time step.
6. FOR008.DAT: This file contains the pressure coefficients for the first airfoil at each time step.
7. FOR009.DAT: This file contains the pressure coefficients for the second airfoil at each time step.

8. FOR010.DAT: This file contains the first airfoil's core vortex (wake) positions at each time step.
9. FOR011.DAT: This file contains the second airfoil's core vortex (wake) positions at each time step.
10. FOR012.DAT: This file contains the AOA at each time step.
11. FOR013.DAT: This file contains the DHY (translational motion) at each time step.
12. FOR014.DAT: This file contains the required input for the Phase program.
13. FOR020.DAT: This file contains the computed average pressure coefficient for the first airfoil.
14. FOR021.DAT: This file contains the computed average pressure coefficient for the second airfoil.

***b. Program Corrections***

There were several errors noted in the original program and corrected. First, the code cannot be executed with only one airfoil as implied by the input variable NAIRF, or number of airfoils. Two airfoils must be defined to run the program. If single airfoil results are desired, one must position the second airfoil at a sufficient distance (approx. 30 chord lengths) away from the first airfoil to ensure no interference effects. This procedure was used to compare the USPOTF2 code against the single airfoil code, U2DIIF. At first, the results did not match. This was when an error in the subroutine Press was discovered and corrected. Now, if one selects NGIES equal to 0.0, which is the



unsteady Kutta condition of equal pressures at the trailing edge panels, the two codes produce the same results.

Next, an error in the convergence criteria was detected. Originally, the code would not reset the variable TOL, which is used by the code to set up the tolerance criteria for convergence. If, for a particular time step, the code required a higher tolerance to converge, the code would use this higher tolerance for follow-on time steps. This was corrected by resetting the variable TOL to its original value at the end of each time step.

The original code computes the moment coefficient about the leading edge. Although this is not an error, it is usually desirable to have the moment coefficient about the pitch axis. This change was made in the modified code.

### ***c. Airfoil Motion***

This was the largest modification made to this code. As stated earlier, the original code was restricted to in-phase and out-of-phase motion. The code was modified so the airfoils can move independently of each other. This was done by adding the following variables into the code: DALP2, TCON2, FREQ2, and PIVOT2. The entire logic for airfoil motion was rewritten to include the new variables which allowed the airfoils to move independently. Corrections for this modification were made as needed in the subroutines. Figure 3.1 shows a sample input file, FOR001.DAT, required for the modified version of USPOTF2. Figures 3.2 and 3.3 demonstrate some of the new

capabilities of the modified code. In Figure 3.2, the first airfoil is stationary at  $10^\circ$  AOA, while the second airfoil is oscillating in pure translation ( $DHY = .1$ ) at a reduced frequency of 2.0. The aerodynamic forces clearly show an influence of the second airfoil's oscillation (drag coefficient) on the first airfoil's lift coefficient. In Figure 3.3, both airfoils are oscillating in pure pitch ( $DALP = 10^\circ$ ), but at different reduced frequencies. The top airfoil is oscillating at a reduced frequency of 4.0, while the bottom airfoil is oscillating at a reduced frequency of 1.0. The aerodynamic forces are shown for 4 cycles of the top airfoil which is equivalent to 1 cycle of the bottom airfoil. The interaction of both airfoils can be seen in the aerodynamic forces with the stronger influence from the fast oscillating top airfoil.

Another modification was made in the original code to allow for different size airfoils to be analyzed at the same time. The original code nondimensionalizes both airfoil's chord length to 1.0. The code was modified to include a new variable SCALE. This variable scales the second airfoil by the amount specified as a percent of the first airfoil. Figure 3.4 demonstrates the capability of this added feature.

```

1      NUMBER OF LINES FOR TITLE
2      1
3      TWO NACA0012 OSCILLATING AIRFOILS
4
5      IFLAG  NLOWER  NUPPER
6      00,    30,    30
7      NAIRFO, XSHIFT, YSHIFT, SCALE
8      2,     1.2,   .0,   1.0
9      NACA AIRFOIL TYPE,
10     12,
11     12,
12     ALP1, ALP2, DALP1, DALP2, TCON1, TCON2,
13     0.0, 0.0, 15.0, 0.0, 1.0, 0.0,
14     FREQ1, FREQ2, PIVOT1, PIVOT2
15     0.0, 0.0, 0.0, 0.0,
16     UGUST, VGUST, DELHX1, DELHX2, DELHY1, DELHY2, PHASE1, PHASE2
17     0.0, 0.0, 0.0, 0.0, 0.0, 0.2, 0.0, 0.0,
18     TF, DTS, DTS2, TOL, TADJ, SCL, SCM, SGAM, NGIES
19     1.1, .005, 0.0, .0001, 0.0, 0.0, 0.0, 0.0, 0
20     STEADY OUTPUT
21     false, true
22
23     STEADY--TRUE IF ONLY STEADY SOLUTION. FALSE OTHERWISE.
24     OUTPUT--TRUE IF YOU WANT COMPLETE OUTPUT TO SCREEN.
25     IFLAG : 0 IF AIRFOIL IS NACA XXXX OR 730XX
26             1 OTHERWISE.
27     NLOWER : NO. OF PANELS USED ON BOTH AIRFOIL LOWER SURFACES.
28     NUPPER : NO. OF PANELS USED ON BOTH AIRFOIL UPPER SURFACES.
29     NAIRFO : NUMBER OF AIRFOILS.
30     XSHIFT : RELATIVE X DIST. FROM 2 AIRFOIL PIVOT POSITION WRT
31             GLOBAL COORDINATE SYSTEM.
32     YSHIFT : RELATIVE Y DIST. FROM 2 AIRFOIL PIVOT POSITION WRT
33             GLOBAL COORDINATED SYSTEM.
34     NACA AIRFOIL TYPE : ENTER NACA 4 OR 5 DIGIT CODE FOR AIRFOILS.,
35                       IF NOT A NACA AIRFOIL, SUPPLY AIRFOIL
36                       X(I),Y(I) COORDS. FOR BOTH AIRFOILS IN
37                       FILE CODE 2.
38     ALP1/2 : INITIAL ANGLE OF ATTACK FOR AIRFOILS IN DEGREES.
39     DALP1/2 : CHANGE IN AOA IN DEGREE FOR NON OSCILL. MOTION.
40             MAX AMPLITUDE OF AOA IN DEGREE FOR ROT. HARMONIC MOTION.
41     TCON1/2 : NON-DIMENSIONAL RISE TIME (Vinf,t/c) OF ACA FOR
42             MODIFIED RAMP CHANGE IN AOA.
43     FREQ1/2 : NON DIMENSIONAL OSCILL. (WC/Vinf.) FOR HARMONIC MOTIONS.
44     PIVOT1/2 : LENGTH FROM LEADING EDGE TO PIVOT POINT FOR LOCAL SYSTEM.
45             (THE GLOBAL SYSTEM'S ORIGIN IS THE FIRST AIRFOILS PIVOT POSITION)
46     UGUST : MAG. OF NON-DIM. GUST VELOCITY ALONG GLOBAL X DIRECTION.
47     VGUST : MAG. OF NON-DIM. GUST VELOCITY ALONG GLOBAL Y DIRECTION.
48     DELHX1/2 : NON-DIM. TRANSLATIONAL CHORDWISE AMPLITUDE.
49     DELHY1/2 : NON-DIM. TRANSLATIONAL TRANSVERSE AMPLITUDE (plunging).
50     PHASE1/2 : PHASE ANGLE IN DEGREE BETWEEN CHORDWISE AND TRANSVERSE
51             TRANSLATIONAL OSCILL. WITH THE LATTER REF. TO THAT AIRFOIL.
52     TF : FINAL NON-DIM. TIME TO TERMINATE UNSTEADY FLOW SOLUTION.
53     DTS : STARTING TIME STEP FOR NON-OSCILL MOTIONS(TADJ=0).
54             NO. OF COMPUTATIONAL STEPS PER CYCLE FOR HARMONIC MOTION
55             (FOR 2 FREQ OSCILL. IT USES THE LARGEST FREQ)
56             BASELINE TIME STEP FOR ALL MOTIONS(TADJ NOT =0)
57     DTS2 : STARTING NON-DIM TIME FOR SECOND AIRFOIL MOTION TO BEGIN.
58           (0 TO BEGIN MOTION AT THE SAME TIME).
59     TOL : TOLERANCE CRITERION FOR CONVERGENCE FOR (Uw)k and (Vw)k.
60     TADJ : FACTOR BY WHICH DTS WILL BE ADJUSTED.
61     SCL : STEADY LIFT COEFF. FOR THE SINGLE AIRFOIL AT THE SPEC. ACA.
62     SCM : STEADY MOMENT COEFF. FOR THE SINGLE AIRFOIL.
63     SGAM : STEADY VORTICITY STRENGTH FOR THE SINGLE AIRFOIL.
64     NGIES : OPTION TO CHANGE THE UNSTEADY KUTTA CONDITION.
65            0 EQUAL PRESSURE AT THE TRAILING EDGE PANELS.
66            1 EQUAL TANGENTIAL VELOCITIES AT THE TRAILING EDGE PANELS.

```

**Figure 3.1** Sample input file, FOR001.DAT, required for the modified version of USPOTF2.

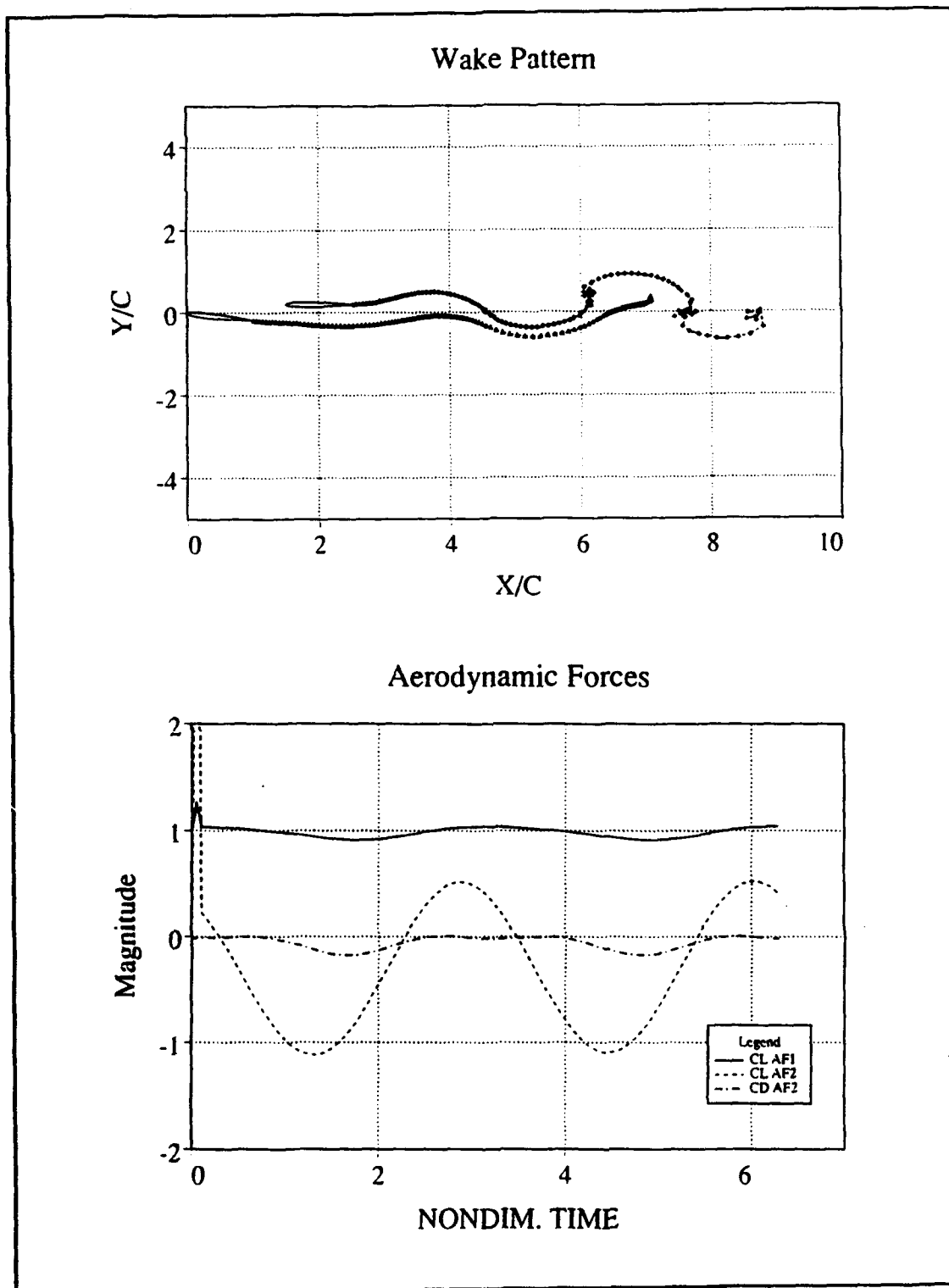


**Figure 3.2** Wake pattern and aerodynamic forces. AF1-10 deg steady, AF2-0 deg unsteady ( $DH Y = .1, k = 2$ )

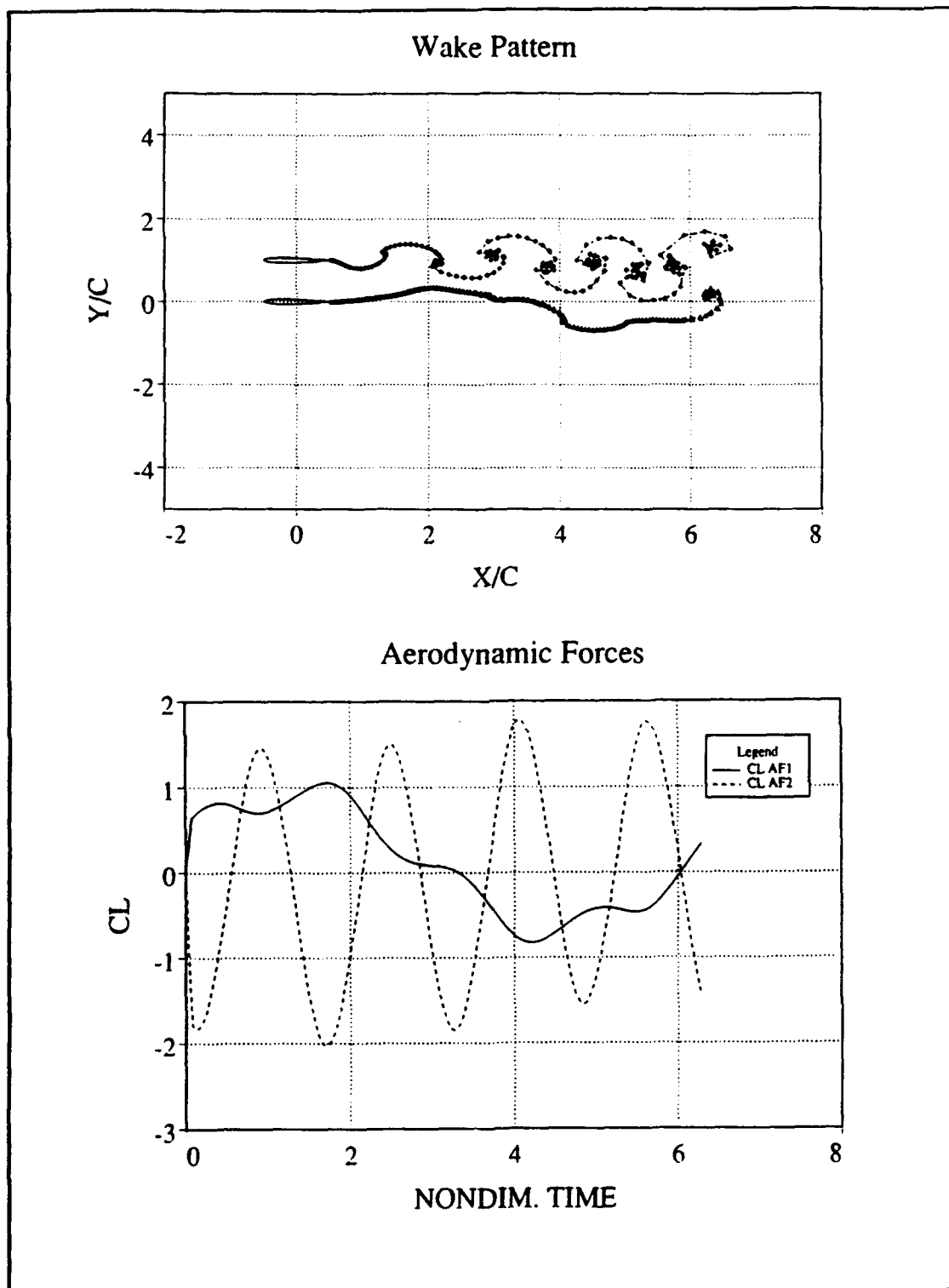


**Figure 3.3** Wake pattern and aerodynamic forces. AF1-unsteady (DALP = 10 deg,  $k = 1$ ), AF2-unsteady (DALP = 10 deg,  $k = 4$ ).

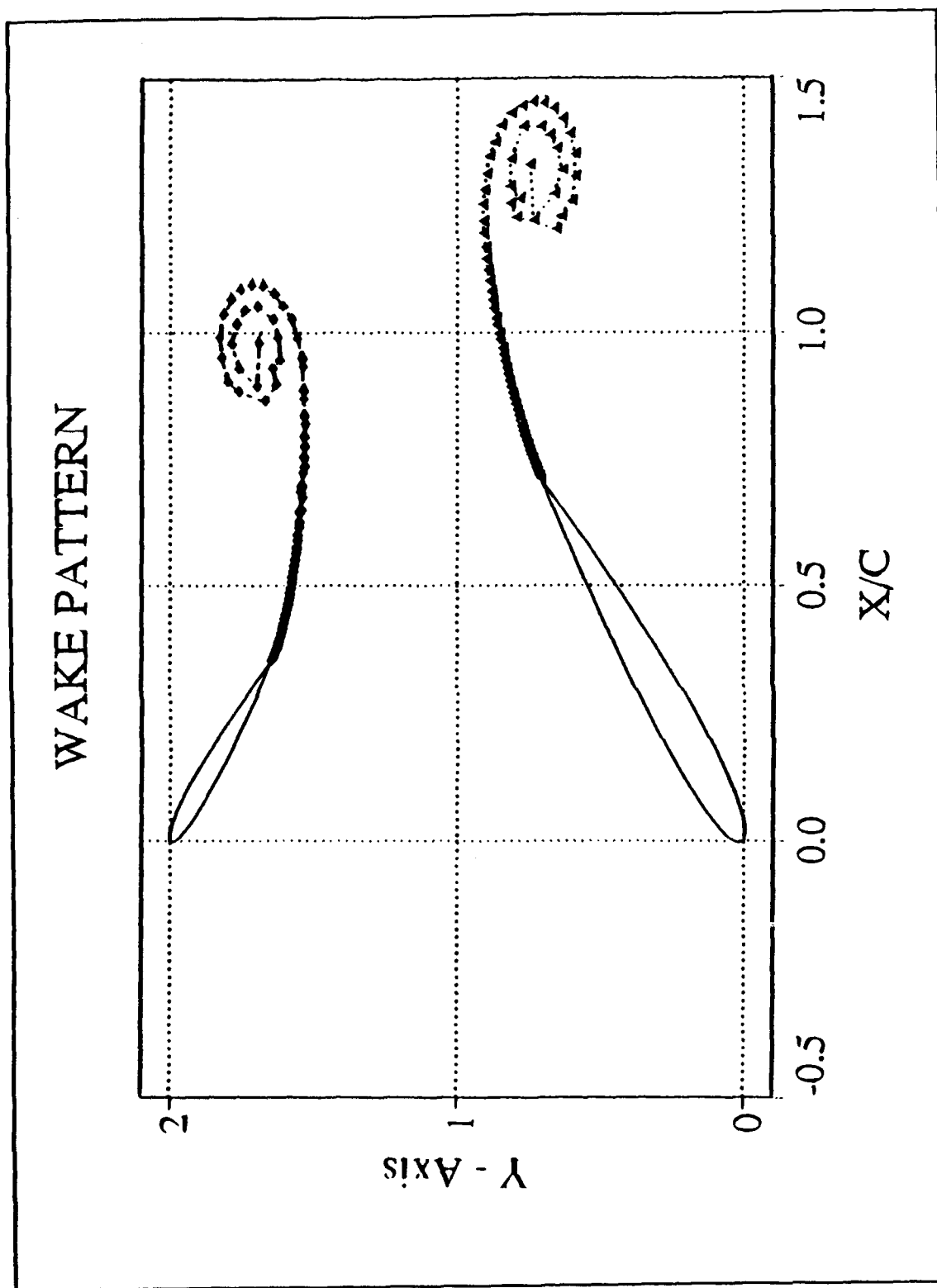
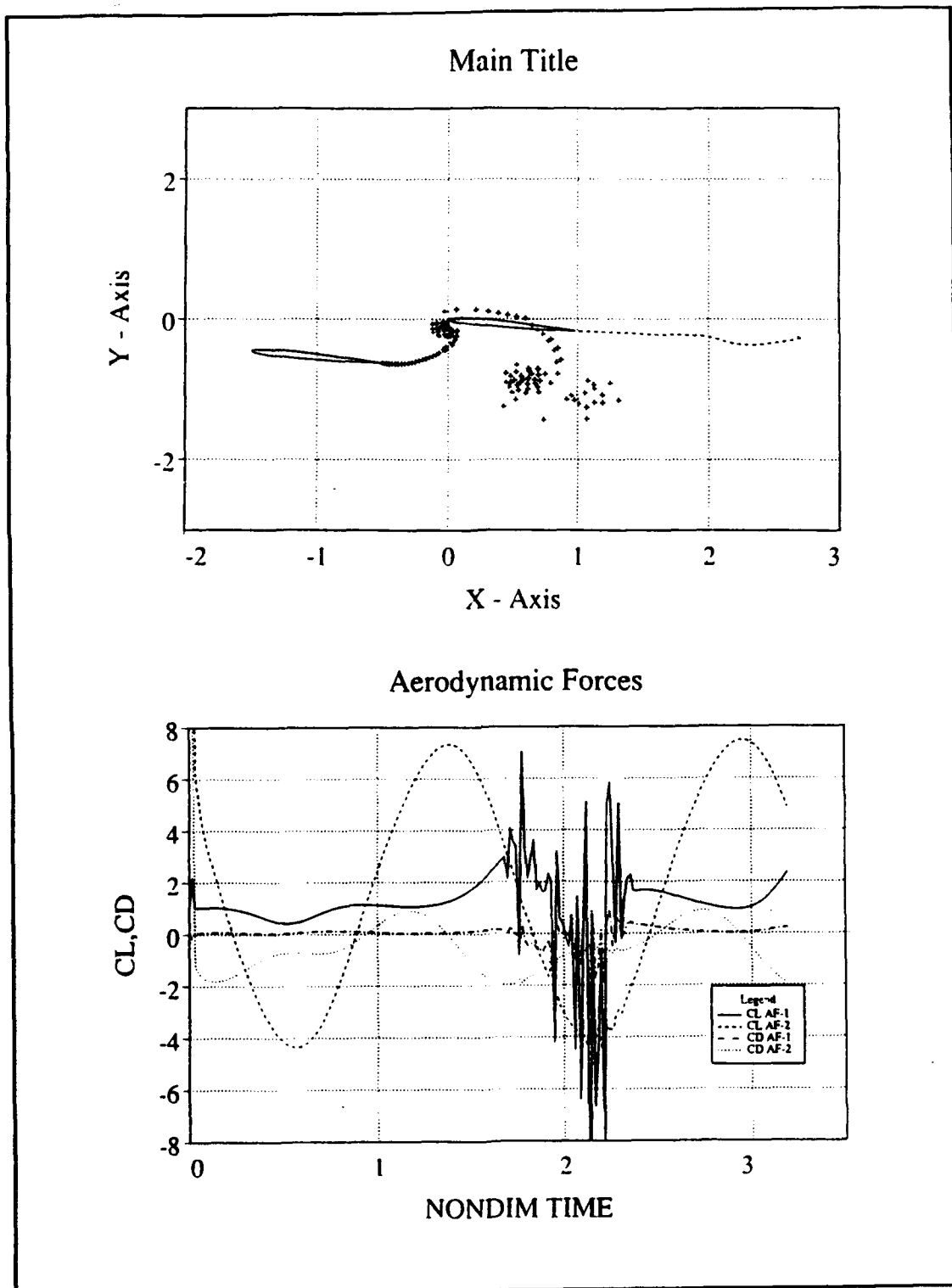


Figure 3.4 Wake pattern. Top airfoil scaled by .5 of bottom airfoil. Both undergoing a step input of 45 degrees.

#### ***d. Limitations***

There are several important limitations that must be understood thoroughly before attempting to use this program. First, the core vortices that make up the airfoil's wake must not intersect the panels that define the airfoil geometry. This situation is possible if one places the second airfoil in the wake of the first airfoil. The singularity nature of a core vortex intersecting a source can sometimes cause erroneous output. This can be noted in two ways. One way is to watch the screen output during the program run. If this situation arises, the code will not converge until the tolerance has been changed several times and is easily observed. Another way to identify this problem is to examine both the force, and moment data along with the wake patterns at the conclusion of the run. If the data or wake patterns are discontinuous, then there is a problem. This problem can be less severe if the panel density is increased and the time step is decreased. Unfortunately, if the wake is strong the interference effects are too great and the solution is suspect. Figure 3.5 shows the wake pattern and aerodynamic forces of a stationary airfoil in the strong wake of an oscillating airfoil. This example clearly points out the biggest limitation with this program.

Other limitations include a sensitivity to panel density, time step, and amplitude of motion. When adjusting these parameters one must watch the screen output to ensure the program can converge at each time step.



**Figure 3.5** Wake pattern and Aerodynamic forces showing vortex interference effects. AF1 unsteady, AF2 steady.



## **B. COMPARISON TO EXISTING COMPUTATIONAL RESULTS**

D.D. Liu and Z.X. Yao published results for vortex/wake flow studies in reference 13. For these results a numerical scheme was developed at Arizona State University that uses Panel Methods combined with an unsteady model that sheds vortices into the wake at each time step. The primary difference between this computer code and USPOTF2A is the treatment of the unsteady Kutta condition. Liu and Yao use a linearized model following the approach by Kim and Mook, where USPOTF2A uses the non-linear model developed by Basu and Hancock.

Two case studies were chosen to compare the results. First, consider the case where two NACA0012 airfoils undergo a step change in AOA from 0 to 5°. The second airfoil is placed .5c behind and .2c above the first. The results for wake patterns and aerodynamic forces for USPOTF2A are shown in Figure 3.6. Liu and Yao have revised their results from reference 13. The current results are published here in Figure 3.7. The next case study involved the first airfoil undergoing a step change in AOA from 0 to 5° while the second airfoil remained stationary. Again, the second airfoil was placed .5c behind and .2c above the first. The results obtained by USPOTF2A are shown in Figure 3.8. The revised results obtained by Liu and Yao are shown in Figure 3.9.

It is clear from the results that both codes follow the same trends. They do not produce the exact same results, as expected, due to the different

formulation of the problem. Both results essentially produce the same interference effect and approach steady state conditions. This example is a good verification for both numerical codes.

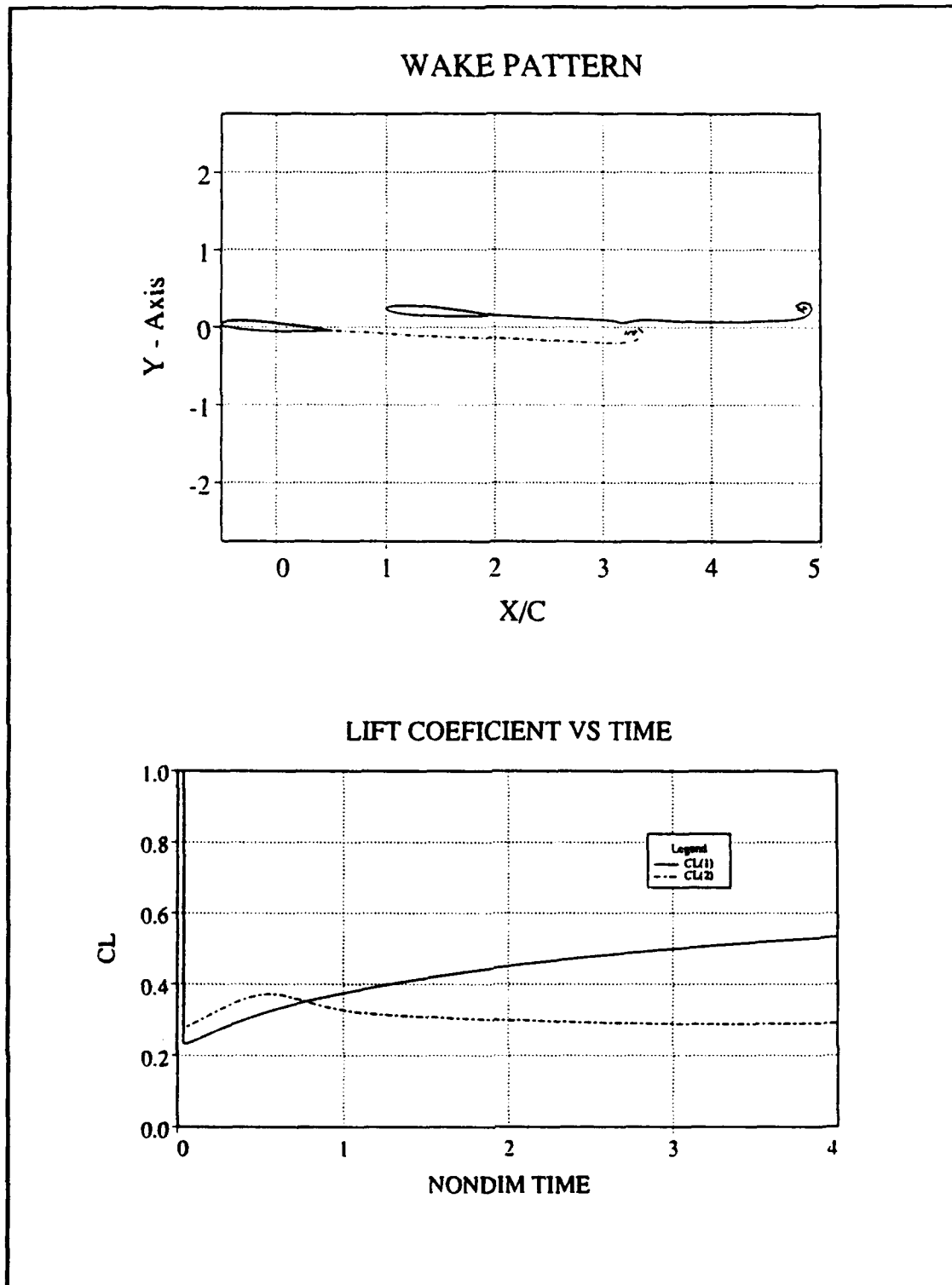


**Figure 3.6** USPOTF2A wake pattern and lift history output for two NACA0012 undergoing a step change in AOA from 0 to 5°.

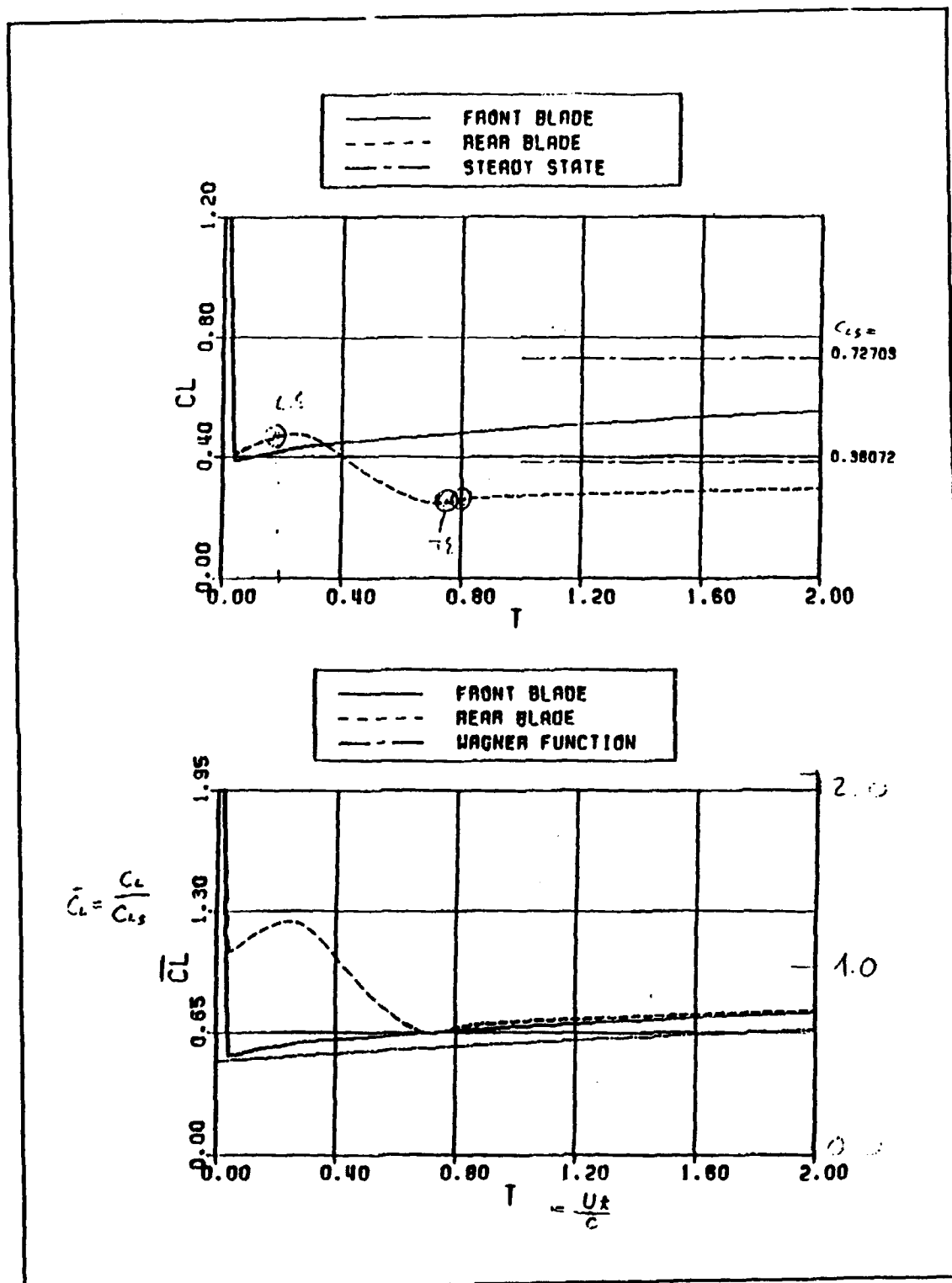
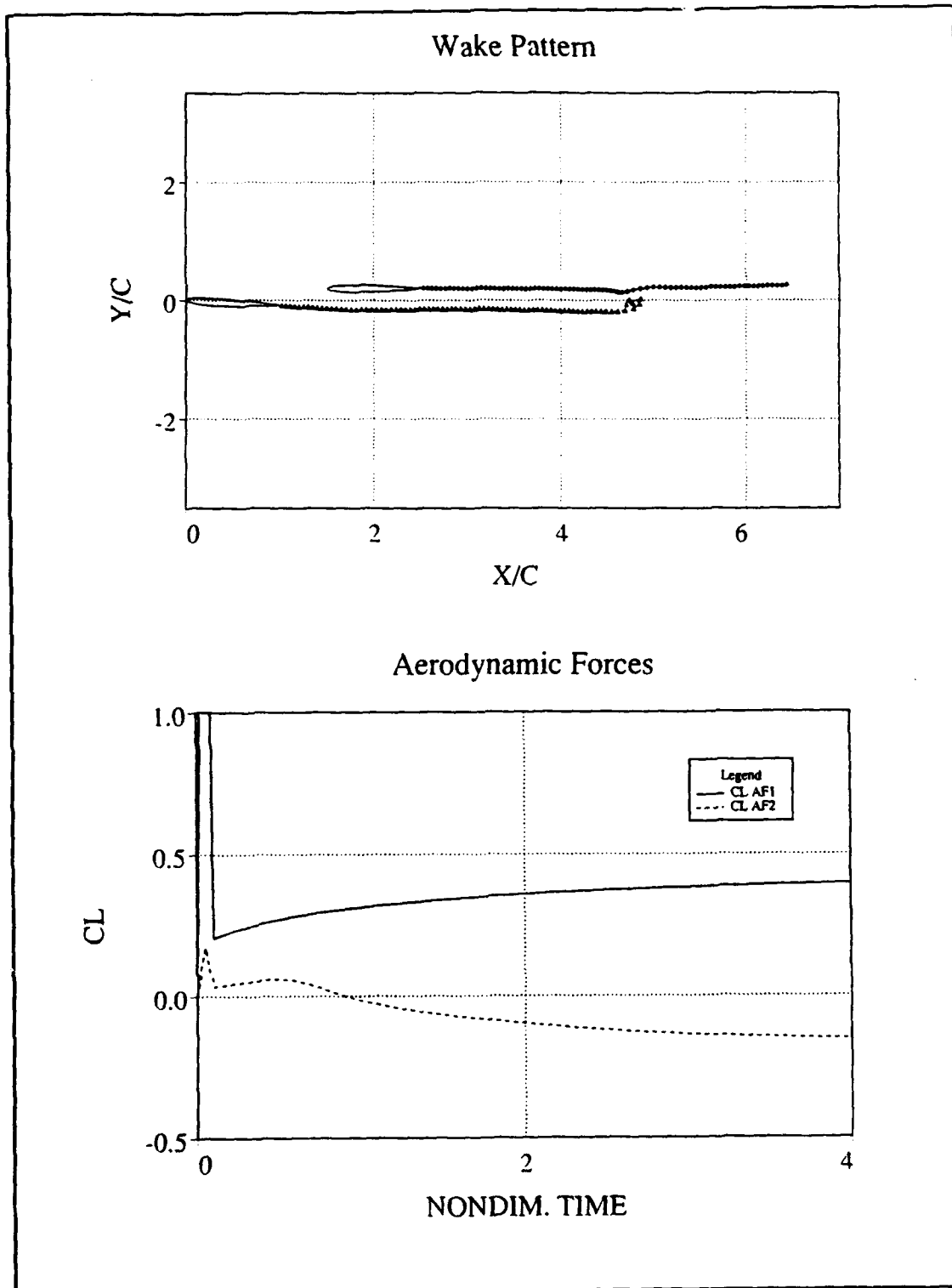
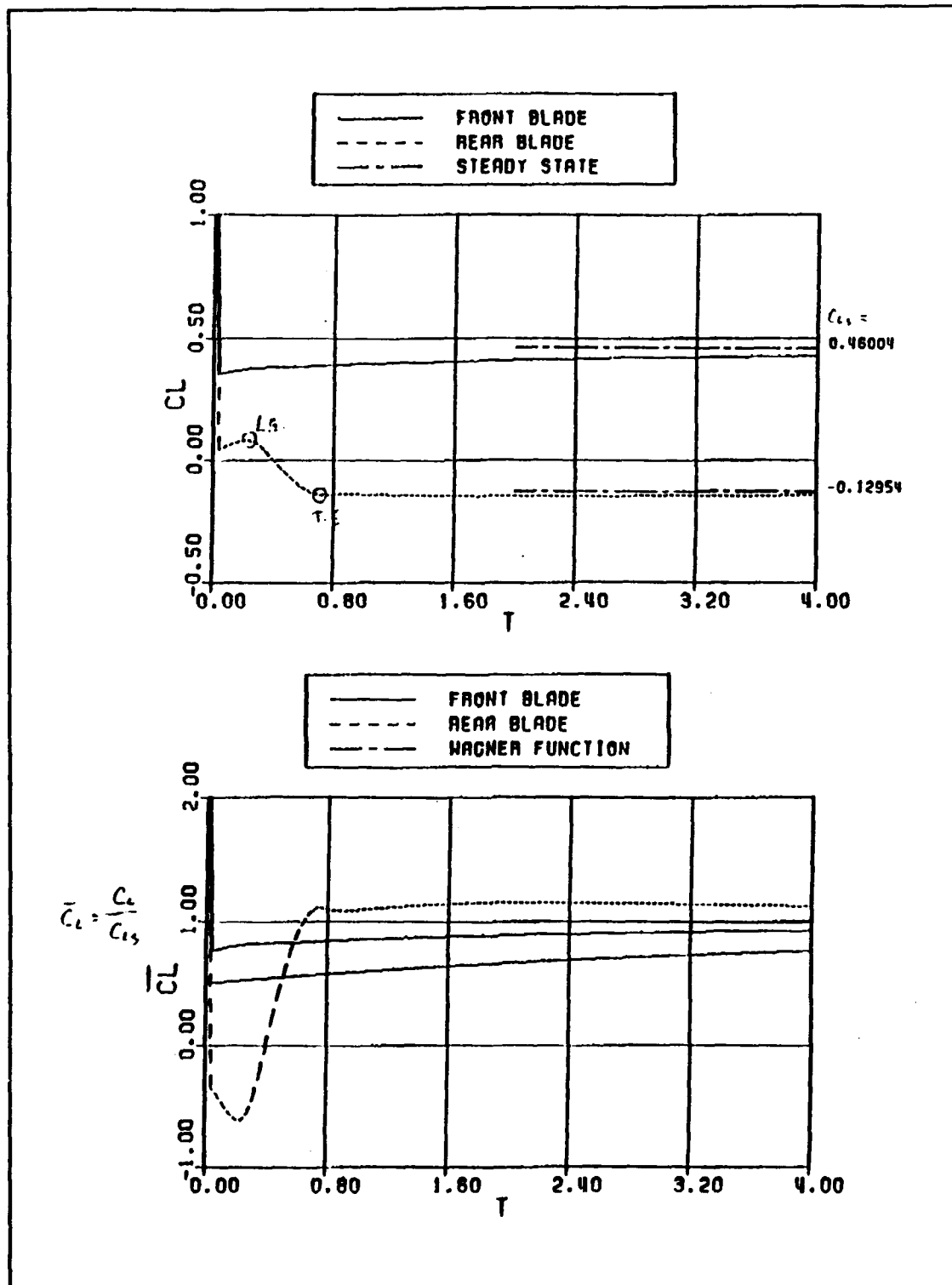


Figure 3.7 Liu's output of lift histories for two NACA0012 airfoils undergoing a step input from 0 to 5°.



**Figure 3.8** USPOTF2A wake pattern and lift history output for two NACA0012 airfoils. AF-1 undergoing a step change in AOA from 0 to 5°.



**Figure 3.9** Liu's output of lift histories for two NACA0012 airfoils, with the first undergoing a step input from 0 to 5°.

## C. PROPULSIVE EFFICIENCY

### 1. Introduction

The purpose of this section is to develop relations for propulsive forces and efficiencies for two airfoils in tandem. There are two configurations discussed in this section (Fig. 3.10). One, the first airfoil oscillates while the second remains stationary. Two, the first airfoil remains stationary, while the second airfoil oscillates. The computational study will only examine the second configuration where the airfoil oscillates in either pitch or plunge. Due to the limitations of the code USPOTF2A, the case where the first airfoil oscillates is discussed with limited computations. The results of the numerical output were compared to the analytical results obtained by Bosch in reference 8.

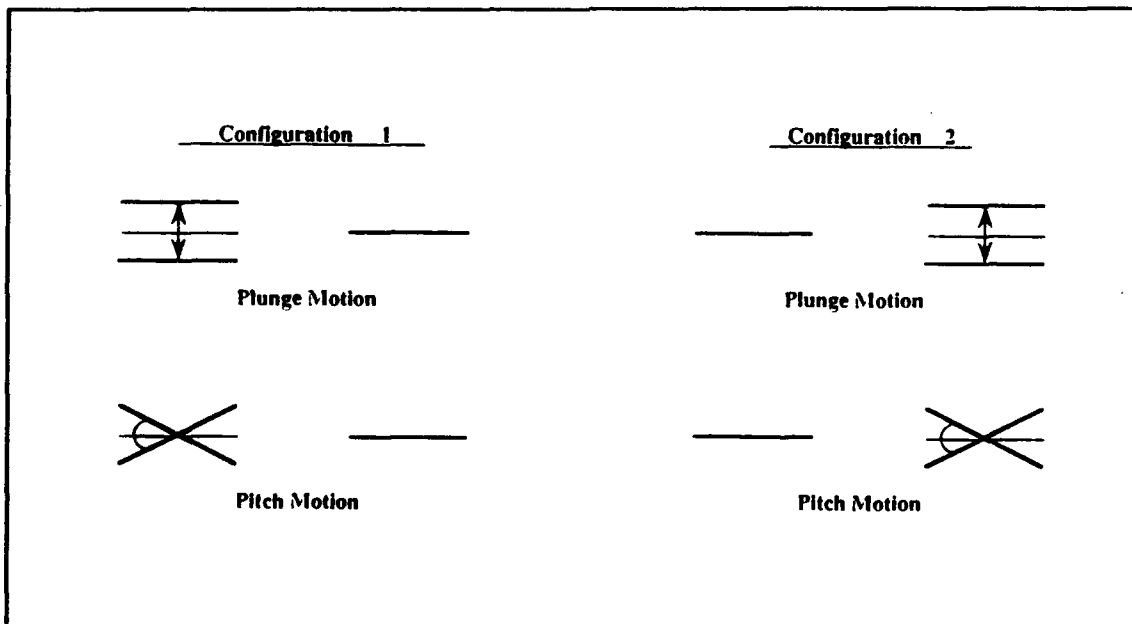


Figure 3.10 The two configurations studied.

## 2. Theory

The theory for the development of propulsive forces and efficiencies for two airfoils in tandem follows closely to the single airfoil case presented in Chapter II. The relationships for work done to the fluid by the two airfoils remain the same as for the single airfoil case since only one of the airfoils is in motion. The relationships for work done by plunge motion is given by equation 2.15 and for pitch motion by equation 2.17. The primary difference between the single airfoil analysis and the two airfoil analysis is in the relationship for efficiency. Although only one airfoil is in motion, both airfoils are capable of producing thrust, and the expression for efficiency becomes:

$$\eta = \frac{(\bar{D}_1 + \bar{D}_2) \cdot v}{\bar{W}} \quad (3.1)$$

where  $\bar{D}_1$ , and  $\bar{D}_2$  are the drag or propulsive forces from the first and second airfoil, respectively.

From the expression for efficiency in equation 3.1, the differences between the two configurations can be examined. In the first configuration, the pressure disturbances from the first airfoil are felt by the second airfoil downstream, or in the first airfoil's wake. This will produce a much stronger effect than the second configuration; where the pressure disturbances must travel upstream to have an effect on the stationary airfoil. Since the production of thrust by the stationary airfoil is entirely dependent on the influence of the



oscillating airfoil, it is clear that the first configuration will have a greater efficiency than the second configuration. Furthermore, as stated in chapter 2, plunge motion has a stronger influence than pitch motion; and the efficiencies associated with plunge motion are greater than those associated with pitch. Bosch concluded this in reference 8. Efficiencies for the first configuration near .9 were obtained for both types of motion with reduced frequencies between 1 and 2. The second configuration reached an efficiency near .5 for plunge motion and .1 for pitch motion for the same range of reduced frequencies.

### **3. Comparison to Flat Plate Theory**

Analytical results for two flat plates undergoing pure pitch and pure plunge motion for both configurations were computed by Bosch [Ref 8.]. To compare the results using USPOTF2A, the same conversions and scaling of the motion as for the single airfoil case were applied. Special consideration was given to the panel density and the time step to reduce the effects of the first airfoil's wake impinging upon the second airfoil. It was shown that when the first airfoil's wake is 'weak', it has a minimal effect on the solution or wake pattern of the second airfoil. The aerodynamic output was carefully observed proceeding each case study to ensure a smooth and continuous curve; this would confirm the impinging wake did not adversely effect the results. The time dependent output was then converted to harmonic output following similar procedures for the single airfoil case using the two airfoil phase-shift code presented in Appendix B. Then, the magnitudes of lift and moment were

divided into real and imaginary parts and plotted against reduced frequency. The results for pitch motion are shown in Figure 3.11; the first plot ( $C_L'$ ) represents the real part, and the second plot ( $C_L''$ ) represents the imaginary part. The agreement is particularly good at the low frequencies and begins to separate at the higher frequencies.

The comparison for thrust and efficiency was done using the second configuration with plunge motion. The expressions for efficiency are given by the following relations:

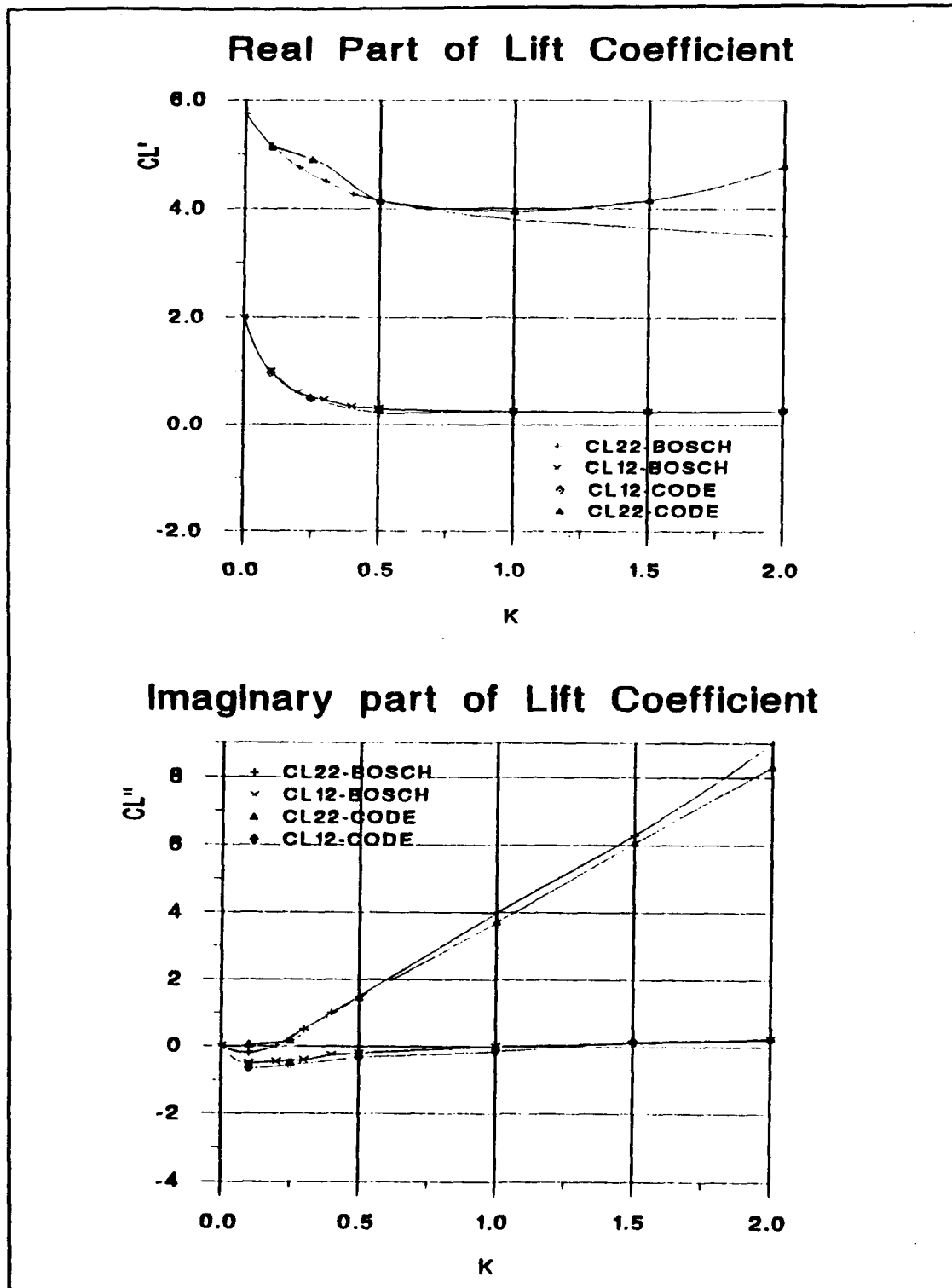
$$\eta_{pitch} = \frac{\overline{C_{D_1}} + \overline{C_{D_2}}}{klm(C_M)}, \quad \eta_{plunge} = \frac{2(\overline{C_{D_1}} + \overline{C_{D_2}})}{klm(C_D)} \quad (3.2)$$

Figure 3.12 shows the propulsive force and efficiency comparisons. Here, the results match well over the entire frequency range with the computed efficiency always being less than that predicted by Bosch. This was anticipated because the non-linear effects in the USPTF2A code would result in a lower efficiency. Furthermore, the consequence of plunge motion producing higher aerodynamic forces for the same frequency as pitch motion, results in less scaling errors.

A final study was done to try and achieve the results by Bosch for the first configuration where the efficiencies are much higher. Unfortunately, as stated this code is unable to converge when the discrete vortices collide with the airfoil. Therefore, the second airfoil was placed  $0.2c$  in front and  $1c$  above

the stationary airfoil. In this configuration, the trailing vortices from the oscillating airfoil would not interfere with the stationary airfoil. The results were recorded for plunging motion ( $DHY = .05$ ) at a reduced frequency of 4.0, and then the oscillating airfoil was brought incrementally closer to the stationary airfoil. This continued until the vortices interacted at  $0.3c$  above the stationary airfoil. The efficiency went from  $\eta = .48$ , to  $\eta = .6$  at  $1c$  and  $.3c$  above the stationary airfoil, respectively. This study shows the correct trend for the efficiency under the limitations of the code.

Overall, the USPOTF2A program was shown to be an effective way to predict the aerodynamic forces, and efficiencies for two interacting airfoils. Unfortunately, the limitations of the program prevent some interesting case studies of strong wake interaction. Finally, one must be cautioned to observe the output with care when studying airfoils in close proximity to the wakes.



**Figure 3.11** Lift coefficient as a function of the reduced frequency  $k$ . Pitching motion using configuration 2.

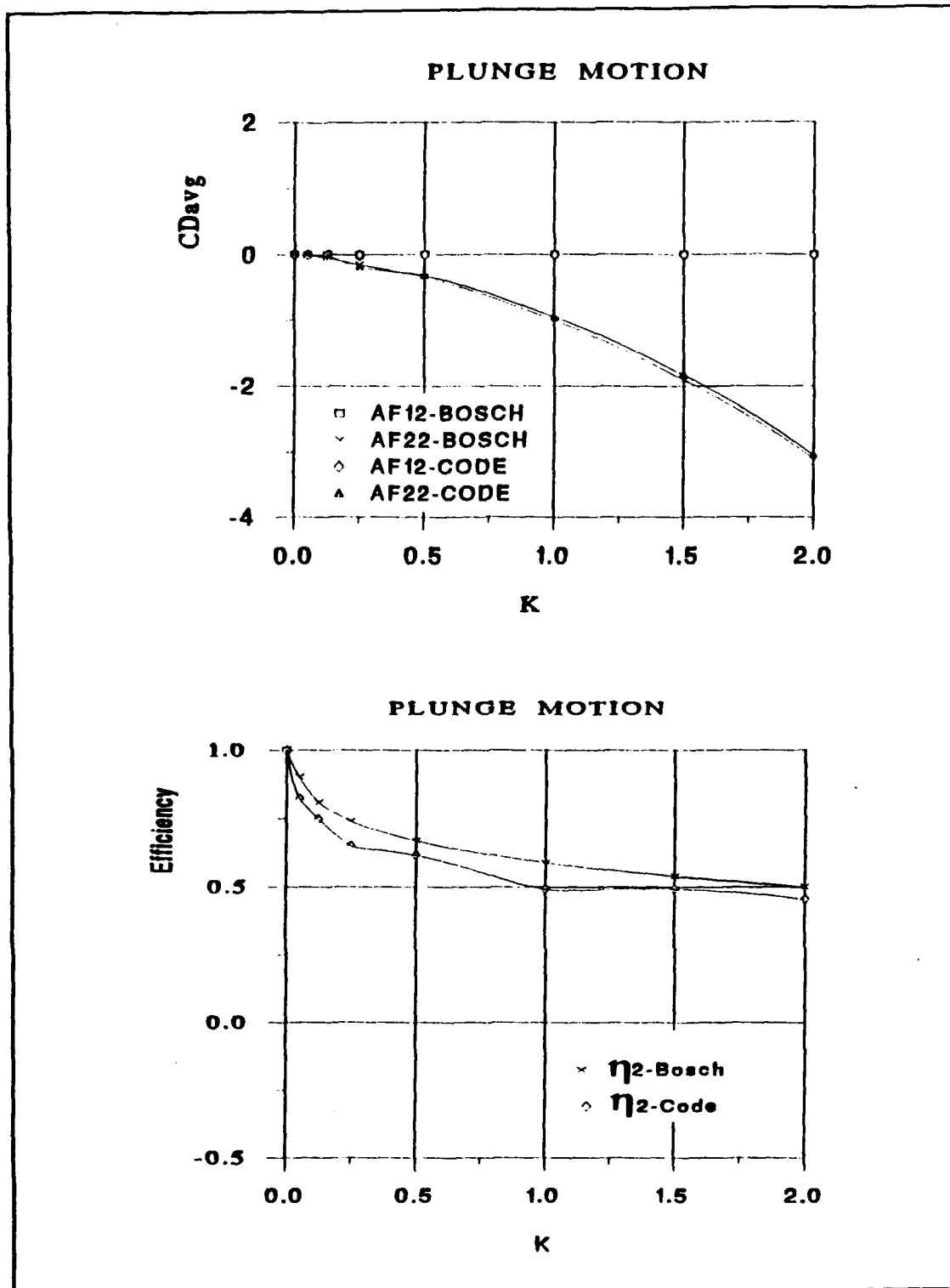


**Figure 3.12** Drag coefficient and propulsive efficiency as a function of the reduced frequency  $k$ . Plunging motion using configuration 2.

## **D. UPWIND INFLUENCE STUDY**

### **1. Introduction**

It has been of interest to understand and study the effects of an oscillating airfoil in the vicinity of a stationary airfoil. The purpose of such a study is to see if there exists a configuration that would enhance the lift on the stationary airfoil. This is of primary interest in the post-stall region, where an oscillating airfoil may have the beneficial effect of delaying boundary layer separation and increasing the steady state lift. In theory, the oscillating airfoil will produce a certain amount of thrust, thereby increasing the flow velocity and creating a more favorable pressure gradient on the stationary airfoil. Although this study is done with the inviscid code, USPOTF2A, useful information on the pressure distributions and gradients are obtained from such an analysis. This information can be used to understand the degree of influence and trends in the integrated forces that determine the effects on a certain configuration. Due to the limitations of the code, only configurations where the oscillating airfoil was behind the stationary airfoil were considered.

### **2. Description**

This study used the modified code, USPOTF2A, to determine the effects of an oscillating airfoil on a stationary airfoil at a high AOA. Two NACA0009 airfoils were used for this study with the first remaining stationary at  $10^\circ$  AOA. The second airfoil was set to oscillate in plunge ( $DHY = .2$ ) at a

reduced frequency of 4.0. The amplitude of motion,  $DH_Y$ , was limited to .2 because of the wake interference problem. The high reduced frequency was chosen to get the maximum effect with the relatively small amplitude of motion used in this study. The study involved changing both the position and mean AOA of the oscillating airfoil; then recording the change in pressure distribution and average lift of the stationary airfoil over steady state values. Two positions for the oscillating airfoil were studied. First, the oscillating airfoil was placed slightly behind ( $XSHIFT = .1c$ ) and above ( $YSHIFT = .6c$ ) the stationary airfoil. Here, the mean AOA of the oscillating airfoil was changed from  $0^\circ$  to  $10^\circ$ . The other position considered was placing the oscillating airfoil slightly behind ( $XSHIFT = .1c$ ) and below ( $YSHIFT = -.6c$ ) the stationary airfoil. Here, the mean AOA of the oscillating airfoil varied from  $0^\circ$ ,  $5^\circ$ ,  $10^\circ$ , and  $15^\circ$ .

### **3. Results**

The numerical results of this study are tabulated in table 3.1. In the first configuration, where the oscillating airfoil was located above the stationary airfoil, the influence was minimal. The increase in lift ranged from 7% to 10%. The important result was the influence of AOA. For a greater mean AOA on the oscillating airfoil, the delta lift on the oscillating airfoil was increased dramatically along with the influence on the stationary airfoil. Furthermore, the production of thrust decreased with increasing mean AOA. The results of the second configuration, where the oscillating airfoil was below the stationary airfoil, proved to be more effective. The increase in lift ranged from 10% to

20%. Again, the influence of mean AOA followed the same trends as the first configuration.

A typical case study is displayed in Figures 3.13 and 3.14. Figure 3.13 shows the steady state pressure distribution super-imposed on the average pressure distribution for one cycle of motion. Furthermore, the pressure gradients for both cases are displayed on the same graph. Figure 3.14 shows the aerodynamic forces for two cycles of motion. The second cycle was analyzed for average data. It is interesting to note the cyclic behavior of the stationary airfoil's lift coefficient which is designated as AF-1. Clearly, the influence of the oscillating airfoil on the stationary airfoil is shown in this graph.

#### **4. Conclusion**

Several important conclusions can be made from the above results. First, there is certainly a favorable influence from an oscillating airfoil in the vicinity of a stationary airfoil. Furthermore, the AOA and position of the oscillating airfoil have a strong influence on the effectiveness of the configuration. It was shown that the most effective configuration was having the oscillator at a high mean AOA and below the stationary airfoil. Finally, it can be concluded that the upwind influence can only produce a maximum of 17% change in lift for an unstalled mean AOA of  $10^\circ$ . Unfortunately, the limitations of the program prevented studying many interesting configurations.



**TABLE 3.1: Numerical results of oscillating airfoil study.**

CL <sub>2</sub> AOA	steady/ average	C <sub>L1</sub>	C <sub>L2</sub>	C <sub>D1</sub>	C <sub>D2</sub>	ΔC <sub>L1</sub>	ΔC <sub>L2</sub>
Position of oscillating airfoil: XSHIFT = .1, YSHIFT = .6							
0°	ss	1.051	-.340	.0281	-.027	.0744	.086
	avg	1.126	-.426	.0336	-.586		
10°	ss	1.257	.8161	-.051	.053	.1019	.199
	avg	1.359	1.016	-.053	-.475		
Position of oscillating airfoil: XSHIFT = .1, YSHIFT = -.6							
0°	ss	1.068	-.300	.0124	-.113	.1027	.0795
	avg	1.170	-.220	.0217	-.586		
5°	ss	1.374	.173	-.019	.020	.140	.236
	avg	1.514	.4089	-.120	-.540		
10°	ss	1.677	.6345	-.061	.065	.1779	.387
	avg	1.856	1.021	-.062	-.466		
15°	ss	1.977	1.082	-.122	.123	.216	.532
	avg	2.193	1.614	-.127	-.364		

# Cp PLOT

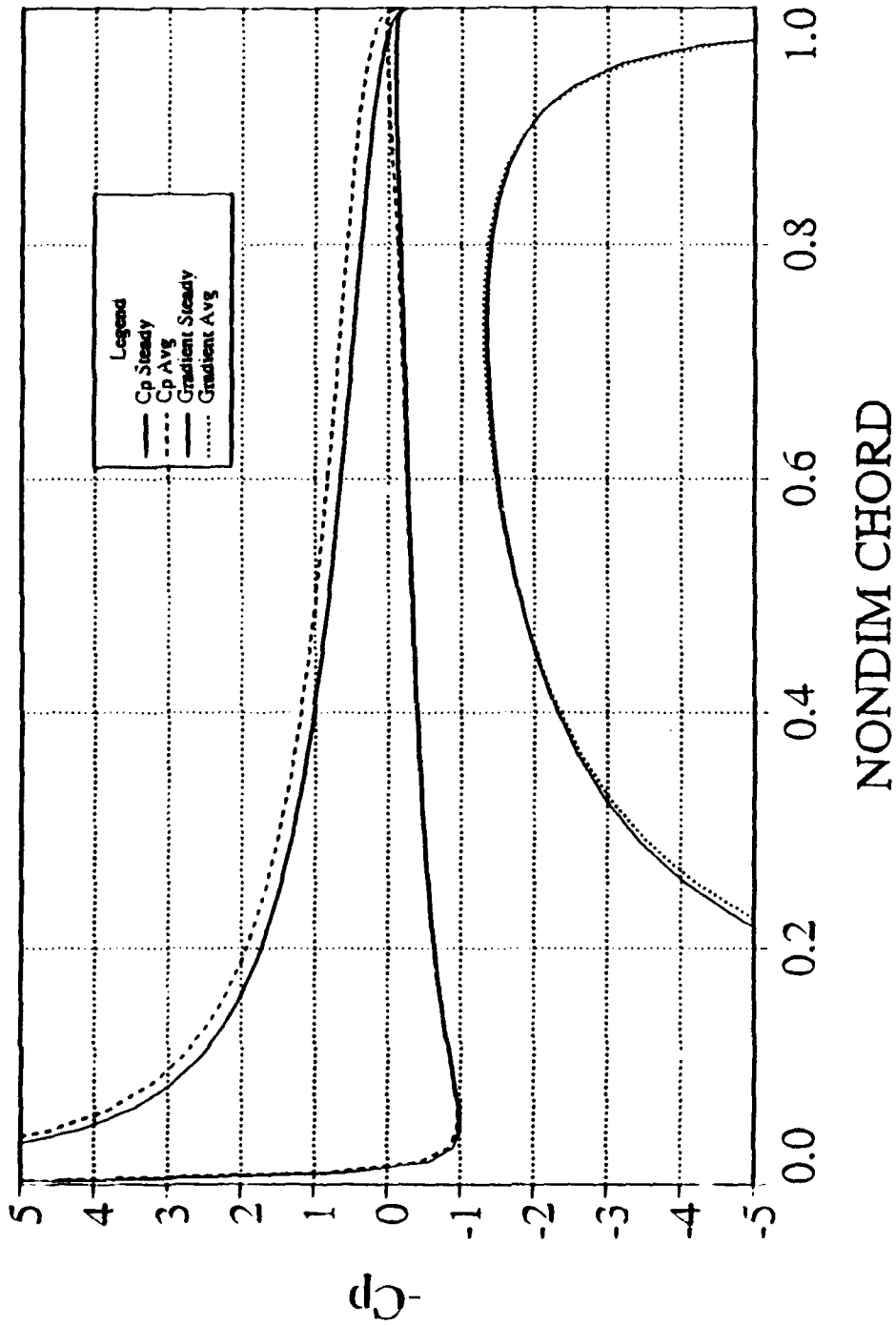
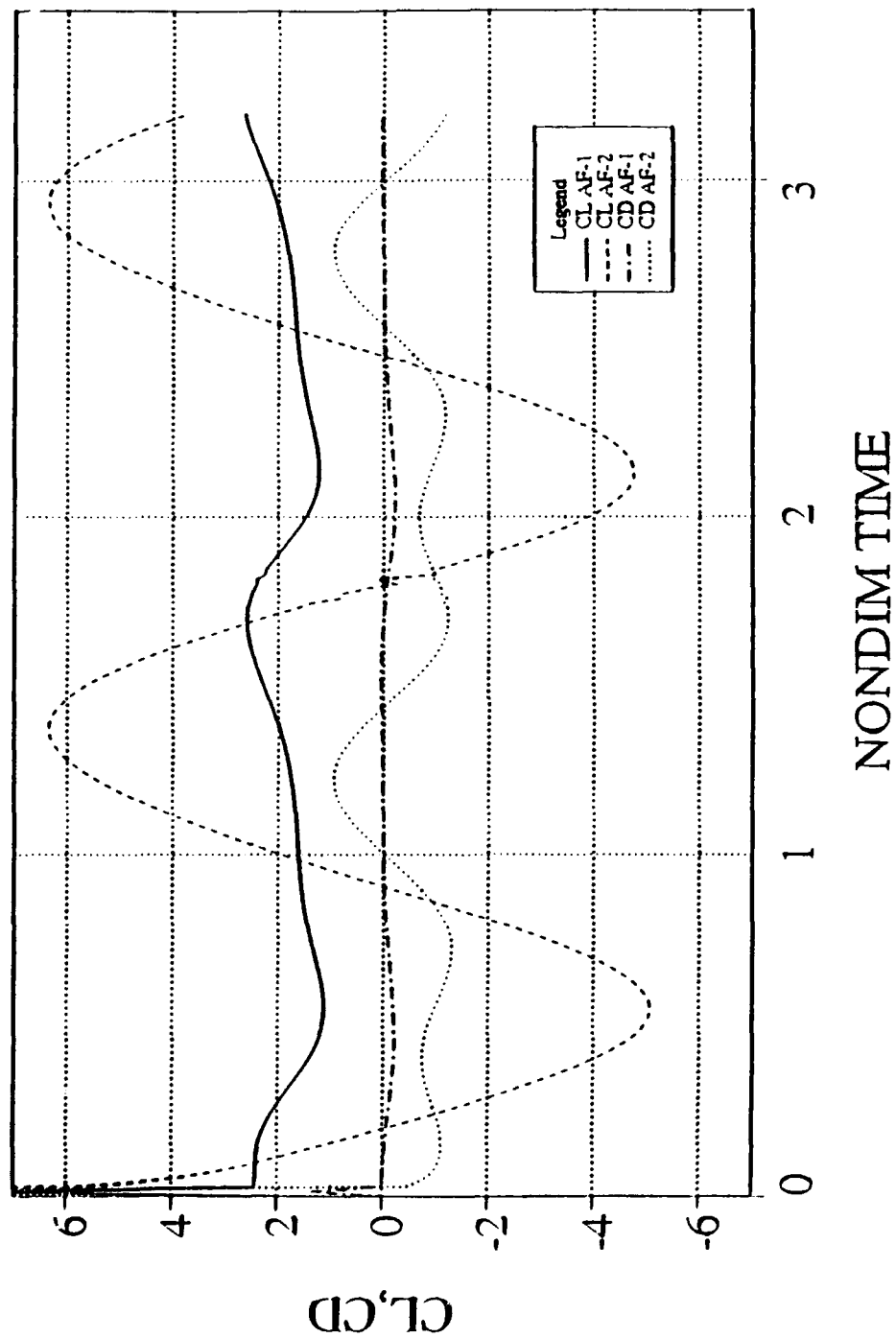


Figure 3.13 Pressure and gradient distribution for two NACA0009 airfoils. AF-1 is stationary at 10° AOA, while AF-2 is oscillating in plunge: AOA = 10°, DHY = .2, k = 4.0, XSHIFT = .1, YSHIFT = -.6.

## Aerodynamic Forces



**Figure 3.14** Aerodynamic forces for two NACA0009 airfoils. AF-1 is stationary at  $10^\circ$  AOA, while AF-2 is oscillating in plunge: AOA =  $10^\circ$ , DHY = .2, k = 4.0, XSHIFT = .1, YSHIFT = -.6.

## **IV. PROPULSIVE FLOW VISUALIZATION EXPERIMENT**

### **A. INTRODUCTION**

The purpose of this experiment was to document the production of thrust by the wave propeller originally built at the Naval Postgraduate School by Carl Dane [Ref. 15]. This was a preliminary experiment to better understand the vortex pattern produced by a wave propeller, and to examine the production of thrust using smoke flow visualization techniques.

An explanation of what constitutes a propulsive vortical signature along with smoke flow visualization of the propulsive vortical patterns is given in reference 16. In this reference, the explanation is given by contrasting the vortical pattern produced by a cylinder (drag) with the vortical pattern produced by a pitching airfoil (thrust). The cylinder produced a vortical street where the top row of vortices rotated clockwise and the bottom row of vortices rotated counterclockwise. This pattern induces a velocity component in the upstream direction (Biot-Savart law). In contrast, the pitching airfoil produced a counterclockwise rotating vortex street on the top row and a clockwise rotating vortex street on the bottom row. This pattern induces a velocity component in the downstream direction. Reproduction of the flow visualization data from reference 16 is shown in Figure 4.1.

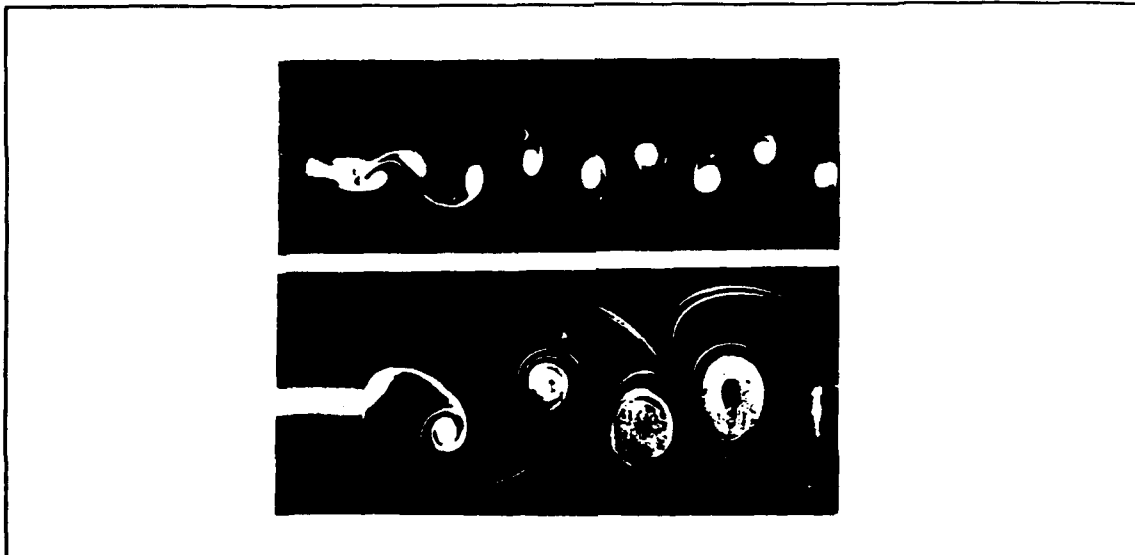


**Figure 4.1** Results from reference 16. Top vortex street shed from a circular cylinder (drag). Bottom vortex street generated by an airfoil pitching about the quarter-chord (thrust).

## **B. THEORY**

A comparison was done using the incompressible panel code, U2DIIIF. The purpose of this study was to examine the vortical pattern produced by the panel code, and determine if the vortical signature matched experimental results. The input to the panel code was set up to best match the conditions of the experiment described in the next section. The panel code was run using a plunge amplitude,  $h_0/c$ , equal to .364, a reduced frequency of 2.5 and a  $0^\circ$  mean AOA. The results of the vortical pattern are shown in Figure 4.2. Aside from the starting vortex, this is clearly a thrust producing vortical street. Furthermore, the vortical pattern is similar to that produced by the experiment

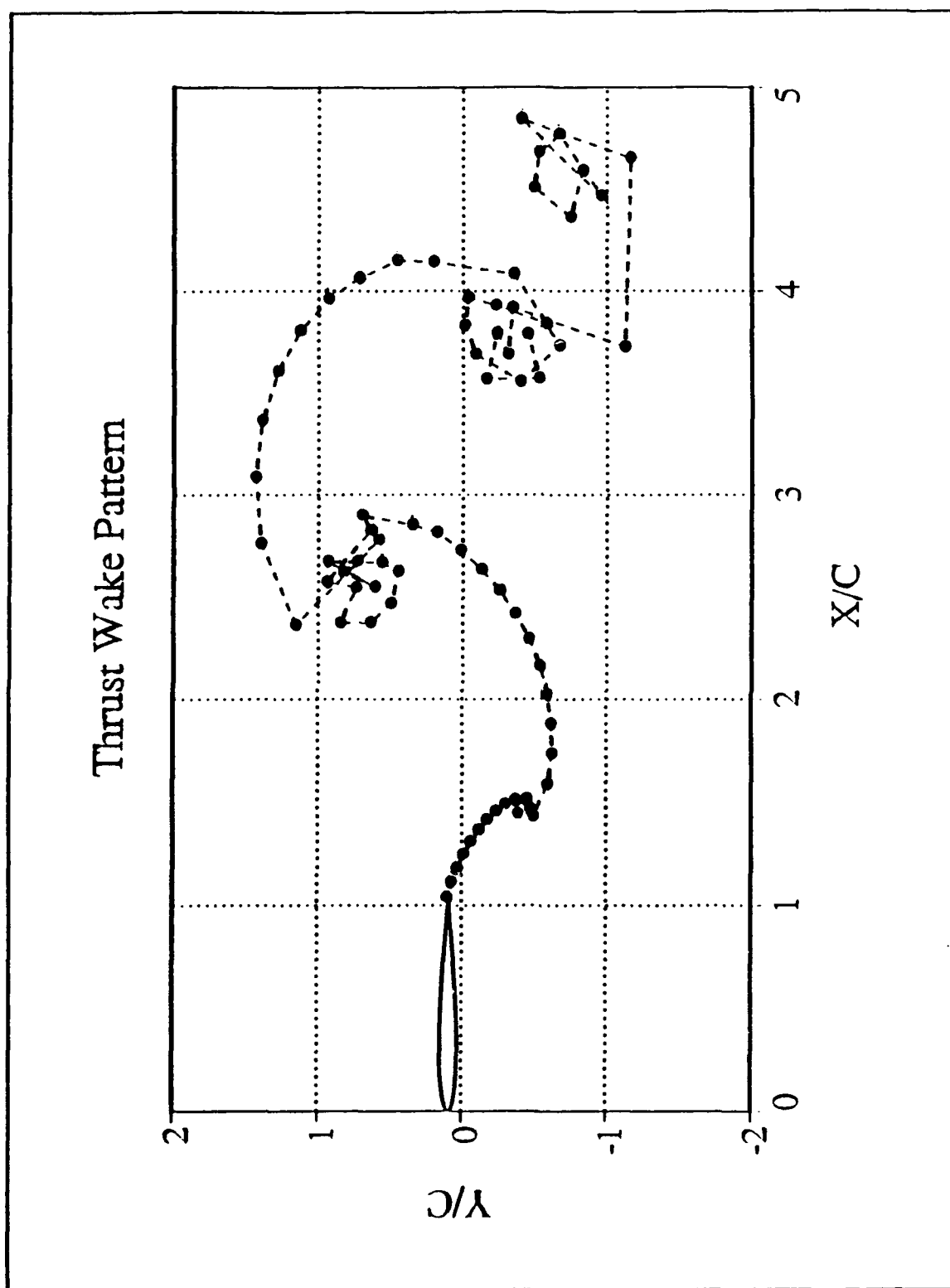


Figure 4.2 Vortical pattern produced by the panel code, U2DIF.  $h_0/c = .364$ , and  $k = 2.5$ .

shown in Figures 4.10 and 4.11. Finally, the theory predicts a drag coefficient (thrust) of  $-0.376$ .

## **C. EXPERIMENTAL SETUP**

### **1. Wave Propeller**

The wave propeller, originally proposed by Wilhelm Schmidt [Ref. 14], used in this paper was a modification of the original construction made by Carl Dane [Ref. 15]. The original mechanism was designed to perform a circular motion while holding the wing at a constant angle-of-attack. The primary modification was the construction of a new wing. The new wing was made from a NACA0012 airfoil section and consisted of a 5.5'' chord and a 22'' span. The wing was built from a foam core covered with a thin plywood skin and finished with a layer of glass-epoxy composite for added fatigue strength. The wave propeller's drive mechanism was rebuilt using added bearings and tighter fittings to allow for less binding at high rotational speeds. The final configuration for the wave propeller is shown in Figure 4.3. The drive motor used was a reversible DC motor rated at 24 volts, and 5 amps. The power supply used was regulated voltage DC power supply rated at 0-35 volts, and 2.5 amps. The motor and power supply combination could provide the wave propeller with a maximum rotational speed of 1500 revolutions per minute (rpm) when placed horizontal.

## **2. Wind Tunnel**

The wind tunnel used in this experiment was a very low speed, low turbulence smoke tunnel at the Naval Postgraduate School. This smoke tunnel is of indraft type and was designed to be a scaled model of an existing smoke tunnel at the NASA Ames Research Center. It is made of plexiglass walls and has a contraction ratio of 2.8:1. The motor provides wind tunnel velocities between 0 and 10 feet per second (fps). The smoke was created using a Rosco smoke generator and piped into the tunnel as a single stream for the streak line flow visualization experiment. The smoke was directed into a rake for the flow field visualization experiment. Figure 4.4 is a photograph of the wind tunnel and smoke rake used in this experiment.





**Figure 4.3** Wave Propeller.

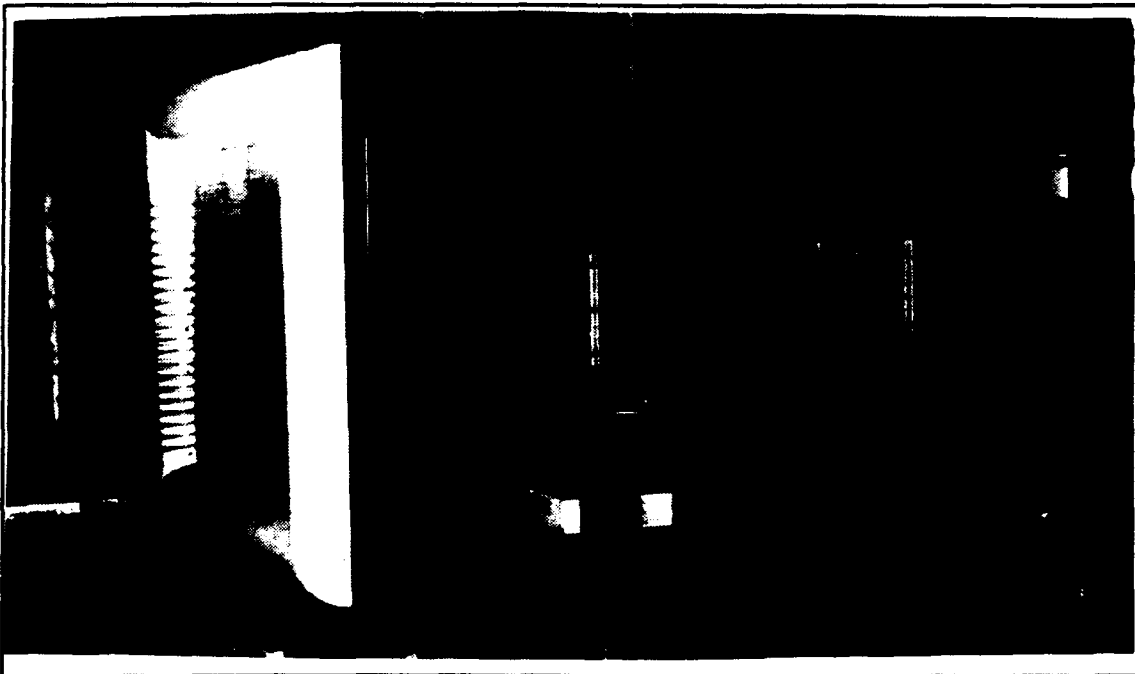


**Figure 4.4** Low speed smoke tunnel.

#### **D. TEST PROCEDURE**

Testing was done in the low speed smoke tunnel for two different conditions. First, with the wind tunnel off (0 velocity), and second with the wind tunnel operating at 10 fps. In the first configuration with the wind tunnel off, the wave propeller was placed in the wind tunnel and the tunnel was filled with smoke; then, the wave propeller was turned on to its maximum rotational speed of 1500 rpm and a rotation diameter of 2 inches. The purpose was to see if the wave propeller would draw the smoke through the tunnel like a fan, thus showing the production of thrust by the wave propeller.

In the second tunnel condition, the smoke tunnel was turned on to its maximum power bringing the tunnel speed to 10 fps (chord Reynolds number of 26,500). The wave propeller was oscillated at three different rotational speeds: 165 rpm, 620 rpm, and 1085 rpm. This equated to reduced frequencies of .792, 2.97, and 5.2 respectively. Furthermore, the angle-of-attack of the wave propeller was varied between 0, 5, 10, and 20 degrees with a rotation diameter of 2 inches. For these configurations, smoke was used to visualize the flow field in two ways. First, smoke was introduced in one tube to visualize the streak line. Next, a rake was used to visualize the entire 2-D flow field.

Photos were taken using a Nikon 35mm camera and Kodak TMAX-400 ASA black and white film. The film speed was set to 1/500 seconds with an aperture setting of 2.0 for the light conditions used at low rotational velocities.

At higher rotational velocities film speeds of 1/1000 and 1/2000 seconds were used with aperture settings of 2.0 and 1.4 respectively.

## **E. RESULTS AND DISCUSSION**

The results for the first tunnel condition flow visualization experiment is shown in Figure 4.5. Here, the wind tunnel is turned off and the wave propeller is oscillating at approximately 1500 rpm. It was shown that the wave propeller accelerated the smoke through the tunnel and out the exit similar to a fan blade. This experiment was done for the cases where the wave propeller oscillated both clockwise and counterclockwise with the same result. This was clear evidence the wave propeller produced thrust; hence, showing that circular motion can simulate plunge motion which is known to produce thrust.

The results of the second tunnel condition flow visualization experiment are shown in Figures 4.6 - 4.20. Figure 4.6 shows the wave propeller at steady state and 0° AOA. It can be seen that the airfoil produces a highly turbulent wake at the very low Reynolds number (26,500) generated in this tunnel. The boundary layer would still remain attached, which was an improvement over the earlier airfoil design. Figures 4.7 through 4.14 show the streak line flow visualization experiment at various AOA's, and frequencies. These photos show several important features about the street vortices produced by different oscillating conditions. Most of these pictures reveal the propulsive vortical street pattern discovered in reference 16. Unfortunately, the

wave propeller was constructed to oscillate at too high an amplitude (diameter) for this tunnel, and many of the vortical patterns would hit the walls and disperse. In Figure 4.10, the vortical pattern shows that the bottom vortex is rotating clockwise, and the top vortex is rotating counterclockwise, which is a thrust producing vortical street. It was observed that the AOA and frequency greatly affect the vortical strength (size). Increasing the AOA and frequency led to an increase in wake vorticity. Furthermore, these increases led to a stronger influence on the streak line in front of the wave propeller. Increasing the AOA beyond  $5^\circ$  led to stall, and subsequently, a decrease in thrust. Figure 4.13 shows the wave propeller in a stalled condition ( $20^\circ$  AOA), and the rotating vortices are both weaker and positioned such that they would not induce significant thrust. In fact, Figure 4.14 shows a dynamic stall vortex building up on the leading edge.

Figure 4.15 - 4.18 contain the rake flow visualization experiment. Figure 4.15 and 4.16 display the propulsive vortical pattern produced by the wave propeller for the 2-D flow field. Figures 4.17 and 4.18 indicate the large region of separation on the airfoil's upper surface. Again, the dynamic stall vortex is seen to form at the leading edge in Figure 4.17. These pictures best reveal the stalled condition of the wave propeller operating at low Reynolds number and high amplitude. Both of these conditions were limitations in the design and test equipment.

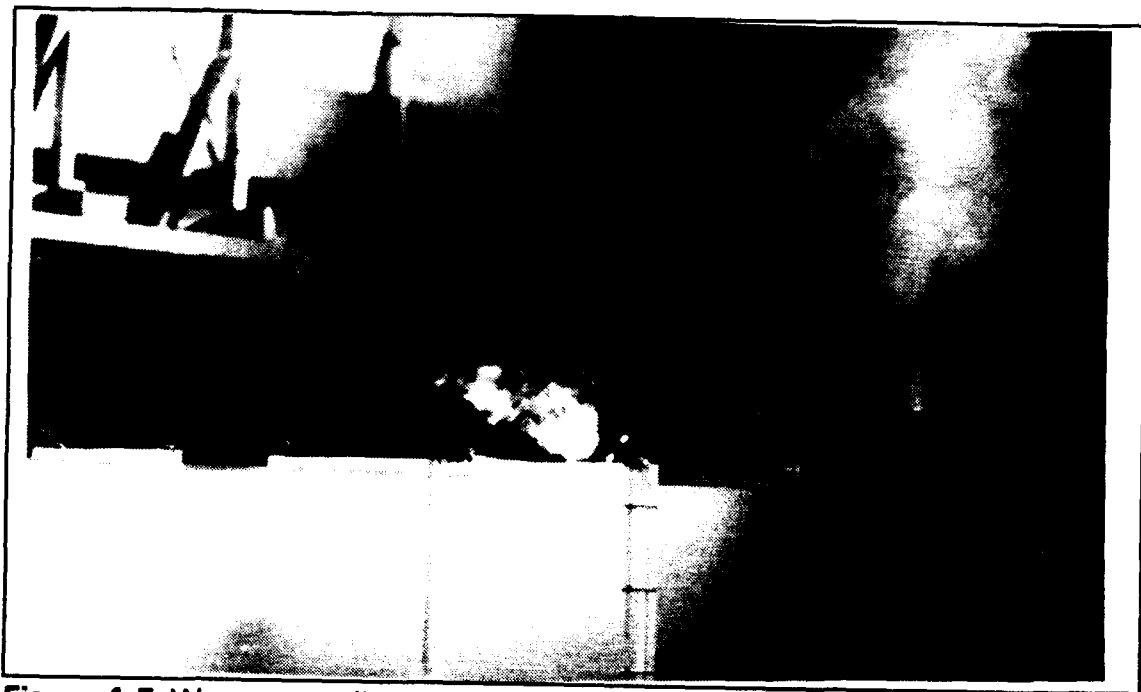


**Figure 4.5** Wave propeller operating at 1500 rpm, 0° AOA with the wind tunnel off.

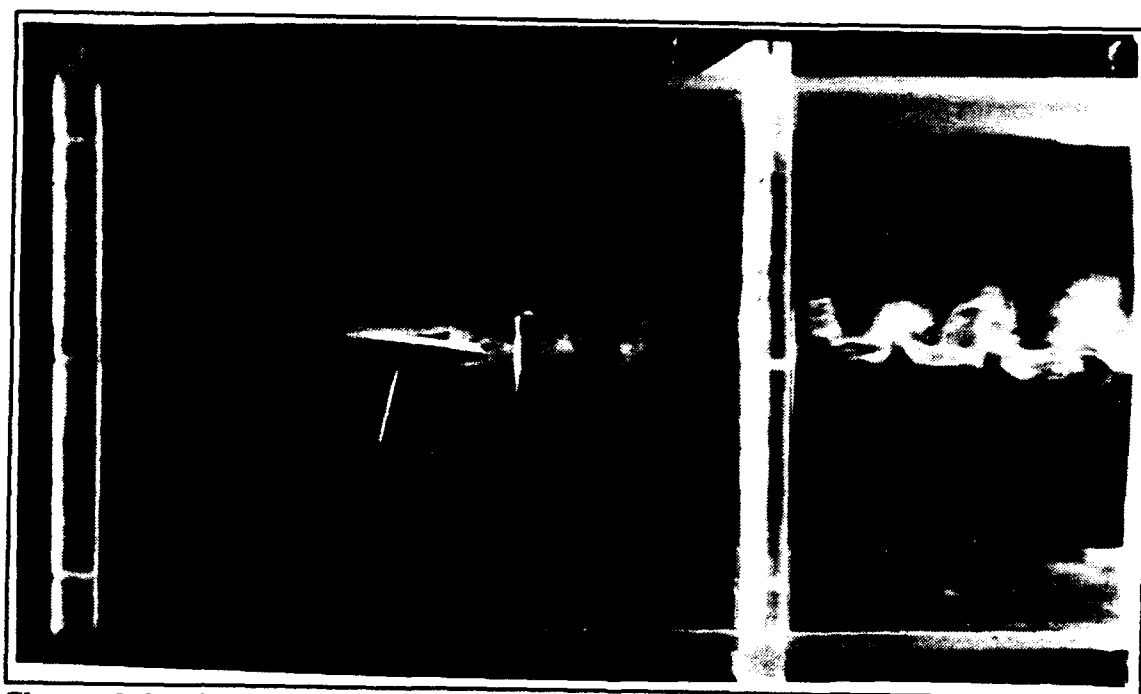


**Figure 4.6** Steady state, 0° AOA.

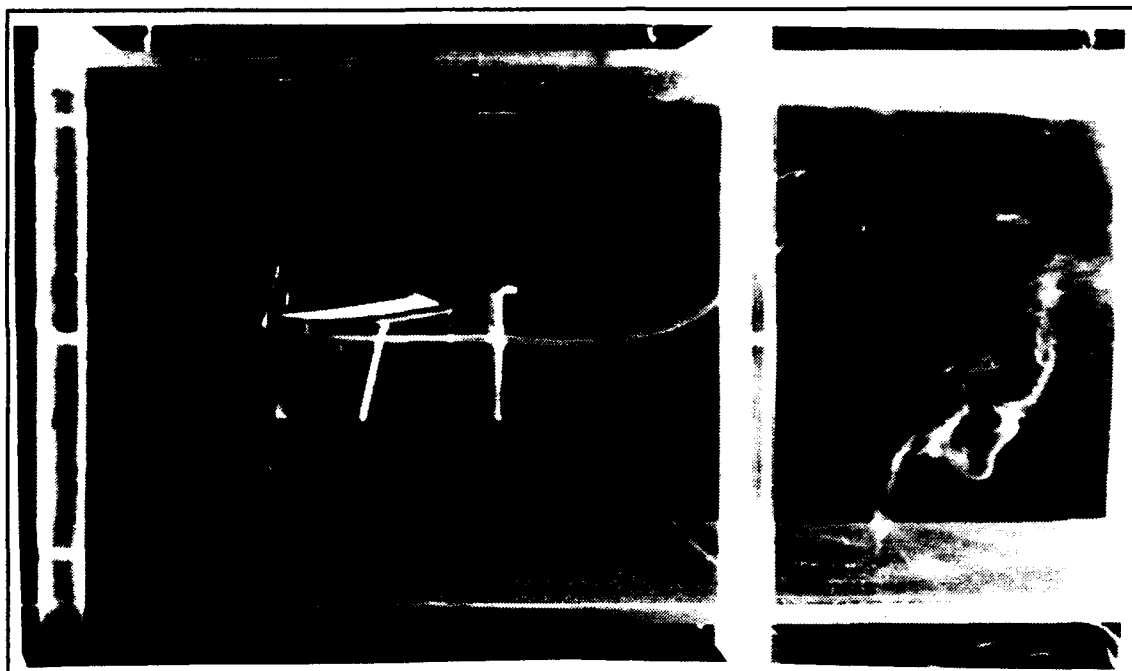


**Figure 4.7** RPM = 1085, AOA = 0°, rotating counterclockwise.

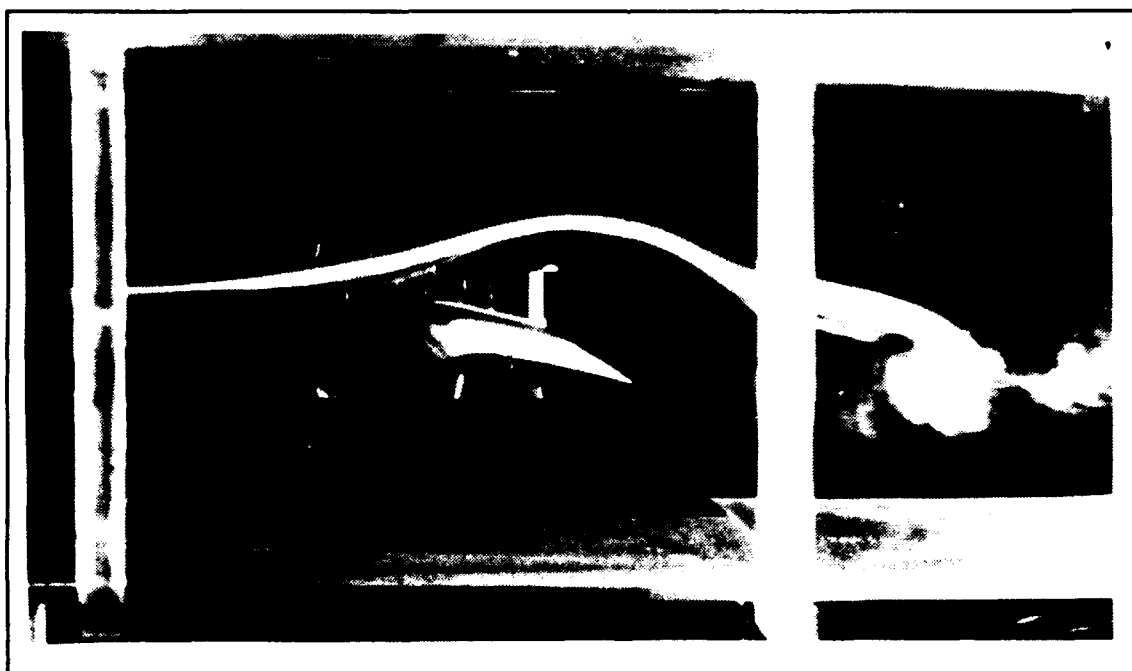


**Figure 4.8** RPM = 165, AOA = 5°, rotating counterclockwise.



**Figure 4.9** RPM = 620, AOA = 5°, rotating clockwise



**Figure 4.10** RPM = 1085, AOA = 5°, rotating clockwise.

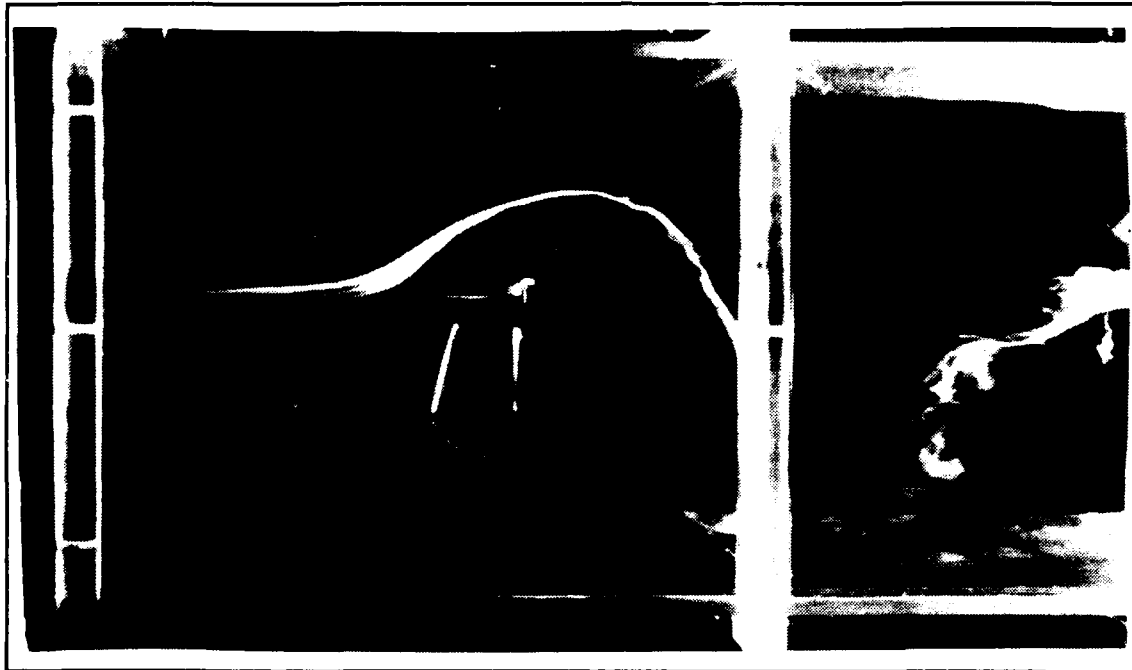


**Figure 4.11** RPM = 620, AOA = 10°, rotating counterclockwise

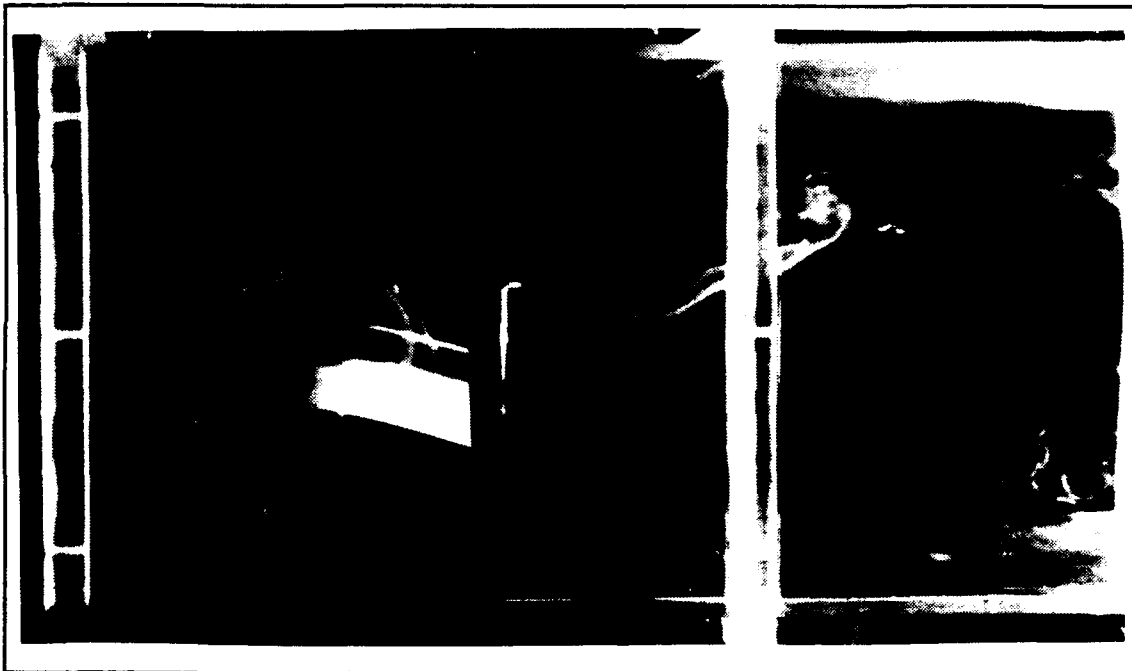


**Figure 4.12** RPM = 1085, AOA = 10°, rotating counterclockwise



AD-A258 019

A COMPUTATIONAL AND EXPERIMENTAL INVESTIGATION OF THE  
PROPULSIVE AND LIFT... (U) NAVAL POSTGRADUATE SCHOOL  
MONTEREY CA K S NEACE SEP 92 XB-NPS

2/2

UNCLASSIFIED

NL

END  
FILMED  
3-91  
DTIC

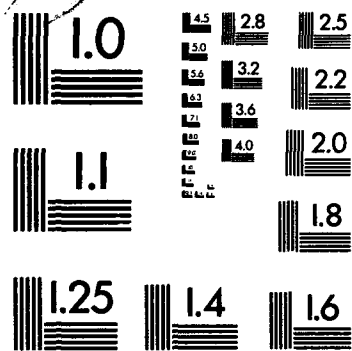




**Figure 4.13** RPM = 620, AOA = 20°, rotating counterclockwise.

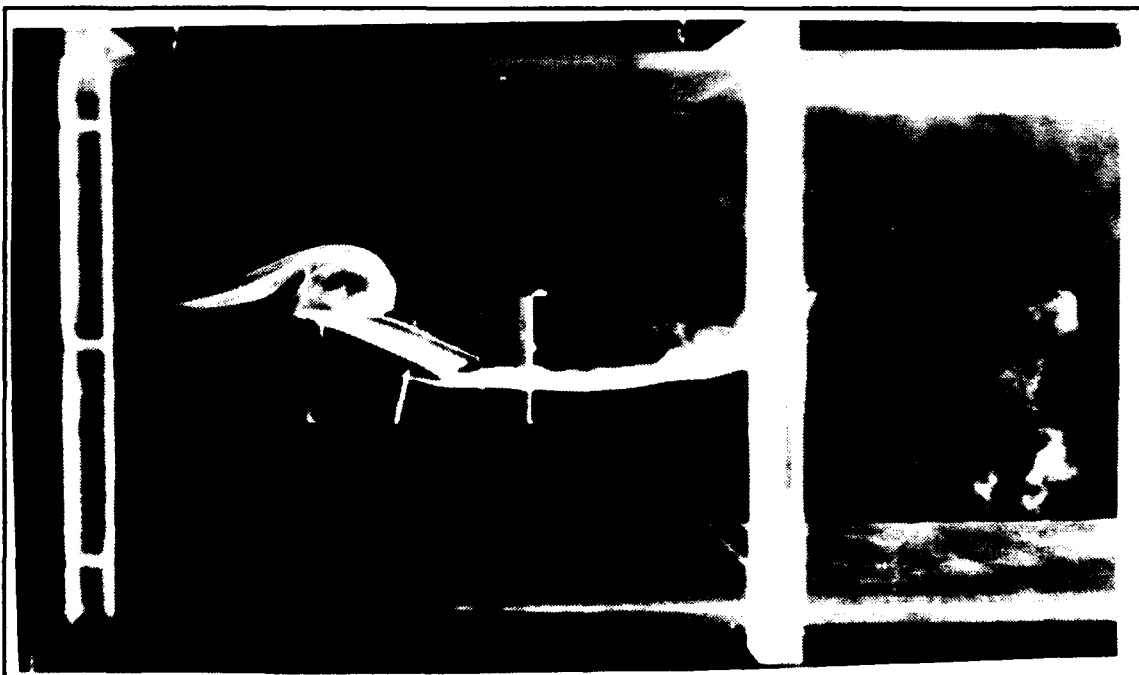


**Figure 4.14** RPM = 1085, AOA = 20°, rotating counterclockwise.

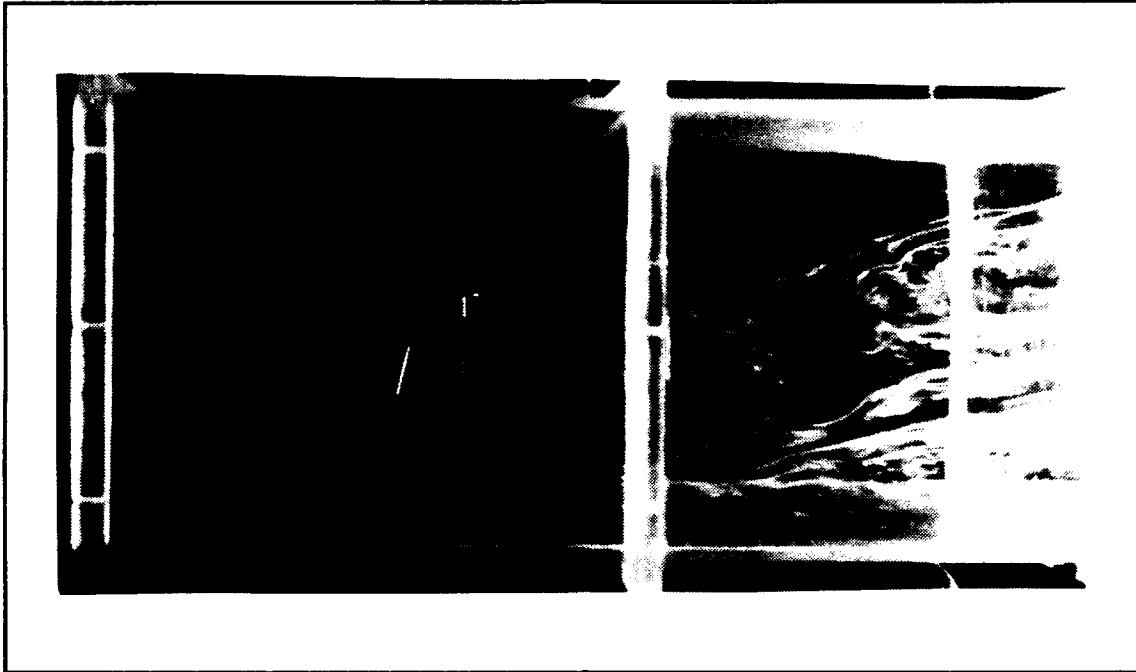


**Figure 4.15** RPM = 620, AOA = 0°, rotating counterclockwise

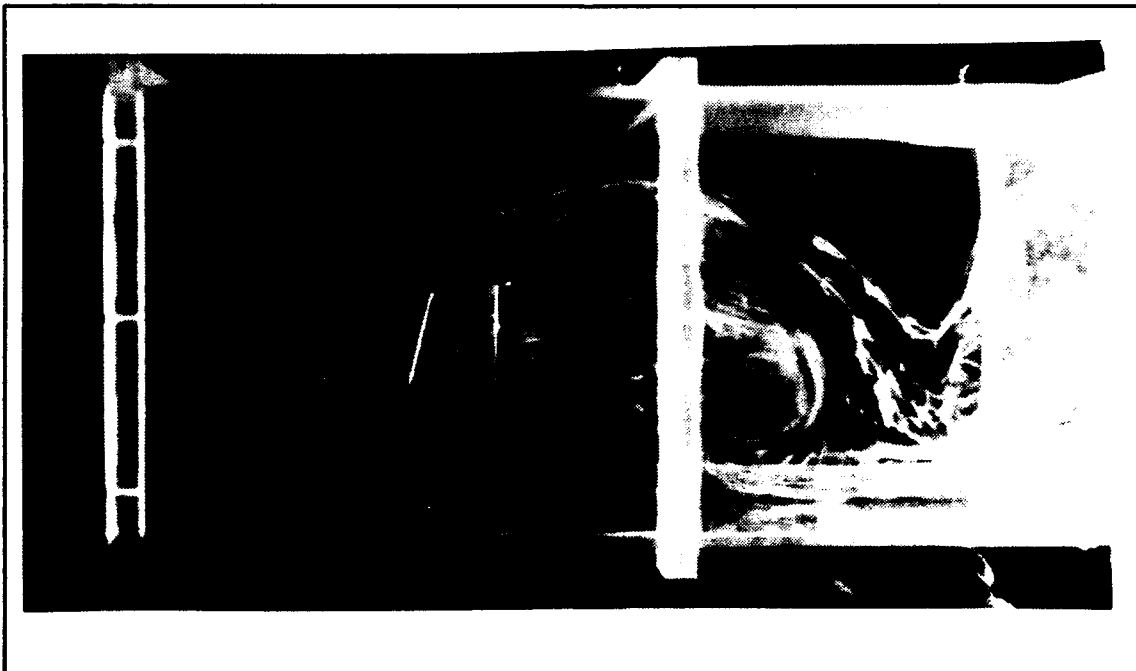


**Figure 4.16** RPM = 1085, AOA = 0°, rotating counterclockwise

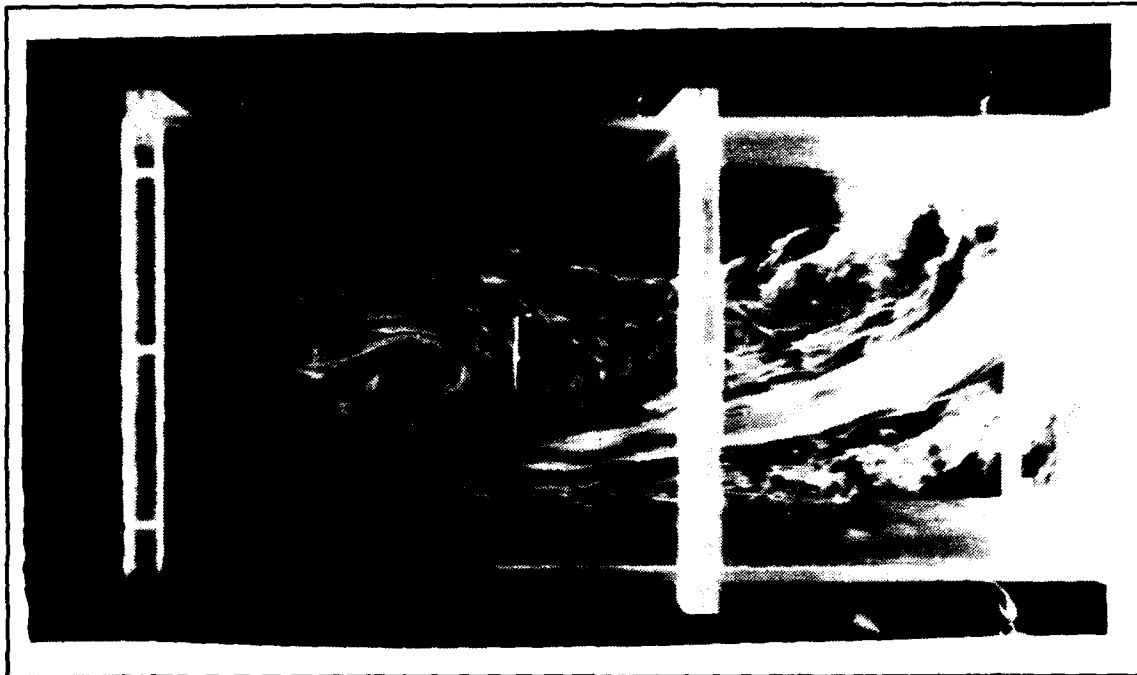


**Figure 4.17** RPM = 1085, AOA = 0°, rotating counterclockwise



**Figure 4.18** RPM = 1085, AOA = 0°, rotating counterclockwise

## **V. ENHANCED LIFT FLOW VISUALIZATION EXPERIMENT**

### **A. INTRODUCTION**

Experimental research in high angle-of-attack flight has long been an area of great interest. The area of active research centers around understanding and controlling the boundary layer to enhance lift in the post-stall region. To this end, many steady-state boundary layer control devices have been installed in an attempt to delay separation.

Boundary layer control has also been attempted through unsteady excitation mechanisms. The most promising method is the wave propeller first suggested by Wilhelm Schmidt in the German Journal of Flight Sciences in 1965 [Ref. 14]. Schmidt's wave propeller consisted of a single wing that performed a plunging motion perpendicular to the freestream. The oscillating wing was mounted between two stationary main lifting wings. In this arrangement the angle-of-attack of the wave propeller was varied to achieve optimum performance. Results from Schmidt's work indicate that with the optimum configuration the steady-state stall angle-of-attack could be increased to beyond  $25^\circ$  and the corresponding lift coefficient increased by four times.

The results on flow visualization in this report was a continuation of the on-going research at the Naval Postgraduate School to better understand the beneficial effects of a wave propeller operating in the vicinity of a main wing.

The initial research and construction of the wave propeller was undertaken by a former NPS student, Carl Dane. Carl Dane's thesis [Ref. 15] contains the results of pressure distributions on a main wing with the wave propeller configured to oscillate aft and slightly above the wing. Unfortunately, the wave propeller was designed poorly due to construction limitations and no beneficial effects were observed. The purpose of this research was to build a more efficient wave propeller; then, through flow visualization, understand the effects of the wave propeller on a stationary wing.

## **B. EXPERIMENTAL SETUP**

### **1. Wave Propeller and Stationary Wing**

The wave propeller was the same as described in Chapter IV (Figure 4.3). In this experiment, the wave propeller was mounted vertically in the NPS low speed wind tunnel behind a stationary wing. The wing had a 12-inch chord and a 28-inch span, the vertical length of the test section [Ref. 15]. The wing was constructed of a NACA 66(215)-216 airfoil section and could be set between 0 and 20 degrees AOA. Unfortunately, the wave propeller operated less efficiently in the vertical position. This was most likely a result of the increased weight on the bearings. A new power supply was used to provide increased rotational speeds of the wave propeller. A DC reversible power supply rated at a constant 48 volts, and 15 amps was used. With this power supply, the wave propeller operated at a rotational speed of 600 RPM.

## **2. Wind Tunnel**

The experiment was conducted in the 32x45 inch low speed wind tunnel located at the Navel Postgraduate School [Ref 17]. This tunnel was designed at the Aerolab Development Company of Pasadena, California as a closed circuit, single-return wind tunnel that is 64 feet long and 25.5 feet wide. The tunnel is powered by a 100 horse power motor which drives a three blade variable pitch fan by a four-speed International truck transmission. This motor and transmission can efficiently drive tunnel velocities up to 180 mph. Fan induced swirl is removed by eight stator blades located directly downstream of the fan. The tunnel cross section gradually expands from the fan to the settling chamber while turning through three sets of 90° corner vanes. The settling chamber includes two fine wire mesh anti-turbulence screens designed to break up large turbulent fluctuations. The flow accelerates to the test section through a 10:1 contraction cone.

The test section is made up of transparent glass sidewalls (access doors) and upper wall for illumination and viewing. The test section is designed to operate at atmospheric pressure, and has a breather slot located aft of the test section to compensate for leakage losses throughout the tunnel.

## **3. Smoke Generator**

The smoke was generated using the same Rosco smoke machine described in Chapter IV. The smoke was piped from the top of the tunnel into a blast tube. The blast tube directed the smoke into the tunnel slightly



upstream of the test section. In this configuration, the smoke was injected into the test section directly at the stationary wing.

### **C. TEST PROCEDURE**

The wave propeller was mounted vertically from the top of the wind tunnel to extend down into the test section slightly behind the stationary wing (Figures 5.1 and 5.2). In this position, the wave propeller could rotate both clockwise or counterclockwise at various angle-of-attack settings.

The tunnel was operated at speeds between 10-30 fps. The smoke was injected in the tunnel slightly upstream of the stationary wing. At this point, the wing angle-of-attack was increased until the boundary layer was just beginning to separate. Then, the wave propeller was turned on, and observations concerning the boundary layer were made. This continued for different AOA settings and rotational directions of the wave propeller.

### **D. RESULTS AND DISCUSSION**

Figures 5.3 and 5.4 show the best pictures taken in the series of experiments. Figure 5.3 is a picture of the flow over the stationary wing with the wave propeller turned off. The flow is shown to be slightly separated. Figure 5.4 shows the flow over the stationary wing with the wave propeller on. Here, the flow is seen to be more attached. Although many pictures were taken, very few came out clearly because of the poor lighting conditions and

limited time available to set appropriate flow visualization conditions for this experiment.

Visual observations of the wave propeller's influence on the stationary wing were more convincing than the pictures. It was clear that the wave propeller had a beneficial effect on the stationary wing that energized the boundary layer at high angle-of-attack and delayed separation. It was observed that the rotation direction, AOA, and relative position of the wave propeller all controlled the degree of influence on the stationary wing. It was noted that a clockwise direction, and increase in AOA had a stronger positive influence on the stationary wing. It was unclear as to the best relative position of the wave propeller. This was complicated by the limited area available in the test section to move the wave propeller. It was further noted that the beneficial influence was stronger at lower tunnel speeds. This was a result of the low rotational velocities achieved by the wave propeller. Apparently, the ratio of oscillation frequency to forward speed is critical for upstream influence. The higher the rotational speed of the wave propeller, the faster the freestream velocity can be and still achieve a beneficial upstream influence.



**Figure 5.1** Top view of stationary wing and wave propeller.



**Figure 5.2** Side view of stationary wing and wave propeller.

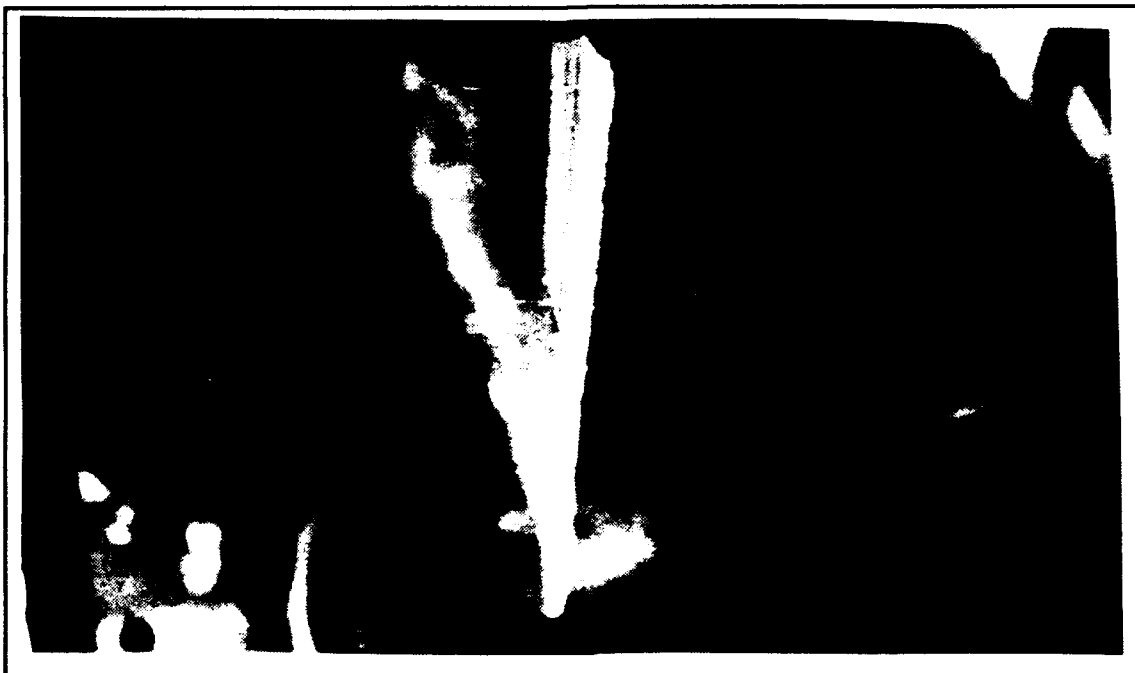


**Figure 5.3** Wave propeller is off.

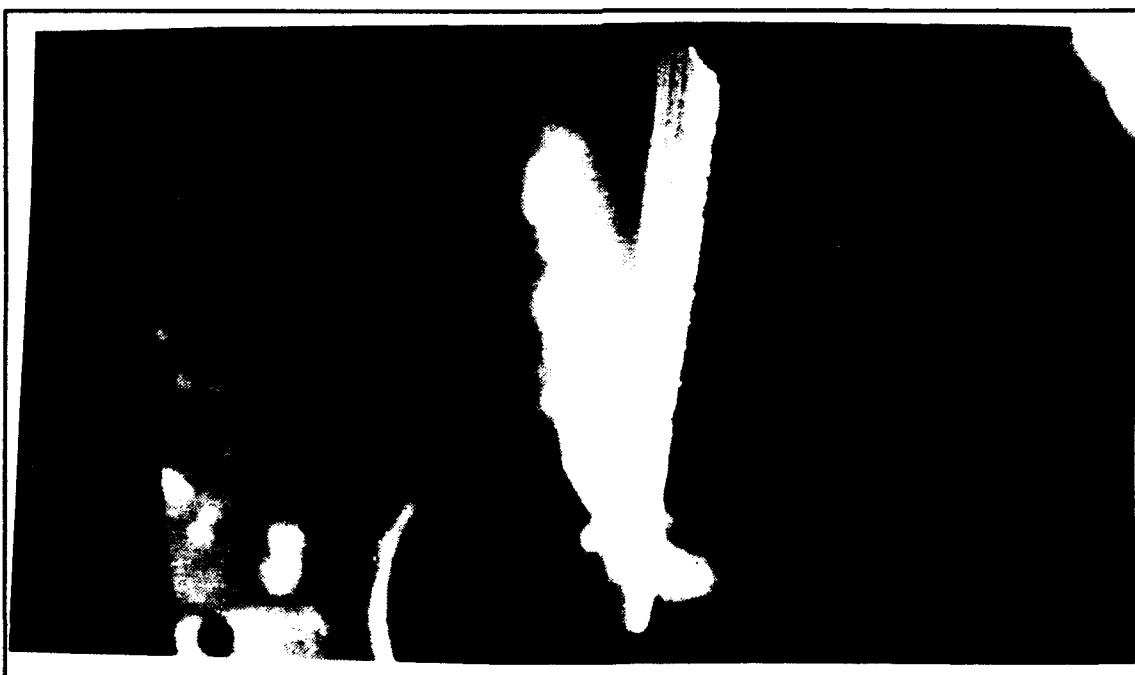


**Figure 5.4** Wave propeller is on.

## **VI. CONCLUSION AND RECOMMENDATIONS**

### **A. SINGLE AIRFOIL ANALYSIS**

The non-linear theory presented here for harmonic motion, and the phase lag relationships that exist between the airfoil motion and build-up of aerodynamic forces has been extensively verified with existing linear theory. Furthermore, a non-linear theory has been presented that predicts the propulsive forces and efficiencies associated with pitching, and plunging airfoils. Finally, a theory has been presented that suggests a definite link between quasi-steady ramp motion (dynamic lift), and a delayed steady state event.

More extensive studies of the quasi-steady phenomenon are recommended to thoroughly understand the relationships that exist between steady and unsteady motion. Another area of research is the study of the effect of airfoil geometry on aerodynamic flutter. A computational method can be developed using the presented codes and Theodorsen theory to solve the two-dimensional flutter determinant.

### **B. TWO AIRFOIL ANALYSIS**

The modified version of USPOTF2A has been verified against existing theoretical studies. Furthermore, a limited theory has been presented that

predicts the thrust and efficiency associated with two airfoils in close proximity. Finally, it was shown in the upwind influence study that an oscillating airfoil will have a beneficial influence on the pressure distribution and pressure gradient of a stationary airfoil.

In Chapter III the current limitations of the USPOTF2A code were noted. The limitation exists when the discrete vortices from one airfoil's wake interact with the other airfoil. The code should be improved to eliminate this difficulty. This would greatly enhance the capability of this code when working with large amplitude motions or when the airfoils are in tandem.

### **C. FLOW VISUALIZATION EXPERIMENTS**

The flow visualization experiment successfully showed the development of thrust produced by the wave propeller. Furthermore, the vortex street was analyzed to determine which conditions were more favorable for thrust production and which conditions induced stall. The enhanced lift flow visualization study was not a complete success. The wave propeller did not operate smoothly in the vertical position, and the upwind influence was only minor. Visual observation indicated a beneficial effect, but further photography is needed to document the event. Unfortunately, there was not sufficient time for experiments to produce adequate pictures of the phenomenon.

It is recommended that further experiments be conducted in the low speed smoke tunnel. The wave propeller should be modified for a smaller rotational

diameter (smaller plunge amplitude). Smaller amplitudes will prevent vortex interactions with the tunnel walls. Finally, it is recommended that the wave propeller be rebuilt so binding in the bearings will not inhibit the motion in the vertical position. Further experiments with smoke visualization and pressure measurements are required to better understand the influence of the wave propeller on the stationary wing. Certainly, the ability to move the wave propeller to various positions around the stationary wing must be included in follow-on experiments.

## APPENDIX A

```

CCCC
C THIS PROGRAM TAKES THE INPUT FILE (FILE CODE 14) CREATED BY
C U2DIIF AND CONVERTS THE DATA TO A FREQUENCY, AMPLITUDE, AND
C PHASE SHIFT. IT ALSO DETERMINES THE PROPULSIVE FORCES AND
C EFFICIENCY.
CCC
    PROGRAM PHASESHIFT
    DIMENSION PHASE(3),CL(400),CM(400),CD(400),
+ ALPHA(400),TIME(400),T(400),AMP(3),CKT(400),
+ FN(400),R(400),DAT(400),FNT(3,400),HY(400)
    LOGICAL FLAG
    REAL L1,L2,L3,L4,M1,M2,M3,M4
    PI = ACOS(-1.0)
C  READ TYPE OF MOTION (0=PITCH, 1=PLUNGE)
    READ(14,*) MOTION,ALP1
C  READ NUMBER OF DATA POINTS AND FREQ
    READ(14,*) NPTS, W
C  READ DATA (TIME, CL,CM,CD)
    DO I=1,NPTS
    READ(8,*) TIME(I),CL(I),CM(I),CD(I)
    END DO
    DO I=1,NPTS
    READ(12,*) T(I),ALPHA(I)
    END DO
    DO I=1,NPTS
    READ(13,*) T(I),HY(I)
    END DO
    DO 200, J = 1,2
    DO I = 1,NPTS
    IF (J .EQ. 1) THEN
    DAT(I) = CL(I)
    ELSE IF(J .EQ. 2) THEN
    DAT(I) = CM(I)
    END IF
    END DO
C  READ POSITION DATA
    IF(MOTION .EQ. 1) THEN
    DO I=1,NPTS
    ALPHA(I) = HY(I)
    END DO
    ZERO = .00001
    ELSE
    ZERO = .01
    END IF
15  N=2

```



```

DO I=2,NPTS
  IF(ALPHA(I).LE.ZERO .AND. ALPHA(I) .GE. -ZERO) GOTO 16
  N=N+1
END DO
16 M=1
DO I=N+1,NPTS
  IF(ALPHA(I).LE.ZERO.AND.ALPHA(I) .GE. -ZERO) GO TO 10
  M = M+1
END DO
10 CALL AMPLITUDE(DAT,AMP,NPTS,J)
  PRINT*, 'AMPL = ',AMP(J)
C
C DETERMINE PHASE SHIFT
C
25 PHI = 0
  ERR = 10000
  TOL = .01
  CN = 1.0
  ITTER = 500
  COUNT = 0
  NUM = 1
  PRINT*, 'N,M,J = ',N,M,J
C
C BEGIN ITERATION TO CONVERGENCE
C
30 IF(ERR .LT. TOL) GO TO 35
  SUM = 0
  DO I = N,N+M
    FN(I) = AMP(J)*SIN(W*T(I) + PHI)
    R(I) = ABS(FN(I) - DAT(I))
    SUM = SUM + R(I)
  END DO
  IF((SUM - ERR) .GT. 0) THEN
    CN = CN/2.0
    NUM = NUM +1
    IF(NUM/2.0 .EQ. INT(NUM/2.0)) THEN
      FLAG = .FALSE.
    ELSE
      FLAG = .TRUE.
    END IF
  END IF
  IF(FLAG) THEN
    PHI = PHI + CN*PI/180.0
    COUNT = COUNT + 1
  ELSE
    PHI = PHI - CN*PI/180.0
    COUNT = COUNT + 1
  END IF
  IF(COUNT .GT. ITTER) GOTO 500
  ERR = SUM

```

```

      GOTO 30
35   PHASE(J) = PHI*180.0/PI
      PRINT*, 'ERR = ', ERR
      GO TO 100
500  PRINT*, 'ITTERATION GREATER THEN 500...INCREASING TOL'
      TOL = 10*TOL
      COUNT = 0
      GO TO 30
100  IF(J .EQ. 1) WRITE (6,20) PHASE(J)+180.0
      IF(J .EQ. 2) WRITE (6,21) PHASE(J)
20   FORMAT(1X, ' CL PHASE =', F12.6)
21   FORMAT(1X, ' CM PHASE =', F12.6)
      DO I = 4, NPTS
          FNT(J, I) = AMP(J)*SIN(W*T(I) + PHASE(J)*PI/180.0)
      END DO
200  CONTINUE
      DO I = 4, NPTS
          WRITE(15, *) T(I), FNT(1, I), FNT(2, I), FNT(3, I)
      END DO

C
C   DETERMINE THE PROPULSIVE EFFICIENCY
C
      PHASE(1) = PHASE(1)*PI/180.0
      PHASE(2) = PHASE(2)*PI/180.0
      CDTOT = 0
      K = 0
      DO I = 2, N+M
          CDTOT = CDTOT + CD(I) - CD(1)
          K = K+1
      END DO
      DBAR = CDTOT/K
      DBAR = DBAR
      PRINT*, 'AVERAGE DRAG (THRUST), TOTAL DRAG (THRUST)
+   =', DBAR, CDTOT
      IF(MOTION .EQ. 1) THEN
          WBAR = -.5*W*SIN(PHASE(1))*AMP(1)
          ETAS = 2*DBAR/WBAR
      ELSE
          WBAR = .5*W*SIN(PHASE(2))*AMP(2)
          ETAS = DBAR/WBAR
      END IF
      PRINT*, 'ETAS, WBAR = ', ETAS, WBAR

C
      SUBROUTINE AMPLITUDE(DAT, AMP, NPTS, J)
      DIMENSION DAT(200), AMP(3), AMP1(10), AMP2(10)
      N2 = 0
      M2 = 0
      DO I = 1, 10
          AMP1(I) = 0
          AMP2(I) = 0

```

```

END DO
DO I = 2,NPTS-1
  IF(DAT(I+1) .LT. 0 .AND. DAT(I) .LT. 0 ) THEN
    IF(ABS(DAT(I+1)) .GT.ABS(DAT(I))) THEN
      IF((N2+1)/2.0 .EQ. INT((N2+1)/2.0)) N2 = N2+1
      TMP = ABS(DAT(I+1))
    ELSE
      GOTO 10
    END IF
    IF(TMP .GT. AMP1(N2)) THEN
      AMP1(N2) = TMP
      TMP = 0
    END IF
  ELSE
    IF((N2+1)/2.0 .NE. INT((N2+1)/2.0)) N2 = N2+1
    IF(ABS(DAT(I+1)) .GT.ABS(DAT(I))) THEN
      TMP = ABS(DAT(I+1))
    ELSE
      GOTO 10
    END IF
    IF(TMP .GT. AMP2(N2)) THEN
      AMP2(N2) = TMP
      TMP = 0
    END IF
  END IF
END DO
10 IF (AMP1(2) .GT. AMP2(2)) THEN
  IF(AMP1(2) .LT. AMP2(3)) THEN
    COMP = AMP1(2)
  ELSE
    COMP = AMP2(3)
  END IF
ELSE
  IF(AMP2(2) .LT. AMP1(3)) THEN
    COMP = AMP2(2)
  ELSE
    COMP = AMP1(3)
  END IF
END IF
PRINT*, 'COMP = ', COMP
DO I = 2, N2
  IF(ABS(AMP1(I)-COMP) .GT. .1*COMP) GO TO 20
  M2 = M2 + 1
  AMP(J) = AMP(J) + AMP1(I)
  GO TO 30
20 IF(ABS(AMP2(I)-COMP) .GT. .1*COMP) GO TO 30
  M2 = M2 + 1
  AMP(J) = AMP(J) + AMP2(I)
30 PRINT*, 'AMP(I), AMP(I) = ', AMP1(I), AMP2(I), M2
END DO

```

```
IF (J .LT. 3) THEN
  AMP(J) = AMP(J) / (M2)
ELSE
  AMP(J) = AMP(J) / (2*M2)
END IF
RETURN
END
```

## APPENDIX B

CCCCC

C THIS PROGRAM TAKES THE INPUT FILE (FILE CODE 14) CREATED BY  
C USPOTF2A AND CONVERTS THE DATA TO A FREQUENCY, AMPLITUDE,  
C AND PHASE SHIFT. IT ALSO COMPUTES THE PROPULSIVE FORCES AND  
C EFFICIENCIES ASSOCIATED WITH THAT DATA SET.

CCCC

```

      PROGRAM PHASESHIFT2
      DIMENSION PHASE(2,2),CL(2,450),CM(2,450),CD(2,450),
+ K(2),ALPHA(2,450),TIME(450),T(450),AMP(2,2),ALP(2),
+ CDTOT(2),FN(400),R(450),W(2),DAT(2,450),FNT(2,450,2),
+ HY(2,450),T1(450),CP1(450),CP2(450),CP3(450),CP4(450)
      REAL L1,L2,L3,L4,M1,M2,M3,M4
      LOGICAL FLAG, FIRST
      PI = ACOS(-1.0)
C  READ TYPE OF MOTION (0=PITCH, 1=PLUNGE)
      READ(14,*) MOTION,ALP1
C  READ NUMBER OF DATA POINTS AND FREQ
      READ(14,*) NPTS, W(1),W(2)
      PRINT*, MOTION,ALP1
      PRINT*,NPTS,W(1),W(2)
C  READ DATA (TIME, CL,CM,CD)
      READ(7,*)
      READ(7,*)
      READ(7,*)
      DO I=1,NPTS
        READ(7,*) TIME(I),CL(1,I),CL(2,I),CM(1,I),CM(2,I),
+ CD(1,I),CD(2,I)
      END DO
      DO I=1,NPTS
        READ(12,*) T(I),ALPHA(1,I),ALPHA(2,I)
      END DO
      DO I=1,NPTS
        READ(13,*) T(I),HY(1,I),HY(2,I)
      END DO
      IF(MOTION .EQ. 1) THEN
        DO L = 1,2
          DO I=1,NPTS
            ALPHA(L,I) = HY(L,I)
          END DO
        END DO
        ZERO = .00001
      ELSE
        ZERO = .01
      END IF
      IF (W(1) .EQ. 0) THEN

```

```

        FIRST = .FALSE.
        W(1) = W(2)
        DO I = 1,NPTS
            ALPHA(1,I) = ALPHA(2,I)
        END DO
    ELSE IF (W(2) .EQ. 0) THEN
        FIRST = .TRUE.
        W(2) = W(1)
        DO I = 1, NPTS
            ALPHA(2,I) = ALPHA(1,I)
        END DO
    END IF
DO 200, J = 1,2
    DO I = 1,NPTS
        IF (J .EQ. 1) THEN
            DAT(1,I) = CL(1,I)
            DAT(2,I) = CL(2,I)
        ELSE IF (J .EQ. 2) THEN
            DAT(1,I) = CM(1,I)
            DAT(2,I) = CM(2,I)
        END IF
    END DO
C  READ POSITION DATA
    DO 100 L = 1,2
15      N=2
        DO I=2,NPTS
            IF (ALPHA(L,I) .LE. ZERO .AND. ALPHA(L,I) .GE.
+          -ZERO) GO TO 16
            N=N+1
        END DO
16      M=1
        DO I=N+1,NPTS
            IF (ALPHA(L,I) .LE. ZERO .AND. ALPHA(L,I) .GE. -ZERO)
+          GO TO 10
            M = M+1
        END DO
10      PRINT*,W(L)
        CALL AMPLITUDE(DAT,AMP,NPTS,L,J,N)
        PRINT*, 'AMPL = ',AMP(J,L)
C
C  DETERMINE PHASE SHIFT
C
25      PHI = 0
        ERR = 10000
        TOL = .01
        CN = 1.0
        ITTER = 500
        COUNT = 0
        NUM = 1
        FLAG = .TRUE.

```

```

      PRINT*, 'N,M,L,J = ', N,M,L,J
C  BEGIN ITTERATION TO CONVERGENCE
30    IF(ERR .LT. TOL) GO TO 35
      SUM = 0
      DO I = N,N+M
        FN(I) = AMP(J,L)*SIN(W(L)*T(I) + PHI)
        R(I) = ABS(FN(I) - DAT(L,I))
        SUM = SUM + R(I)
      END DO
      IF((SUM - ERR) .GT. 0.0) THEN
        CN = CN/2.0
        NUM = NUM + 1
        IF(NUM/2.0 .EQ. INT(NUM/2.0)) THEN
          FLAG = .FALSE.
        ELSE
          FLAG = .TRUE.
        END IF
      END IF
      IF(FLAG) THEN
        PHI = PHI + CN*PI/180.0
        COUNT = COUNT + 1
      ELSE
        PHI = PHI - CN*PI/180.0
        COUNT = COUNT + 1
      END IF
      IF(COUNT .GT. ITTER) GOTO 500
      ERR = SUM
      GOTO 30
35    PHASE(J,L) = PHI*180/PI
      PRINT*, 'PHASE(J,L) = ', PHASE(J,L)
      PRINT*, 'ERROR = ', ERR
      GO TO 100
500   PRINT*, 'ITTERATION GREATER THEN 500...INCREASING TOL'
      TOL = 10*TOL
      CN = 10*CN
      COUNT = 0
      GO TO 30
100   CONTINUE
      IF(J .EQ. 1) WRITE (6,20) PHASE(J,1)+180.0 , PHASE(J,2)
+    +180.0
      IF(J .EQ. 2) WRITE (6,21) PHASE(J,1), PHASE(J,2)
20    FORMAT(1X, ' CL PHASE(1) =', F10.6, 5X, 'CL PHASE(2)
+    =', F10.6)
21    FORMAT(1X, ' CM PHASE(1) =', F10.6, 5X, 'CM PHASE(2)
+    =', F10.6)
      DO I = 4, NPTS
        FNT(J,I,1) = AMP(J,1)*SIN(W(1)*T(I) + PHASE(J,1)*PI/180.0)
        FNT(J,I,2) = AMP(J,2)*SIN(W(2)*T(I) + PHASE(J,2)*PI/180.0)
      END DO
      PHASE(J,1) = PHASE(J,1)*PI/180.0

```

```

        PHASE(J,2) = PHASE(J,2)*PI/180.0
200    CONTINUE
C
C    DETERMINE THE PROPULSIVE EFFICIENCY
C
C    INPUT DTS
        PRINT*, 'INPUT DTS '
        READ*, DTS
        K1 = 0
        DO L = 1,2
            CDTOT(L) = 0
            K(L) = 0
            DO I =DTS,2*DTS
                CDTOT(L) = CDTOT(L) + CD(L,I)
                K(L) = K(L) + 1
            END DO
        END DO
        DBAR1 = CDTOT(1)/K(1)
        DBAR2 = CDTOT(2)/K(2)
        PRINT*, 'AVERAGE DRAG, TOTAL DRAG (AF 1) =
+ ', DBAR1, CDTOT(1), K(1)
        PRINT*, 'AVERAGE DRAG, TOTAL DRAG (AF 2) =
+ ', DBAR2, CDTOT(2), K(2)
        IF(MOTION .EQ. 1) THEN
            IF (FIRST) THEN
                PHAS = PHASE(1,1)
                AMPL = AMP(1,1)
            ELSE
                PHAS = PHASE(1,2)
                AMPL = AMP(1,2)
            END IF
            WBAR = -.5*W(1)*SIN(PHAS)*AMPL
        ELSE
            IF (FIRST) THEN
                PHAS = PHASE(2,1)
                AMPL = AMP(2,1)
            ELSE
                PHAS = PHASE(2,2)
                AMPL = AMP(2,2)
            END IF
            ALP1 = ALP1*PI/180.0
            WBAR = -.5*W(1)*SIN(PHAS)*AMPL
        END IF
        ETAS = 2*(DBAR1+DBAR2)/WBAR
        PRINT*, 'ETAS, WBAR = ', ETAS, WBAR
        DO I=DTS,2*DTS
            CL1TOT = CL1TOT + CL(1,I)
            CL2TOT = CL2TOT + CL(2,I)
            K1 = K1 + 1
        END DO

```



```

CL1AVG = CL1TOT/K1
CL2AVG = CL2TOT/K1
DELCL1 = CL1AVG - CL(1,1)
DELCL2 = CL2AVG - CL(2,1)
PRINT*, 'CL1AVG, DELCL1 = ', CL1AVG, DELCL1
PRINT*, 'CL2AVG, DELCL2 = ', CL2AVG, DELCL2

C
DO I = 4, NPTS
  WRITE(15, *) T(I), FNT(1, I, 1), FNT(1, I, 2), FNT(2, I, 1),
+   FNT(2, I, 2)
END DO

C
END

SUBROUTINE AMPLITUDE(DAT, AMP, NPTS, L, J, N)
DIMENSION DAT(2, 200), AMP(2, 2), AMP1(10), AMP2(10)
  N2 = 0
  M2 = 0
  DO I = 1, 10
    AMP1(I) = 0
    AMP2(I) = 0
  END DO
  DO I = 2, NPTS-1
    IF(DAT(L, I+1) .LT. 0 .AND. DAT(L, I) .LT. 0) THEN
      IF(ABS(DAT(L, I+1)) .GT. ABS(DAT(L, I))) THEN
        IF((N2+1)/2.0 .EQ. INT((N2+1)/2.0)) N2 = N2+1
        TMP = ABS(DAT(L, I+1))
      ELSE
        GOTO 10
      END IF
      IF(TMP .GT. AMP1(N2)) THEN
        AMP1(N2) = TMP
        TMP = 0
      END IF
    ELSE
      IF((N2+1)/2.0 .NE. INT((N2+1)/2.0)) N2 = N2+1
      IF(ABS(DAT(L, I+1)) .GT. ABS(DAT(L, I))) THEN
        TMP = ABS(DAT(L, I+1))
      ELSE
        GOTO 10
      END IF
      IF(TMP .GT. AMP2(N2)) THEN
        AMP2(N2) = TMP
        TMP = 0
      END IF
    END IF
  END DO
  IF (AMP1(2) .GT. AMP2(2)) THEN
    IF(AMP1(2) .LT. AMP2(3)) THEN

```

```

        COMP = AMP1(2)
    ELSE
        COMP = AMP2(3)
    END IF
ELSE
    IF(AMP2(2) .LT. AMP1(3)) THEN
        COMP = AMP2(2)
    ELSE
        COMP = AMP1(3)
    END IF
END IF
PRINT*, 'COMP = ', COMP
DO I = 2, N2
    IF(AMP1(I) .GT. COMP) GO TO 19
    IF(ABS(AMP1(I) - COMP) .GT. .12*COMP) GO TO 20
19    M2 = M2 + 1
    AMP(J, L) = AMP(J, L) + AMP1(I)
    GO TO 30
20    IF(AMP2(I) .GT. COMP) GO TO 21
    IF(ABS(AMP2(I) - COMP) .GT. .12*COMP) GO TO 30
21    M2 = M2 + 1
    AMP(J, L) = AMP(J, L) + AMP2(I)
30    PRINT*, 'AMP(I), AMP(I) = ', AMP1(I), AMP2(I), M2
END DO
AMP(J, L) = AMP(J, L) / (M2)
RETURN
END

```

## LIST OF REFERENCES

1. Platzer, M.F., *Class Lecture Notes*, Naval Postgraduate School, Monterey, California, Sep 1991, pp. 1-20.
2. Teng, N.H., *The Development of a Computer Code (U2DIIIF) for the Numerical Solution of Unsteady, Inviscid and Incompressible Flow over an Airfoil*, Master's Thesis, Naval Postgraduate School, Monterey, California, Jun 1987, pp. 1-135.
3. Karman, Th. von, and Sears W.R., *Airfoil Theory for Non-uniform Motion*, Journal of Aeronautical Sciences 5, 1936, pp. 379-390.
4. Hess, J.L. and Smith, A.M.O., *Calculation of Potential Flow about Arbitrary Bodies*, Progress in Aeronautical Sciences, Vol. 8, Pergamon Press, Oxford, 1966, pp. 1-138.
5. Basu, B.C. and Hancock, G.J., *The Unsteady Motion of a Two-Dimensional Aerofoil in Incompressible Inviscid Flow*, Journal of Fluid Mechanics, Vol. 87, Jul 1987, pp. 159-168.
6. Giesing, J.P., *Nonlinear Two-Dimensional Unsteady Potential Flow With Lift*, Journal of Aircraft, Vol. 5, No. 2, Mar-Apr 1968, pp. 135-143.
7. Fung, Y.C., *The Theory of Aeroelasticity*, pp. 455-463, Dover, 1969.
8. Bosch, H., *Interfering Airfoils in Two-Dimensional Unsteady Incompressible Flow*, AGARD-CP-227, Feb 1978, pp. 7.1-7.14.
9. McKinney, W. and DeLaurier J., *The Wingmill: An Oscillating-Wing Windmill*, Journal of Energy, Vol 5, No. 2, March-April 1981, pp. 109-115.
10. Nowak, L.M., *Computational Investigation of a NACA0012 Airfoil in Low Reynolds Number Flows*, Master's Thesis, Naval Postgraduate School, Monterey, California, Sep 1992.

11. Chandrasekhara M., Carr, L., and Ahmed, S., *Schlieren Studies of Compressibility Effects on Dynamic Stall of Airfoils in Transient Pitching Motion*, AIAA-90-3038, Aug 20-22, 1990, pp. 346-356.
12. Pang, C.K., *A Computer Code (USPOTF2) for Unsteady Incompressible Flow Past Two Airfoils*, Master's Thesis, Naval Postgraduate School, Monterey, California, Sep 1988, pp. 1-156.
13. Liu, D.D. and Yao, Z.X., *Vortex/Wake Flow Studies for Airfoils in Unsteady Motions*, ASU Report CR-R-90008, Dec 1989, pp. 1-29.
14. Schmidt, Wilhelm., *Der Wellpropeller, Ein Neuer Antrieb Fur Wasser-, Land-, Und Luftfahrzeuge*, Z. Flugwiss, 13(1965), Heft 12, pp. 472-479.
15. Dane, C.W., *Exploratory Experimental Investigation of a Wave Propeller*, Master's Thesis, Naval Postgraduate School, Monterey, California, Mar 1992, pp. 1-57.
16. Freymuth, P., *Propulsive Vortical Signature of Plunging and Pitching Airfoils*, AIAA Journal, Vol. 26, No. 7, Jul 1988, pp. 881-883.
17. *Laboratory Manual for Low Speed Wind Tunnel Testing*, Department of Aeronautics, Naval Postgraduate School, Monterey, California, Oct 1983.
18. Scherer, J.O., *Experimental and Theoretical Investigation of Large Amplitude Oscillating Foil Propulsion Systems*, Hydronautics Research, Inc., Technical Report 662-1 final, May 1968, pp. 1-56.

## INITIAL DISTRIBUTION LIST

1. Defense Technical Information Center .....2  
Cameron Station  
Alexandria, Virginia 22304-6145
2. Superintendent.....2  
Attn: Library, Code 1424  
Naval Postgraduate School  
Monterey, California 93943-5000
3. Chairman, Code AA/CO .....1  
Naval Postgraduate School  
Monterey, California 93943-5000
4. Dr. M.F. Platzter.....5  
Dept. of Aeronautics and Astronautics, Code AA/PL  
Naval Postgraduate School  
Monterey, California 93943-5000
5. Dr. S.K. Hebbar.....2  
Dept. of Aeronautics and Astronautics, Code AA/HB  
Naval Postgraduate School  
Monterey, California 93943-5000
7. Dr. E.R. Wood.....2  
Dept. of Aeronautics and Astronautics, Code AA/EW  
Naval Postgraduate School  
Monterey, California 93943-5000
6. LT. Kerry S. Neace.....1  
2001 Agnes ct.  
Virginia Beach, Virginia 23454